

**NASA CONTRACTOR  
REPORT**



**NASA CR-9**



**NASA CR-992**

**LOAN COPY: RETURN TO  
AFWL (WLIL-2)  
KIRTLAND AFB, N MEX**

**EXPLORATORY FLOW AND CONTAINMENT  
EXPERIMENTS IN A DIRECTED-WALL-JET  
VORTEX TUBE WITH RADIAL OUTFLOW AND  
MODERATE SUPERIMPOSED AXIAL FLOWS**

*by Bruce V. Johnson*

*Prepared by*  
**UNITED AIRCRAFT CORPORATION**  
East Hartford, Conn.

*for*

**NATIONAL AERONAUTICS AND SPACE ADMINISTRATION • WASHINGTON, D. C. • FEBRUARY 1968**



**EXPLORATORY FLOW AND CONTAINMENT EXPERIMENTS  
IN A DIRECTED-WALL-JET VORTEX TUBE WITH RADIAL OUTFLOW  
AND MODERATE SUPERIMPOSED AXIAL FLOWS**

By Bruce V. Johnson

Distribution of this report is provided in the interest of information exchange. Responsibility for the contents resides in the author or organization that prepared it.

Issued by Originator as Report No. F-910091-11

Prepared under Contract No. NASw-847 by  
**UNITED AIRCRAFT CORPORATION**  
East Hartford, Conn.

for

**NATIONAL AERONAUTICS AND SPACE ADMINISTRATION**



## FOREWORD

An exploratory experimental and theoretical investigation of gaseous nuclear rocket technology is being conducted by the United Aircraft Corporation Research Laboratories under Contract NASw-847 with the joint AEC-NASA Space Nuclear Propulsion Office. The Technical Supervisor of the Contract for NASA is Captain W. A. Yingling (USAF). Results of the fluid mechanics portion of the investigation conducted during the period between September 15, 1965 and May 30, 1967 are described in the following four reports (including the present report) which comprise the required fifth Interim Summary Technical Report under the Contract:

1. Travers, A.: Experimental Investigation of Flow Patterns in Radial-Outflow Vortexes Using a Rotating-Peripheral-Wall Water Vortex Tube. UAC Research Laboratories Report F-910091-10, May 1967 (NASA CR-991, 1968).
2. Johnson, B. V.: Exploratory Flow and Containment Experiments in a Directed-Wall-Jet Vortex Tube with Radial Outflow and Moderate Superimposed Axial Flows. UAC Research Laboratories Report F-910091-11, May 1967 (present report, NASA CR-992, 1968).
3. Kendall, J. S., A. E. Mensing, and B. V. Johnson: Containment Experiments in Vortex Tubes with Radial Outflow and Large Superimposed Axial Flows. UAC Research Laboratories Report F-910091-12, May 1967 (NASA CR-993, 1968).
4. Clark, J. W., B. V. Johnson, J. S. Kendall, A. E. Mensing, and A. Travers: Summary of Gaseous Nuclear Rocket Fluid Mechanics Research Conducted Under Contract NASw-847. UAC Research Laboratories Report F-910091-13, May 1967. (Submitted to AIAA for publication.)



Exploratory Flow and Containment Experiments  
in a Directed-Wall-Jet Vortex Tube with Radial Outflow  
and Moderate Superimposed Axial Flows

TABLE OF CONTENTS

	<u>Page</u>
SUMMARY . . . . .	1
CONCLUSIONS . . . . .	2
INTRODUCTION . . . . .	3
Background and Objectives of This Investigation . . . . .	4
DESCRIPTION OF EQUIPMENT AND PROCEDURES . . . . .	6
Vortex Tube Assemblies . . . . .	6
Flow Capabilities of Facilities . . . . .	8
Instrumentation and Procedures . . . . .	9
DISCUSSION OF RESULTS . . . . .	13
Flow Visualization Tests . . . . .	13
Velocity and Static Pressure Measurements . . . . .	15
Heavy-Gas Containment Tests . . . . .	19
SUMMARY OF PRINCIPAL RESULTS . . . . .	25
Flow Visualization Tests . . . . .	25
Velocity Measurements . . . . .	25
Heavy-Gas Containment Tests . . . . .	26
Concluding Remarks . . . . .	27
REFERENCES . . . . .	29
LIST OF SYMBOLS . . . . .	31
APPENDIX - RELATIONS BETWEEN DIMENSIONLESS AND DIMENSIONAL VORTEX FLOW CONTAINMENT PARAMETERS . . . . .	34
TABLES . . . . .	36
FIGURES . . . . .	39

Exploratory Flow and Containment Experiments  
in a Directed-Wall-Jet Vortex Tube with Radial Outflow  
and Moderate Superimposed Axial Flows

SUMMARY

Exploratory fluid mechanics experiments were performed to obtain information applicable to an open-cycle, vortex-stabilized, gaseous-core nuclear rocket. The containment characteristics of confined radial-outflow vortexes with superimposed axial flow were studied to determine whether high average simulated-fuel densities and high ratios of simulated propellant-to-fuel flow rates could be obtained. The experiments concentrated on two factors that influence simulated-fuel containment: (1) simulated-propellant injection methods in which the flow is injected from the peripheral wall of an axial-flow vortex tube with both axial and tangential (circumferential) components of velocity, and (2) simulated-fuel injection methods. The experiments were performed in 10-in.-dia by 30-in.-long vortex tubes. Simulated propellant was injected at the peripheral wall through 600 directed wall jets that could be adjusted to any injection flow angle between the tangential and axial directions.

Flow visualization tests were performed using water with dye as a trace fluid. The dye patterns showed that large-scale turbulent mixing occurred between the central region and the peripheral-wall region when the simulated fuel was injected from ducts at the centers of both end walls (radial outflow). Velocity measurements were made using air as the working fluid. These measurements indicated that injection at the peripheral wall with both axial and tangential components of velocity will substantially decrease the average axial velocities in the central region and will create a larger volume within the vortex that is potentially available for containment of fuel. Containment tests to determine the average dwell time of simulated fuel in the vortex tube were performed using a heavy gas to simulate fuel and a light gas to simulate propellant. Compared with the containment times measured with no axial component of injection velocity, improvements in containment time of as much as a factor of three-and-one-half were obtained in this investigation using injection with both axial and tangential components of velocity. The improvements that can be obtained using different fuel injection methods are smaller. However, the maximum containment times that were measured were approximately one to two orders of magnitude less than the value now estimated to be required for an economically practical, open-cycle, gaseous-core nuclear rocket.

## CONCLUSIONS

1. Velocity measurements indicated that the average axial velocities in the central region of an axial-flow vortex tube were substantially decreased for some, but not all, configurations in which the simulated propellant was injected with an axial component of velocity in addition to the tangential component. Compared with configurations in which the simulated propellant was injected only tangentially, the volume potentially available for simulated-fuel containment was increased substantially for the best configurations.

2. The heavy-gas dwell times (the average time that the heavy gas or simulated fuel remained in the vortex tube) were higher in tests with an axial component of light-gas (simulated propellant) injection velocity. The maximum heavy-gas dwell times were three-and-one-half times those measured in tests with no axial component of injection velocity, but were only seven times the average light-gas dwell time. The heavy-gas dwell times were not appreciably affected by changes in the heavy-gas injection configuration.

3. Flow visualization tests using water as the working fluid showed that turbulent mixing was a dominant feature even with the injection configurations that provided the highest heavy-gas dwell times and the highest average heavy-gas densities. Large-scale eddies occurred between the central region and high-axial-velocity region near the peripheral wall for all peripheral-wall injection configurations. These eddies probably account for the failure to obtain greater improvements in the heavy-gas dwell times.

4. The best combination of simulated-propellant and simulated-fuel injection methods provided containment parameters that are between one and two orders of magnitude less than are now estimated to be required for an economically practical full-scale, open-cycle engine.

## INTRODUCTION

An experimental and theoretical investigation of gaseous nuclear rocket technology is being conducted by the United Aircraft Research Laboratories under Contract NASw-847 administered by the joint AEC-NASA Space Nuclear Propulsion Office. The research performed under this contract is applicable to two vortex-stabilized gaseous nuclear rocket concepts: the open-cycle concept and the nuclear light bulb engine concept.

In the open-cycle concept, hydrogen propellant is injected from the peripheral wall of the rocket chamber to drive the vortex. It then flows axially in a narrow region near the peripheral wall into an exhaust annulus at one end of the chamber and through the exhaust nozzle. Gaseous nuclear fuel is contained in the central region of the vortex flow. Heat is transferred by thermal radiation from the gaseous nuclear fuel to the hydrogen propellant passing over the fuel region. Details of the engine concept -- including the fluid mechanics, heat transfer, nucleonics and structure -- are described in Ref. 1.

In the nuclear light bulb concept, propellant is heated by thermal radiation passing through an internally cooled transparent wall located between the fuel and the propellant. Coolant gas is injected tangent to the inner surface of the transparent peripheral wall to drive a vortex. A vortex flow pattern is utilized to contain gaseous nuclear fuel and keep it away from the transparent wall.

Two factors which determine the flow patterns in confined vortices are (1) whether or not there is a superimposed axial flow near the peripheral wall, and (2) whether or not the net flow of fluid is radially inward or outward with respect to the centerline of the vortex. In a vortex with superimposed axial flow, fluid is injected at the peripheral wall and is withdrawn through an annulus located near the outer edge of one end wall. The radial-inflow vortex is formed by removing a small amount of fluid through ports at the centers of the end walls. The radial-outflow vortex is also driven by injecting fluid at the peripheral wall, but in this case additional fluid is injected through the ports at the centers of the end walls.

Flow visualization tests of radial-inflow vortices (Refs. 2 and 3) have indicated that the flow in the central region can be relatively laminar and, hence, may lead to satisfactory containment of gaseous nuclear fuel. However, two-component-gas tests with radial-inflow vortices (Refs. 4, 5, and 6) have indicated that the density of the heavy gas in the simulated fuel-containment region of the vortex (i.e., the relatively laminar central region) can be only slightly greater than that of the surrounding light gas before instabilities and turbulence occur. In an open-cycle engine the density of the fuel must be considerably greater than that of the surrounding propellant; performance studies indicate that the fuel-to-propellant density ratios attainable with a radial-inflow vortex are not large enough for such

an engine. However, since the nuclear light bulb engine could utilize a heavy gas such as neon between the fuel and the transparent wall, radial-inflow vortexes appear suitable for nuclear light bulb engines.

Initial flow visualization tests of radial-outflow vortexes (Ref. 2) indicated that the flow was turbulent in the central region. Two-component-gas tests (Refs. 5 and 6) indicated that the density of the heavy gas in the simulated fuel containment region could be increased to a value substantially greater than the density of the surrounding light gas. However, very few measurements had been made of heavy-gas loss rates, particularly for conditions with large amounts of superimposed axial flow. Thus, further research was required to determine whether radial-outflow vortexes would be suitable for application to an open-cycle engine.

Three different experimental investigations were conducted concurrently to investigate the characteristics of radial-outflow vortexes for potential application to an open-cycle engine. The results of flow visualization tests directed toward obtaining fundamental information on the stability and flow patterns of radial-outflow vortexes are reported in Ref. 7. The results of an exploratory investigation that included flow visualization tests, flow-field velocity measurements and heavy-gas containment tests are presented in this report. The results of heavy-gas containment tests conducted at Reynolds numbers up to those that would be required in a full-scale engine are reported in Ref. 8. A summary of the principal results of the fluid mechanics research conducted under Contract NASw-847 and a comparison of the observed vortex flow characteristics with those that would be required in both an open-cycle engine and a nuclear light bulb engine are presented in Ref. 9.

#### Background and Objectives of This Investigation

Several experimental studies have been performed to investigate the flow and fuel-containment characteristics in axial-flow vortexes for application to an open-cycle engine. Velocity measurements were made using water and air as working fluids in the tests reported in Refs. 3, 10, and 11. The results indicated that the axial velocities in the central region (the fuel-containment region) of the vortexes were undesirably large. Heavy-gas containment measurements were also made to determine the average dwell time of simulated fuel (Refs. 4, 5, and 12). The average dwell times measured for axial-flow vortexes were only one-half to one-third of those measured for basic vortexes, i.e., vortexes without superimposed axial flow. The measured containment parameters were substantially less than those estimated to be required for a full-scale, open-cycle engine (Ref. 1). Thus, improvements in flow and containment characteristics are needed if axial-flow vortexes are to be used for open-cycle engines.

In vortex tubes investigated previously, an axial pressure gradient was required to accelerate the flow toward the axial-flow exhaust annulus. The resulting

flows had a region of high axial velocities which extended inward from the peripheral wall about half the distance to the center of the vortex tube. This region encompassed approximately three-fourths of the volume of the vortex tube. Injecting the simulated propellant from the peripheral wall with an axial component of velocity (in addition to the tangential component) should decrease or eliminate the required axial pressure gradient and increase the volume within the vortex tube having low axial velocities. If, in addition, the method used to inject simulated fuel is compatible with the flow patterns induced by the simulated propellant injection configuration, improvements in containment should result.

The objectives of the research reported herein were (1) to determine the effectiveness of injecting simulated propellant from the peripheral wall with an axial component of velocity (in addition to the tangential component) as a method for decreasing the axial velocities in the central region of radial outflow vortices, (2) to determine whether the containment time and simulated-fuel-to-propellant density ratio can be increased using these peripheral-wall injection configurations, and (3) to determine the effects of different simulated-fuel injection methods on containment when used with these peripheral-wall injection configurations.

## DESCRIPTION OF EQUIPMENT AND PROCEDURES

### Vortex Tube Assemblies

A sketch showing the most important geometrical features of the vortex tube assemblies used for this program is presented in Fig. 1. Two separate vortex tube assemblies were constructed. In both assemblies the vortex tube had an inside diameter of 10 in. and a length of 30 in. The assembly for the flow visualization tests was constructed using lucite for the end walls, the peripheral wall, and the outer cylindrical shell. The assembly for the velocity measurements and the heavy-gas containment tests was constructed entirely of metal. In all tests the simulated propellant (water or air) was injected from the peripheral wall through 600 directed wall jets that were adjusted to various injection flow angles between the tangential (i.e., circumferential) and axial directions. Additional flow to simulate fuel (water, air or heavy gas) was usually injected from the nonaxial-flow end wall, the axial-flow end wall, or both end walls. The mixture of simulated propellant and simulated fuel was exhausted from the vortex tube through an annulus at the outer edge of the axial-flow end wall. In some cases, a small amount of flow was withdrawn at the center of the axial-flow end wall or at the centers of both end walls. The simulated propellant was injected at the peripheral wall from ten plenums between the vortex tube and the outer cylindrical shell of the assembly (see Fig. 1). The flow through each plenum was metered using a variable-area flow meter.

A photograph of the vortex test apparatus assembled for velocity measurement tests is shown in Fig. 2. The plumbing to and from the vortex tube assembly was varied slightly for the flow visualization tests and for the heavy-gas containment tests.

### Peripheral-Wall Configurations

A sketch of a typical insert for the directed-wall-jet peripheral-wall injection system is shown in Fig. 3a. The insert provides a duct for delivering flow from the plenum through the peripheral wall of the vortex tube. The injection slot was created by fastening a cap to the insert base. The slot width for all caps was 0.300 in. and the slot heights varied from 0.030 in. to 0.060 in. in increments of 0.005 in. (a total of seven different slot heights).

A sketch of the insert installation is shown in Fig. 3b, and a photograph of inserts installed in the vortex tube is shown in Fig. 4. The inserts could be rotated a full 360 deg. In the present program, flow angles from  $\beta_j = 0$  deg (the tangential direction) to  $\beta_j = 90$  deg (the axial direction) were investigated. This provided ratios of the axial component of injection velocity to the tangential component from  $V_{z,j} / V_{\phi,j} = 0$  to infinity. The inserts were arranged in 20 rings at

equally spaced axial stations with 30 inserts in each ring (Fig. 4). The flow to each set of two rings of inserts was supplied from the surrounding plenum. The plenums were separated by silicon rubber seals which were inflated after the vortex tube was installed inside the outer cylindrical shell.

A total of seven different peripheral-wall injection configurations were tested. Details of these configurations, including the injection angle and slot height distributions, are summarized in Table I.

### End Wall Configurations

The nonaxial-flow end wall configuration for the flow visualization tests and the velocity measurements consisted of a flat disk with a 0.9-in.-dia duct at the center for flow injection or withdrawal. A variety of nonaxial-flow end wall configurations were used for the heavy-gas containment tests; all of these had provisions for injection of heavy gas, and some had provisions for injection of both heavy gas and light gas. These different end-wall injection configurations are discussed below.

The axial-flow end wall configuration for all of the flow visualization tests, and for most of the velocity measurements and heavy-gas containment tests, consisted of a flat disk which provided an axial-flow exhaust annulus from a radius of  $r_3 = 4.5$  in. to the peripheral wall ( $r_1 = 5.0$  in.). The disk had a 0.9-in.-dia duct at the center for flow injection or withdrawal. A photograph of the axial-flow end wall used in most of the velocity measurements and heavy-gas containment tests is shown in Fig. 5. As noted in Fig. 5, for some velocity measurements the inner radius of the axial-flow exhaust annulus,  $r_3$ , was changed to 4.75 in., 4.50 in., 4.00 in., 3.50 in., and 3.00 in. Some of the axial-flow end walls used in the heavy-gas containment tests also had provisions for both heavy-gas and light-gas injection (see discussion below).

### Heavy-Gas Injection

Sketches of the heavy-gas injection configurations used are shown in Fig. 6. The primary heavy-gas injection configuration consisted of injection through the 0.9-in.-dia duct at the center of the nonaxial-flow end wall (Fig. 6a). A few tests were also made with heavy-gas injection through the duct at the center of the axial-flow end wall and simultaneously through the ducts at the centers of both end walls. Seven other heavy-gas injection configurations were also investigated. The details of these other configurations are presented in Figs. 6b through 6h and in Table II. The configurations included a centerline porous tube (Fig. 6b), a "showerhead" (Fig. 6c), a 6-in.-dia screen (Fig. 6d), three different configurations having injection with swirl (Figs. 6e through 6g), and axial injection through twelve ducts

(Fig. 6h). The heavy-gas injection areas of these configurations varied from 0.106 to 78.5 sq in.

### Light-Gas Injection with Swirl

Photographs of the end walls used for the tests with light-gas injection from the end walls with swirl are shown in Fig. 7. Light gas was injected tangentially from all of the wall jets on the axial-flow end wall (Fig. 7b) and from the outer three rings of wall jets on the nonaxial-flow end wall (Fig. 7a). Heavy gas was injected through the four wall jets in the center ring and through the eight wall jets in the second ring on the nonaxial-flow end wall (heavy-gas injection configuration shown in Fig. 6g). The details of the light-gas slot size and wall jet locations are shown in Fig. 7. The light-gas flow to each of the end walls was metered by three variable-area flow meters. The inner radius of the axial-flow exhaust annulus was 4.5 in.

### Flow Capabilities of Facilities

Water was used as the working fluid for the flow visualization studies. The capacity of the flow meters limited the flow rate through the peripheral-wall directed wall jets to 170 gpm. Additional flow was injected or withdrawn through the ducts at the centers of both end walls. The water circulation system described in Ref. 3 was used for the flow visualization tests.

Room-temperature air was drawn into the vortex tube assembly through the plenums and directed wall jets for the velocity measurements. The pressure in the vortex tube was approximately 0.9 atm. The ten variable-area flow meters used had a maximum total flow rate limitation of 0.9 lb/sec for room-temperature air. Additional flow was injected through the ducts at the centers of both end walls, or some flow was withdrawn through the same ducts. The room-temperature air was used as both a simulated propellant and a simulated fuel for these tests.

Air heated to approximately 260 F was drawn into the vortex tube to simulate propellant in the heavy-gas containment tests. The ten flow meters had a maximum total flow rate limitation of 0.75 lb/sec at this temperature and at pressures slightly less than 1 atm. The pressure in the test section during these tests was approximately 10 psi. The simulated fuel for most of the tests was a fluorocarbon (FC-77, molecular weight approximately 400) manufactured by the Minnesota Mining and Manufacturing Corporation. The maximum heavy-gas flow rate was 0.22 lb/sec. Approximately 0.001 lb/sec of iodine was also injected with the heavy gas to serve as a tracer. In some tests, flow was also withdrawn from the center of the axial-flow end wall.

## Instrumentation and Procedures

For all of the tests discussed in this report, the flow conditions for the simulated propellant are described in terms of Reynolds numbers which are defined on the basis of a local velocity or an average flow rate in the vortex tube. These nondimensional parameters are useful in applying the results to performance analyses of full-scale, open-cycle engines. The tangential injection Reynolds number is defined as

$$Re_{t,j} = V_{\phi,j} r_1 \rho_{P_1} / \mu_{P_1} \quad (1)$$

The axial-flow Reynolds number is defined as

$$Re_{z,w} = W_p / (7/16) \pi r_1 \mu_{P_1} \quad (2)$$

where  $W_p$  is the weight flow rate of simulated propellant ( $Re_{z,w}$  is based on the average axial velocity through an axial-flow exhaust annulus extending from  $0.75 r_1$  to  $r_1$ ). The radial Reynolds number is defined as

$$Re_r = W_t / 2 \pi \mu_{P_1} L \quad (3)$$

where  $W_t$  is the weight flow rate through the ducts at the centers of the end walls. This parameter was used as a measure of the rate at which flow was injected ( $Re_r < 0$ ) or withdrawn ( $Re_r > 0$ ) through the ducts at the centers of both end walls in the flow visualization tests and velocity measurements. It was also used as measure of the rate at which the mixture of heavy gas and light gas was withdrawn through the duct at the center of the axial-flow end wall in some heavy-gas containment tests (the heavy-gas injection flow rate was indicated by  $W_p$ ).

### Flow Visualization Procedures

Water with fluorescent dye as a tracer was used as the working fluid for the flow visualization tests. Dye was injected at one or more locations on the nonaxial-flow end wall or on the peripheral wall. Microflash photographs of the dye patterns were taken at various times after injection when the dye concentrations were near the peripheral wall or in the central region. The purpose of the photographs was to show the scale of turbulence or the laminar character of the flow in various regions of the vortex. A sketch of the optical system used to obtain dye photographs is shown in Fig. 8. As indicated in Fig. 8, an adjustable slit was used with a microflash lamp to illuminate a plane in the fluid at the desired axial location. The microflash lamp had an illumination duration of 0.1 microsecond. The photographs were taken through the transparent nonaxial-flow end wall. All photographs presented in this report were taken with the slit at a distance of  $z = 7.5$  in. from the nonaxial-flow end wall.

## Velocity Measurement Procedures

A schematic of the equipment used for the velocity measurements is shown in Fig. 9. The velocity measurements were made using a cobra probe which is shown in Views B-B and C-C. The total pressure was obtained at pressure tap B. The direction of the flow was determined by balancing the pressure at tap A with the pressure at tap C (pressure taps A and C are on planes approximately 45 deg to the plane of pressure tap B). Taps A and C were connected to a transducer which provided a null or activation signal to the controller. The probe angle,  $\beta_p$ , was automatically adjusted by the controller. The transducer and probe were sensitive to pressure differences as small as about 0.002 psi. At a flow velocity of approximately 100 ft/sec the probe sensitivity was such that the probe angle could be set to within 0.5 deg. At higher velocities the flow angle could be determined more accurately due to the increased dynamic pressure. Calibration tests were made to determine the ratio between  $p_B$  minus  $p_C$  (measured on the slant-board manometer) and the total velocity head. The ratio obtained was then used in the tests to determine the flow velocities from pressure measurements at tap B and tap C. The radial location of the probe was set manually using the controller.

## Heavy-Gas Containment Measurement Procedures

The heavy gas used to simulate the gaseous nuclear fuel consisted of a mixture of iodine vapor and a heavy fluorocarbon vapor, FC-77. The iodine was used as a trace gas since it absorbs light at wavelengths easily detected and measured. An iodine absorptometer was installed on the vortex tube exhaust ducts to permit the density of iodine vapor to be determined from the amount of light absorbed. The theoretical aspects of the absorptometer are discussed in Ref. 12; a description of the unit employed in the present test is given in Appendix I of Ref. 12.

The amount of heavy gas stored within the vortex tube was determined from the rate of iodine flow out of the vortex tube after the heavy gas shut-off valve was closed. With the vortex-tube geometry and the light-gas flow parameters established, heavy gas was injected at a constant rate. The rate of flow of heavy gas out of the vortex was monitored using the iodine absorptometer located in the axial-flow exhaust duct (and, when used, in the thru-flow exhaust duct at the center of the axial-flow end wall). When the rate of flow of heavy-gas out of the vortex tube reached a steady-state condition, the heavy-gas shut-off valve was closed. The amount of heavy gas that had been contained in the vortex tube under steady-state conditions was obtained from the volume flow rate of the mixture in the axial-flow exhaust duct and the integral of the iodine density determined from the time-dependent absorptometer signal.

The iodine vapor was the only portion of the mixture that was detected by the absorptometer. The ratio of the FC-77 weight flow to the iodine weight flow in the exhaust ducts was assumed to be the same as in the heavy-gas injection duct. This assumption is valid since, for the flow conditions of this study, there were no significant forces within the vortex which would separate the iodine vapor from

FC-77 vapor within the time period required for the heavy gas to flow through the vortex. Allowances were made for the heavy gas in the injection lines and exhaust ducts when calculating the total heavy gas stored in the vortex tube from the measurements. The injection lines (downstream of the shut-off valve) were purged shortly after shut-off in each test.

Several parameters were calculated from the heavy-gas containment test data to describe the containment characteristics. The average heavy-gas density in the vortex is defined as

$$\bar{\rho}_{F_1} = W_F / V \quad (4)$$

where  $W_F$  is the total weight of heavy gas stored and  $V$  is the volume of the vortex tube. The heavy-gas density ratio is  $\bar{\rho}_{F_1} / \rho_{P_1}$ ; although it is a dependent variable (the weight flow rate of heavy gas,  $W_F$ , was the independent variable in the experiments), it will be used as the abscissa when discussing the containment results.

The average heavy-gas dwell time,  $t_F$ , is the average time the heavy gas remains within the vortex tube. It is given by

$$t_F = W_F / W_P \quad (5)$$

The minimum dwell time for the light gas, if no heavy gas were contained in the vortex, is given by

$$t_{F \text{ MIN}} = V \rho_{P_1} / W_P \quad (6)$$

where  $W_P$  is the light-gas weight flow rate and  $\rho_{P_1}$  the light-gas density at injection. The containment parameter is the ratio of the average heavy-gas dwell time to the minimum dwell time,

$$\tau_{F_1} / \tau_{F_1 \text{ MIN}} = t_F / t_{F \text{ MIN}} \quad (7)$$

The containment parameter will be used as the dependent variable when the results are discussed. The light- to-heavy-gas weight flow rate ratio,  $W_P / W_F$ , can be calculated from

$$\frac{W_P}{W_F} = \frac{V \rho_{P_1} / t_{F \text{ MIN}}}{W_F / t_F} = \left( \frac{\tau_{F_1}}{\tau_{F_1 \text{ MIN}}} \right) / \left( \frac{\bar{\rho}_{F_1}}{\rho_{P_1}} \right) \quad (8)$$

A numerical example which relates the dimensionless and dimensional flow parameters is given in the Appendix.

## DISCUSSION OF RESULTS

This report summarizes the results of exploratory studies of flow in an axial-flow vortex tube performed in an attempt to increase the fraction of the vortex tube filled with heavy gas for a given ratio of simulated-propellant flow rate to simulated-fuel flow rate. The specific objectives of this research were to study the effects on the containment characteristics of changes in both the peripheral-wall simulated-propellant injection configurations and simulated-propellant (heavy-gas) injection configurations.

An outline of each of the three types of tests reported herein is presented in Table III. The flow visualization tests and velocity measurements were performed first in an effort to understand the flow characteristics of the vortices. The heavy-gas containment tests concluded the test program.

Results for three simulated-propellant injection configurations ( $\beta_j = 0, 45,$  and  $0$  to  $45$  deg) were obtained for all three types of tests noted in Table III. Velocity measurements were obtained with three additional simulated-propellant configurations ( $\beta_j = 26.5, 63.5,$  and  $0$  to  $63.5$  deg) and heavy-gas containment results were obtained for two additional simulated-propellant injection configurations ( $\beta_j = 90$  and  $0$  to  $63.5$  deg). Results presented for the flow visualization tests and velocity measurements were limited to a single simulated-fuel injection configuration, i.e., injection through ducts at the centers of both end walls. A total of ten heavy-gas injection configurations (see Table II and Fig. 6) are reported for the heavy-gas containment tests.

### Flow Visualization Tests

The characteristics of flow in the axial-flow vortex tube were studied using water as the working fluid and dye as a tracer. With water as the working fluid rather than air, the time scale of the flow is decreased by a factor of approximately 20 for the same Reynolds number due to the differences in density and viscosity. As a result, the laminar or turbulent character of the flow can be more easily discerned and a judgment about the desirability of a given flow condition for simulated-fuel containment can be quickly made. Flow patterns were observed for three peripheral-wall injection configurations:  $\beta_j = 0, 45,$  and  $0$  to  $45$  deg. For all the flow visualization tests reported herein, a constant peripheral-wall injection flow rate was maintained which provided an equivalent axial-flow Reynolds number of approximately 53,000.

### Flow Patterns with Flow Injected at Centers of End Walls (Radial Outflow)

Photographs of dye patterns in the vortex tube with the peripheral-wall injection configuration  $\beta_j = 0$  are shown in Fig. 10. The radial and tangential

injection Reynolds numbers for this case were  $Re_r = -40$  and  $Re_{t,j} = 164,000$ , respectively. The upper photograph shows dye patterns near the peripheral wall where, as expected, the flow was turbulent for all flow conditions; the scale of the eddies near the peripheral wall was 0.1 to 0.5 in. The lower photograph shows the size and shape of the turbulent cells in the central region of the vortex tube. Flow from the peripheral-wall region was convected into the cells; flow from the central region was, in turn, convected to the peripheral wall region. The eddies were large, encompassing almost one-half of the vortex-tube diameter, and the mixing was rather irregular.

Photographs of dye patterns for flow conditions with  $\beta_j = 45$  deg and  $Re_r = -40$  deg are shown in Fig. 11. The tangential injection Reynolds number was less than that in Fig. 10 ( $Re_{t,j} = 116,000$ ) since the injection area was the same as for  $\beta_j = 0$  but the jets were oriented at 45 deg to the local  $r-\phi$  plane. The eddies in the central region of the vortex were approximately the same large size as for  $\beta_j = 0$ .

Photographs for flow conditions with  $\beta_j = 0$  to 45 deg are shown in Fig. 12. The radial and tangential injection Reynolds numbers were  $Re_r = -40$  and  $Re_{t,j} = 164,000$ , respectively. The lower photograph shows well-ordered secondary vortex cells which were superimposed upon the steady-state rotation. The center of two cells can be clearly seen at the lower left-hand corner and midway along the right side of the lower photograph. The secondary cells are rotating in the same direction as the injected flow at the outside of the vortex. The secondary cells appear to be laminar. Visual observations also indicated that the flow in the center of the cells passed from the center of the vortex tube toward both end walls. However, the flow between the secondary cells had a relatively large eddy size and no regular pattern. Similar eddies are shown in Ref. 7.

The conclusion from observing the flow patterns shown in the three preceding figures was that turbulent mixing was the dominant feature of the flow for all of the peripheral-wall injection configurations with radial outflow. Large-scale eddies occurred in the central region of the vortex with much mixing between the central region and the peripheral-wall region.

#### Flow Patterns with Flow Withdrawn at Centers of End Walls (Radial Inflow)

Photographs of dye patterns in the vortex tube with the peripheral-wall injection configuration  $\beta_j = 0$  are shown in Fig. 13. The radial flow rate withdrawn through the ducts at the centers of both end walls is the same as the flow rate injected in the three previous figures ( $Re_r = +40$ ). The peripheral-wall region was turbulent as expected; however, the central region of the vortex appeared laminar with well-defined dye striations. A set of small eddies with a diameter of 0.5 to 1 in. was superimposed upon the flow, regularly spaced around the circumference at a radius of approximately 2.5 in.

Photographs of dye patterns in the vortex tube with  $\beta_j = 45$  deg are shown in Figs. 14 and 15. The flow rates for the former figure were the same as for Fig. 13, i.e.,  $Re_r = +40$ ; however, the tangential injection Reynolds number is lower,  $Re_{t,j} = 116,000$ . In Fig. 14, large-scale eddies, similar to those in the photographs with radial outflow, occurred in the central region of the vortex from the center to  $r = 4.5$  in. Thus the central regions of this vortex was not stabilized as was the vortex with  $\beta_j = 0$  deg and the same thru-flow rate. Photographs of dye patterns with the same peripheral-wall injection configuration and double the radial flow rate of Fig. 14 are shown in Fig. 15. The flow near the peripheral wall was turbulent, similar to that shown in the previous five figures. At  $r \approx 3$  in., the turbulence had decreased to a low level. The central region of the vortex tube had the laminar characteristics seen in Fig. 13; the flow was symmetric, had well-defined dye striae, and did not have the large-scale mixing which appeared in the previous figure. The conclusion from this discussion was that a larger amount of radial inflow was needed to stabilize the flow for  $\beta_j = 45$  deg compared with similar flow conditions for  $\beta_j = 0$  deg. This was probably because large secondary flows were induced when all of the jets were directed at 45 deg.

#### Velocity and Static Pressure Measurements

Axial and tangential velocity profiles and the peripheral-wall static pressures were measured at several axial locations for six peripheral-wall injection configurations, as indicated in Table III. The equivalent axial-flow Reynolds number for these tests was approximately 108,000 rather than 53,000 as in the flow visualization tests. The flow rate was increased to increase the velocity and dynamic pressure levels within the vortex tube and hence increase the sensitivity of the velocity probe measurements.

#### Effects of Peripheral-Wall Injection Configurations on Velocity Profiles

##### Velocity Profiles at Different Axial Stations

Axial and tangential velocity profiles are shown in Figs. 16 to 21 for peripheral-wall injection configuration of  $\beta_j = 0, 0$  to 45, 0 to 63.5, 26.5, 45, and 63.5 deg. Profiles were measured with flow injected at the centers of both end walls. For  $\beta_j = 0, 0$  to 45, and 0 to 63.5 deg (Figs. 16 to 18), the tangential velocity profiles appeared to be independent of axial station for a given flow condition. The axial velocity increased regularly from the nonaxial-flow end wall to the axial-flow end wall in the high-axial-velocity region. This regularity will be shown again later. In Fig. 16, the region of high axial velocity extended well past the inner radius of the axial-flow annulus,  $r_3$ , into the central region of the vortex tube ( $r_3$  was 4.5 in. for these tests). The axial velocity profiles for  $\beta_j = 0$  deg show a relatively large amount of counterflow in the central region of the vortex tube from a radius of 3 in. to approximately 1 in., i.e., a region of

axial velocity toward the nonaxial-flow end wall. The tangential velocity profiles for  $z = 28.5$  in. were not identical to those at the other axial locations; this was probably because a large amount of secondary flow occurred along the axial-flow end wall and influenced the tangential velocity profile by the recirculation of flow radially outward in this region. That is, near the axial-flow end wall there was a relatively large amount of flow (1) radially inward along the end wall, (2) axially at mid-radii from the end wall toward the central region of the vortex tube, and (3) radially outward into the high-axial-velocity region at values of  $z$  greater than approximately 22 in.

For  $\beta_j = 0$  to 45 deg, Fig. 17, the counterflow at the central region of the vortex tube was less at  $r = 2.5$  in. than for  $\beta_j = 0$  deg. The average axial velocities were less than 5 ft/sec at most of the axial stations for radii less than approximately 3.0 in. and appeared to provide a favorable flow condition for heavy-gas containment. For  $\beta_j = 0$  to 63.5 deg, Fig. 18, the region of relatively high axial flow was confined to radii greater than 3.5 to 4 in. The maximum counterflow velocity near the axial-flow end wall was less than 10 ft/sec and the counterflow velocities at the other stations were less than 5 ft/sec.

The tangential velocity profiles for  $\beta_j = 26.5$  deg (Fig. 19) do not vary much with axial location. However, when  $\beta_j$  was increased to 45 deg (Fig. 20), the tangential velocity profiles changed appreciably from  $z = 4.5$  in. to  $z = 28.5$  in. The axial variation of the tangential velocity profiles was even more pronounced for  $\beta_j = 63.5$  deg (Fig. 21); for this case, the tangential velocity near the nonaxial-flow end wall is very low at all radii, characteristic of very strong radial outflow. The axial velocity profiles for  $\beta_j = 26.5, 45$  and 63.5 deg (Figs. 19 to 21) show a counterflow at  $z = 4.5$  in. between radii of 4.5 in. and 3.5 in.

#### Reduced Axial Velocity Profiles

The reduced axial velocity profiles for  $\beta_j = 0, 0$  to 45, and 0 to 63.5 deg (Fig. 22) were obtained by dividing the local axial velocities by the local  $z$ . In all tests discussed so far, the injection flow rate per unit length along the vortex tube was constant; therefore, the average axial velocity was proportional to  $z$ . For these configurations, the axial velocity profiles for  $z \geq 10.5$  in. can be represented by a common curve for each flow condition. The reduced axial velocity profiles for  $z = 4.5$  in. were not the same as the common curve because the flow in this region was influenced by the secondary flow on the nonaxial-flow end wall.

Recall (Figs. 16 to 18) that the tangential velocity profiles for these cases were independent of axial location. Analysis showed that, for constant total viscosity and conditions where the tangential profile is independent of axial location and where the axial flow is proportional to  $z$ , a similarity parameter for an axial-flow vortex can be obtained. The flow in the high-velocity region of these vortices appears to be subject to such analysis.

### Comparison of Axial and Tangential Velocity Profiles for All Injection Configurations

Comparisons of the axial and tangential velocity profiles obtained at  $z = 16.5$  in. are shown in Fig. 23 for  $\beta_j = 0, 0$  to  $45$  and  $0$  to  $63.5$  deg and in Fig. 24 for  $\beta_j = 0, 26.5, 45,$  and  $63.5$  deg. The velocity profiles in Fig. 23 show that the tangential velocity increases with a decrease in radius for radial regions where there is a high axial velocity (caused by the inflow of angular momentum due to the large radial flow rate required to fill the axial velocity profile). The tangential velocity for  $\beta_j = 0$  increased from the wall to a radius of  $3.5$  in.; the profile for  $\beta_j = 0$  to  $63.5$  deg increased only from the wall to a radius of  $4.7$  in. In Fig. 24, the tangential injection velocities are different for the four cases because the jet injection velocity,  $V_j$ , was constant and  $V_{\phi,j} = V_j \cos \beta_j$ . Of the axial profiles shown in Fig. 24, the profile for  $\beta_j = 45$  deg has the lowest velocity in the central region of the vortex tube and appeared most favorable for heavy-gas containment.

### Effects of Peripheral-Wall Injection Configuration on Pressure Distributions

The peripheral-wall static pressure distributions for  $\beta_j = 0, 0$  to  $45,$  and  $0$  to  $63.5$  deg and for  $\beta_j = 0, 26.5, 45,$  and  $63.5$  deg are shown in Figs. 25 and 26, respectively. The static pressures were measured at the same axial stations as the velocity profiles. For  $\beta_j = 0$  deg (Fig. 25), the peripheral-wall pressure distribution decreased nearly parabolically with distance from the nonaxial-flow end wall. This pressure decrease was necessary to induce axial velocities in the high-axial velocity region. The static pressure decrease from  $z = 4.5$  in. to  $z = 30$  in. was approximately twice the dynamic head of the maximum axial velocity at  $z = 30$  in. The pressure distribution for  $\beta_j = 0$  to  $45$  deg is almost constant along the entire length of the vortex tube; this characteristic was desired because it was felt that a constant peripheral-wall pressure distribution would minimize the counterflows in the central region of the vortex tube and minimize the heavy-gas loss for a given configuration. The pressure distribution for  $\beta_j = 0$  to  $63.5$  deg shows a relatively large pressure rise with increasing  $z$ . This was probably because the increase in axial injection velocity with distance  $z$  was greater than required to overcome the axial pressure gradient required to accelerate the flow axially.

The pressure distributions for the cases with constant  $\beta_j$  (Fig. 26) show variations with axial location for all cases. For  $\beta_j = 26.5$  deg, the pressure is constant in the central region of the vortex tube from  $z = 10$  in. to  $z = 22.5$  in.; however, a pressure drop occurs near the axial-flow end wall. This pressure drop was probably necessary to accelerate the flow through the axial-flow exhaust annulus.

## Comparison of Tangential Velocity Profiles Obtained with Probe and End-Wall Static Pressure Measurements

The tangential velocity profiles for  $z = 4.5$  in. presented in Figs. 16, 17, 18, 20 and 21 are shown as dashed lines in Fig. 27. The velocity profiles obtained from radial gradients of end-wall pressure are shown as solid lines. Good agreement between the two methods was obtained for  $\beta_j = 0, 0$  to  $45$ , and  $0$  to  $63.5$  deg. These were configurations which had small counterflow velocities near the nonaxial-flow end wall. The poor agreement obtained for  $\beta_j = 45$  and  $63.5$  deg was probably due to the large radial variation of counterflow velocities near the nonaxial-flow end wall; consequently, a radial variation in the axial pressure gradient between  $z = 4.5$  in. and the peripheral wall was required to decelerate this flow. Another reason for the poor agreement may be that the pressure differences for these cases are smaller, due to the lower tangential velocities for these two cases.

## Effects of Changes in Radial Reynolds Number

The effects of changes in radial Reynolds number on axial and tangential velocity profiles are shown in Figs. 28 and 29 for  $\beta_j = 0$  to  $45$  deg and for  $\beta_j = 0$  to  $63.5$  deg, respectively. Profiles were obtained at  $z = 16.5$  in. for constant peripheral-wall injection conditions for each configuration. In both figures, the tangential velocity profiles obtained for  $Re_r = -105, 0,$  and  $+24$  are approximately the same. When the  $Re_r$  was increased to  $+100$ , the tangential velocity distribution showed an increase in angular velocity ( $V_\phi/r$ ) with decreasing radius. The axial velocity profiles for both of these cases are independent of radial Reynolds number.

## Effects of Inner Radius of Axial-Flow Exhaust Annulus on Velocity Profiles

The effects of changes of the inner radius of the axial-flow exhaust annulus on the velocity profiles for  $\beta_j = 0$  to  $63.5$  deg are shown in Fig. 30. For this peripheral-wall injection configuration, the axial velocity profiles were virtually unaffected by changes in the inner radius for  $r_3 = 3.0, 3.5, 4.0, 4.5$  and  $4.75$  in. The tangential velocity profiles are also essentially independent of  $r_3$  for  $r_3 \geq 3.5$  in. For  $r_3 = 3.0$  in., the tangential velocity profile shows a moderate increase in tangential velocity with decrease in radius compared with the tangential velocity profiles obtained for the previous four cases.

## Conclusions from Velocity Measurements and Flow Visualization Tests

Results from some of the velocity measurements, e.g.,  $\beta_j = 0$  to  $45$  deg, indicate that axial-flow vortexes with superimposed axial flow should have favorable heavy-gas containment characteristics since low axial velocities were obtained in the central region of the vortex tube. However, the flow visualization studies showed that large-scale turbulent mixing occurred even though the average axial

velocities were relatively low. Thus, the overall results from the one-component flow studies show that although the desired objective of obtaining low axial velocities in the central region of the vortex tube was obtained, the total result of having a desirable fuel-containment region was not obtained. Analytical stability studies for turbulent flow (Ref. 13) or for laminar flow with small disturbances (Ref. 14) show that radial gradients of axial velocity (axial shear) decrease the stability of a given flow. From the flow visualization photographs (Fig. 12) and the velocity profiles (Fig. 17) it is concluded that, at least for some conditions, the axial shear caused the flow to become unstable and form a regular flow pattern of small-scale vortices. A similar effect was reported in Ref. 7 when moderate axial flows were superimposed on a vortex flow. The effect of peripheral-wall injection with an axial velocity component on heavy-gas containment will be discussed in subsequent sections.

### Heavy-Gas Containment Tests

The amount of heavy gas in the vortex tube during steady-state flow conditions was measured for five peripheral-wall injection configurations and ten heavy-gas injection configurations. The principal flow condition consisted of an equivalent axial-flow Reynolds number of approximately  $Re_{z,w} = 74,000$  and heavy-gas injection at the center of the nonaxial-flow end wall. Containment times for this flow condition were measured for  $\beta_j = 0, 45, 90, 0$  to  $45$  and  $0$  to  $63.5$  deg. An outline of the containment tests including other variations in geometry and flow rates is shown in Table III.

### Heavy-Gas Injection at the Centers of the End Walls

#### Standard Configurations

The variation of containment parameter with heavy-gas density ratio is shown in Fig. 31 for all peripheral-wall injection configurations tested with heavy-gas injection at the center of the nonaxial-flow end wall or the centers of both end walls. For some peripheral-wall injection configurations, data were also obtained with heavy-gas injection at the center of the axial-flow end wall. For reference, lines indicating a constant ratio of light-gas flow rate to heavy-gas flow rate,  $W_p/W_F$ , are shown. The light-gas (air) was injected at a constant flow rate per unit length for these tests with an axial-flow Reynolds number of approximately  $Re_{z,w} = 74,000$ . The containment parameters were usually highest for heavy-gas injection at the nonaxial-flow end wall and lowest for heavy-gas injection at the axial-flow end wall (see, for example, Figs. 31c and 31d). The containment parameters for heavy-gas injection at the center of both end walls were not much less than for injection at the center of the nonaxial-flow end wall. Curves are faired through the data from tests with heavy-gas injection at the nonaxial-flow end wall. For all configurations except  $\beta_j = 90$  deg, the containment parameter

was a maximum at low values of density ratio and decreased to approximately half the maximum value at a density ratio of 0.7. For  $\beta_j = 90$  deg, the containment parameter was almost constant for changes in heavy-gas density ratio from 0.06 to 0.7 (Fig. 31f).

A comparison of the variation of containment parameter with heavy-gas density ratio for tests with all peripheral-wall injection configurations and with heavy-gas injection at the nonaxial-flow end wall are presented in Fig. 32. The highest containment parameters were obtained for peripheral-wall injection configurations of  $\beta_j = 45$  and 0 to 63.5 deg. Containment data were obtained with the vortex-tube axis horizontal for  $\beta_j = 0, 0$  to 45, 0 to 63.5, and 45 deg; containment data were obtained with the vortex-tube axis vertical for  $\beta_j = 45$  and 90 deg. The data for  $\beta_j = 45$  deg with the vortex-tube axis horizontal and vertical show no appreciable effect of axis orientation on the variation of containment parameter with heavy-gas density ratio. The variation of the containment parameter at a heavy-gas density ratio of 0.2 with the maximum injection angle for each peripheral-wall injection configuration is shown in Fig. 33. These containment parameters are from Fig. 32. For the injection configurations where  $\beta_j$  is a constant along the length of the tube, the containment parameter appears to peak between  $\beta_j = 45$  and 90 deg. For  $\beta_j = 0$  to 45 and 0 to 63.5 deg, the containment parameter increased appreciably as the maximum injection angle was increased. However, it is desirable to minimize the maximum angle in a full-scale engine since propellant flows with very large axial velocities near the peripheral wall require a larger propellant flow rate to absorb the radiant heat transfer from the fuel region (Ref. 15).

#### Effect of Flow Withdrawal at Axial-Flow End Wall

The effect of flow withdrawal at the center of the axial-flow end wall on the variation of containment parameter with heavy-gas density ratio is shown in Fig. 34. Other parameters for these tests were  $\beta_j = 0$  to 63.5 deg, heavy-gas injection at the center of the nonaxial-flow end wall,  $Re_{z,w} \approx 74,000$  and  $Re_{t,j} \approx 230,000$ . Heavy-gas containment parameters were obtained for radial Reynolds numbers (a measure of the amount of thru-flow withdrawn) of  $Re_r = +51, +68$  and  $+93$ . The results show no large effect of radial Reynolds number on the variation of containment parameter with heavy-gas density ratio. The containment parameters at heavy-gas density ratios of about 0.15 are approximately 30 percent less than were obtained with no thru-flow and the same peripheral-wall and heavy-gas injection configurations; the containment parameters at heavy-gas density ratios of 0.6 are approximately the same. For these tests with thru-flow, at least 90 percent of the heavy gas was exhausted through the axial-flow annulus. The ratio of the weight flow rate withdrawn at the center of the axial-flow end wall to the heavy-gas weight flow rate injected at the center of the nonaxial-flow end wall varied from 0.13 to 1.0; however, the ratio of the volume flow rates varied from 1.8 to 14.

### Effect of Axial Variation of Light-Gas Injection Flow Rate

The effect of changes in light-gas injection flow rate with axial distance along the peripheral wall on the variation of containment parameter with heavy-gas density ratio is shown in Fig. 35. Containment data were obtained for  $\beta_j = 0$  to 63.5 deg, heavy-gas injection at the center of the nonaxial-flow end wall and  $Re_{z,w} \approx 43,000$ . The results for injection flow rate constant along the peripheral wall were similar to those previously shown in Fig. 31c for  $Re_{z,w} = 74,000$ . The tangential injection Reynolds number for this flow condition was  $Re_{t,j} = 125,000$ .

The first change was to remove the seals between the plenums and to equalize the pressure in the plenums. This provided approximately constant total injection velocity but a tangential component which varied from a large value at the nonaxial-flow end wall to a low value at the axial-flow end wall; the tangential injection Reynolds number at  $z = 0$  was  $Re_{t,j} = 171,000$  and at  $z = 30$  in. was  $Re_{t,j} = 76,000$ . The containment parameters are slightly less than were obtained for the previous condition.

The second change was to increase the light-gas injection flow rate linearly with distance so that the injection flow rate at the axial-flow end wall was 50 percent greater than at the nonaxial-flow end wall. The tangential injection velocity and the tangential injection Reynolds number were increased proportionally,  $Re_{t,j}$  varying from 100,000 to 150,000. The containment parameters for tests with this second change were increased 40 to 60 percent at the same heavy-gas density ratios compared with the standard condition (injection flow rate constant along the wall). For this second change, the average distance that the injected flow travels within the tube decreased compared with the standard condition. If a larger simulated-propellant flow rate were injected immediately upstream of the axial-flow end wall annulus, the containment parameters would be increased further; however, this is not practical for a full-scale engine since the propellant would not absorb a significant amount of heat from the fuel region in the short time it was in the cavity.

### Effect of Changes in Axial-Flow Reynolds Number

The variations of containment parameter with heavy-gas density ratio for  $Re_{z,w} = 40,000$  and 74,000 are compared in Fig. 36. Containment parameters are compared for  $\beta_j = 0, 45$  and 90 deg with heavy gas injected at the center of the nonaxial-flow end wall. In the tests with  $\beta_j = 0$  the vortex-tube axis was horizontal; in the tests with  $\beta_j = 45$  and 90 deg the vortex-tube axis was vertical. The containment results for  $\beta_j = 45$  and 90 deg show very little effect of axial-flow Reynolds number. Although the containment parameters for  $\beta_j = 0$  are higher for  $Re_{z,w} = 40,000$  than for  $Re_{z,w} = 74,000$ , the principal effect on the containment parameter appears to be the peripheral-wall injection configuration.

## Heavy-Gas Injection at Other Locations

### Results of Tests with Other Configurations Without Heavy-Gas Swirl

The effect of heavy-gas injection from a porous tube along the centerline (Fig. 6b) on the variation of containment parameter with heavy-gas density ratio is shown in Fig. 37. Other flow parameters were  $\beta_j = 0$  to 45 deg and  $Re_{z,w} = 74,000$ . The containment parameters obtained with the porous tube are about 20 percent higher than with heavy-gas injection at the center of the nonaxial-flow end wall for a heavy-gas density ratio of 0.1, and approximately double for a heavy-gas density ratio of 0.6. Although the containment parameters were higher with a porous tube, additional testing was not pursued because the porous tube is not practical for the full-scale engine.

The effect of heavy-gas injection from a "showerhead" on the variation of containment parameter with heavy-gas density ratio is shown in Fig. 38. The "showerhead" consisted of 30 hypo tubes mounted at the center of the nonaxial-flow end wall (see Fig. 6c). Tests were made with and without thru-flow withdrawal at the center of the axial-flow end wall (radial Reynolds numbers of  $Re_r = 0, +50$  and  $+110$ ). Other flow parameters for these tests were  $\beta_j = 0$  to 63.5 deg and  $Re_{z,w} = 74,000$ . The variations of containment parameter with heavy-gas density ratio were not affected by these changes in radial Reynolds number. The containment parameter obtained with the "showerhead" at heavy-gas density ratios of 0.2 were approximately the same as were obtained with injection at the center of the nonaxial-flow end wall; however, an increase in the containment parameters was obtained for heavy-gas density ratios above about 0.5.

To further decrease the average heavy-gas axial velocity at injection, a 6-in.-dia screen was mounted on the nonaxial-flow end wall (Fig. 6d). Containment parameters were obtained for this heavy-gas injection configuration with  $\beta_j = 0$  to 63.5 deg, with  $Re_{z,w} = 74,000$ , and with and without thru-flow withdrawal at the center of the nonaxial-flow end wall (radial Reynolds numbers of  $Re_r = 0, +74$ , and  $+110$ ). The variation of containment parameter with heavy-gas density ratio (Fig. 39) was again independent of radial Reynolds number. The containment parameters are 30 to 40 percent lower than those obtained with heavy-gas injection through the center of the nonaxial-flow end wall for heavy-gas density ratios of 0.15 but are slightly higher for heavy-gas density ratios above 0.5.

### Effect of Heavy-Gas Injection with Swirl

Heavy gas was injected with swirl through 16 wall jets mounted on the nonaxial-flow end wall (Fig. 6e). Other flow parameters for this test were  $\beta_j = 0$  deg,  $Re_{z,w} = 74,000$  and radial Reynolds numbers of  $+67$  and  $+100$ . The variation of containment parameter with heavy-gas density ratio (Fig. 40) shows that containment parameters of approximately 4 to 5 were obtained for density ratios as high as 0.4.

These containment parameters, which appear to be independent of heavy-gas density ratio, are 2 to 3 times as high as the containment parameters obtained for  $\beta_j = 0$  with heavy-gas injection at the center of the nonaxial-flow end wall (the curve from Fig. 31a is shown for reference). The ratio of the heavy-gas weight flow through the axial-flow annulus to the total heavy-gas weight flow through the vortex is shown in Fig. 41 as a function of heavy-gas density ratio for the configuration of Fig. 40. A large fraction of the heavy gas was exhausted at the center of the axial-flow end wall for tests with relatively low heavy-gas density ratios.

Additional tests were performed using a mixture of nitrogen and iodine as the heavy gas rather than the mixture of FC-77 and iodine used for all other tests reported herein. For the configuration of Fig. 40, essentially all of the heavy gas was exhausted from the vortex at the center of the axial-flow end wall. The heavy-gas density ratios obtained were less than 0.05 but the heavy-gas volume fraction of the vortex tube was approximately the same as for the tests with FC-77. A limited number of containment parameters were measured for  $\beta_j = 0$  to 45 deg with the nitrogen and iodine injected with swirl. Comparison of the data for peripheral-wall injection configurations  $\beta_j = 0$  and  $\beta_j = 0$  to 45 showed that approximately the same containment parameters were obtained for both peripheral-wall injection configurations. This was probably because higher thru-flow rates have to be withdrawn to stabilize the vortex flow with  $\beta_j > 0$ . The conclusion was that the heavy-gas injection configuration has to be compatible with the flow conditions existing due to the peripheral-wall injection configuration and thru-flow withdrawal in order to obtain increased or optimum heavy-gas time constants.

Containment tests were made with heavy-gas injection through 15 1/8-in.-dia hypo tubes mounted at  $z = 1.5$  in. and  $r = 4.5$  in. along the peripheral wall. The ends of the hypo tubes were bent to 60-deg angles with the local tangent (Fig. 6f). Other flow parameters for these tests were  $\beta_j = 0$  deg,  $Re_{z,w} = 40,000$ , and radial Reynolds numbers of  $Re_r = 0, +59$ , and  $+104$ . The variation of containment parameter with heavy-gas density ratio (Fig. 42) showed essentially no effect of radial Reynolds number on the containment parameter. The containment parameters increased slightly with increasing heavy-gas density ratio. The concentrations of heavy gas in the axial-flow annulus and in the thru-flow duct at the center of the axial-flow end wall were approximately equal; thus, the flow was almost fully mixed near the axial-flow end wall.

#### Effect of Light-Gas Injection with Swirl from the End Walls

Light gas was injected with swirl from the axial-flow end wall or both end walls in an attempt to induce a rotating flow with moderate angular momentum and low average axial velocities in the central region of the vortex. Photographs of the end walls used for these tests are presented in Fig. 7 along with details of the injection configuration. Heavy gas was also injected from the nonaxial-flow end wall with swirl (Fig. 6g) and without swirl (Fig. 6h). Other flow parameters

for these tests were  $\beta_j = 0$  to 45 deg,  $Re_{z,w} \approx 40,000$  and  $V_{\phi,j} \approx 150$  ft/sec. Data were obtained for approximately 10 combinations of light-gas injection flow rates and heavy-gas injection configurations. Data for three combinations which illustrate the principal effects are presented in Figs. 43 and 44. A comparison of the containment parameters for tests with light-gas injection with swirl at both end walls and at only the axial-flow end wall are shown in Fig. 43 for heavy-gas injection with swirl from the nonaxial-flow end wall. The light-gas injection velocities at the end walls were 227 ft/sec at the axial-flow end wall and 173 ft/sec at the nonaxial-flow end wall, compared with 150 ft/sec for the tangential injection velocity,  $V_\phi$ . The purpose of high end-wall velocities is to promote a secondary flow outward along the end walls. Analysis and experiments in a basic vortex tube for this secondary-flow control method are reported in Ref. 11.

The variation of containment parameter with heavy-gas density ratio shows that containment parameters of approximately 4 to 5 were obtained for light-gas injection from the axial-flow end wall only (Fig. 43). Lower heavy-gas containment parameters were obtained for light-gas injection from both end walls. The decrease in containment parameter with injection from the nonaxial-flow end wall was probably due to entrainment of the heavy gas by the swirling light gas. The curve for heavy-gas injection at the center of the nonaxial-flow end wall (from Fig. 31a) is also shown for comparison. The containment parameters obtained for light-gas injection from only the axial-flow end wall were approximately 30 percent higher than for heavy-gas injection from the center of the nonaxial-flow end wall.

A comparison of containment parameters for heavy-gas injection from the nonaxial-flow end wall with swirl and without swirl is shown in Fig. 44 for light-gas injection with swirl from only the axial-flow end wall. The containment results for heavy-gas injection with swirl from the nonaxial-flow end wall are approximately 20 to 30 percent higher for heavy-gas density ratios from 0.3 to 0.7 compared with the containment results for heavy-gas injection without swirl through twelve 0.5-in.-dia ducts (see Fig. 6h). The results for injection without swirl through the twelve 0.5-in.-dia ducts are approximately equal to those obtained for heavy-gas injection through a duct at the center of the nonaxial-flow end wall. Since injection from the twelve 0.5-in.-dia ducts provides about the same results as injection from the center of the nonaxial-flow end wall, it was concluded that there was no net effect of light-gas injection from the axial-flow end wall for this peripheral-wall injection configuration.

## SUMMARY OF PRINCIPAL RESULTS

A large number of geometries and flow conditions are in the preceding sections. Since many of the tests were exploratory, some of the test results are less significant than others. In this section, the principal results are outlined without detail but with reference to particular figures. Further discussion of a particular test or result can be obtained from the preceding sections.

### Flow Visualization Tests

Flow visualization tests were performed with fluid (simulated-fuel) injected from ducts at the centers of both end walls (radial-outflow vortexes) or with fluid withdrawn through these ducts (radial-inflow vortexes). Tests were made with peripheral-wall injection configurations in which the axial component of the injection velocity was zero ( $\beta_j = 0$ ), equal to the tangential component of the injection velocity ( $\beta_j = 45$  deg), and proportional to the distance from the nonaxial-flow end wall ( $\beta_j = 0$  to 45 deg). The principal results of these tests are:

1. Large-scale mixing occurred between the central region and the peripheral-wall region for all peripheral-wall configurations with radial-outflow vortexes (Figs. 10 to 12).
2. Approximately 2 percent of the flow had to be withdrawn from the center of the end walls to obtain laminar flow in the central region for  $\beta_j = 0$  (Fig. 13). Approximately 4 percent had to be withdrawn to obtain laminar flow in the central region for  $\beta_j = 45$  deg and  $\beta_j = 0$  to 45 deg (Figs. 14 and 15).
3. The region near the peripheral wall was turbulent for all peripheral-wall configurations and flow conditions tested (Figs. 10 to 15).

### Velocity Measurements

Pitot-probe measurements were made with peripheral-wall injection configurations of  $\beta_j = 0, 0$  to 45, 0 to 63.5, 26.5, 45 and 63.5 deg. Flow was injected or withdrawn through ducts at the centers of both end walls. The principal results of these measurements are:

1. Measurements in radial-outflow vortexes indicated that the average axial velocities in the central region were substantially decreased for some peripheral-wall injection configurations (Figs. 17 and 20). Therefore, the volume of the vortex

potentially available for simulated-fuel containment was increased.

2. The axial velocity profiles were similar at different axial stations for  $\beta_j = 0, 0$  to  $45$ , and  $0$  to  $63.5$  deg (Fig. 22) and the reduced axial velocity profiles,  $V_z/z$ , were essentially independent of axial location for these peripheral-wall injection configurations. Also, the tangential velocity profiles did not change appreciably with axial location.
3. The axial and tangential velocity profiles for  $\beta_j = 26.5, 45$  and  $63.5$  deg varied with axial location and thus were not similar (Figs. 19 to 21).
4. For a given peripheral-wall configuration, axial velocity profiles were not appreciably altered by (a) changing from radial-outflow to radial-inflow vortexes (Figs. 28 and 29), or (b) changing the inner radius of the axial-flow exhaust annulus (Fig. 30) for  $\beta_j = 0$  to  $63.5$  deg.

#### Heavy-Gas Containment Tests

The average time the heavy gas remained in the vortex tube (dwell time or time constant) was measured using air as the simulated propellant and a heavy gas (a fluorocarbon, FC-77) as the simulated fuel. Dwell times were measured for peripheral-wall configurations of  $\beta_j = 0, 45, 90, 0$  to  $45$  and  $0$  to  $63.5$  deg with ten heavy-gas injection configurations. The results were expressed in terms of the containment parameter  $\tau_{F_1}/\tau_{F_1,MIN}$  (the ratio of the average dwell time of the heavy gas to the average dwell time of the light gas) and the heavy-gas density ratio  $\bar{\rho}_{F_1}/\rho_{P_1}$  (the ratio of the weight of heavy gas stored divided by the total volume of the vortex tube to the density of the light gas at injection). Most of the tests were performed at an axial-flow Reynolds number of  $Re_{z,w} = 74,000$  and with heavy-gas injection from a duct at the center of the nonaxial-flow end wall (radial outflow). The values of the simulated-fuel containment and flow parameters required for a practical full-scale engine are  $\tau_{F_1}/\tau_{F_1,MIN} = 150$ ,  $\rho_{F_1}/\rho_{P_1} = 10$ , and  $Re_{z,w} = 500,000$  (Ref. 9). The principal results of these tests are:

1. The containment parameters obtained with an axial component of peripheral-wall injection velocity ( $\beta_j > 0$ ) were higher than those obtained with zero axial component ( $\beta_j = 0$ ). Maximum containment parameters of approximately  $\tau_{F_1}/\tau_{F_1,MIN} = 7$  were obtained for  $\beta_j = 45$  and  $0$  to  $63.5$  deg at heavy-gas density ratios between  $\rho_{F_1}/\rho_{P_1} = 0.1$  and  $0.2$ . This was approximately three-and-one-half times as large as the maximum containment

parameter obtained with  $\beta_j = 0$  at the same heavy-gas density ratios (Fig. 32).

2. For most peripheral-wall injection configurations tested, the containment parameter decreased to approximately 50 percent of the maximum value at heavy-gas density ratios of approximately  $\bar{\rho}_{F_1}/\rho_{P_1} = 0.7$ . However, for  $\beta_j = 90$  deg, the containment parameter did not vary with density ratio (Fig. 32).
3. No significant improvements in the containment parameter were obtained with changes (a) in the axial-flow Reynolds number (Fig. 36), (b) in the amount of flow withdrawn at the center of the axial-flow end wall (Fig. 34), and (c) in the orientation of the axis of the vortex tube from horizontal to vertical (Fig. 32).
4. No significant improvements in the containment parameter were obtained (a) with heavy-gas injection through a 6-in.-dia screen and a "showerhead" at the center of the nonaxial-flow end wall (Figs. 38 and 39), and (b) with light-gas injection with swirl from the axial-flow end wall or from both end walls (Figs. 43 and 44).
5. The best combination of simulated-propellant and simulated-fuel injection methods provided containment parameters that are between one and two orders of magnitude lower than are required for a practical full-scale engine (Fig. 32 and Ref. 9).

#### Concluding Remarks

The velocity measurements indicate that the time-averaged axial velocities in the central region of the vortex could be substantially decreased for some flow conditions and peripheral-wall injection configurations. However, the flow visualization tests showed that turbulent mixing was also a dominant feature in vortices where low average axial velocities were obtained in the central region. In fact, the turbulence and large-scale eddies appeared to increase for tests with  $\beta_j > 0$ . Theoretical studies of rotating flows also indicate that axial shear will decrease the stability of laminar flows to small disturbances (Ref. 14) and will decrease the damping of turbulent fluctuations (Ref. 13). Concurrent experimental studies (Ref. 7) indicated that increasing the axial flow, and hence the shear, will cause turbulence or instabilities in an established laminar rotating flow.

Results from the heavy-gas containment tests indicate a moderate increase in containment parameter could be obtained for peripheral-wall injection configurations with  $\beta_j > 0$ . However, the increase in heavy gas stored due to decreased axial convection was probably offset somewhat by the increased turbulent diffusion and radial

convection. The increased containment parameters obtained in this investigation were not obtained in the investigation reported in Ref. 8 in which containment measurements were made at Reynolds numbers up to the value required for a full-scale engine ( $Re_{z,w} = 480,000$ ). In conclusion, the containment parameters obtained from the present tests and the containment parameters obtained from the present tests and the tests of Ref. 8 are more than one order of magnitude less than the value now estimated to be required for economical operation of a full-scale, open-cycle gaseous-core nuclear rocket.

## REFERENCES

1. McLafferty, G. H.: Analytical Study of the Performance Characteristics of Vortex-Stabilized Gaseous Nuclear Rocket Engines. United Aircraft Research Laboratories Report D-910091-20, prepared under Contract NASw-847, September 1965. To be issued as NASA Contractor report.
2. Travers, A.: Experimental Investigation of Peripheral-Wall Injection Techniques in a Water Vortex Tube. United Aircraft Research Laboratories Report D-910091-7, prepared under Contract NASw-847, September 1965. To be issued as NASA Contractor report.
3. Travers, A. and B. V. Johnson: Measurements of Flow Characteristics in an Axial-Flow Vortex Tube. United Aircraft Research Laboratories Report C-910091-3, prepared under Contract NASw-847, September 1964. Also issued as NASA CR-277.
4. Mensing, A. E. and J. S. Kendall: Experimental Investigation of Containment of a Heavy Gas in a Jet-Driven Light-Gas Vortex. United Aircraft Research Laboratories Report D-910091-4, prepared under Contract NASw-847, March 1965. To be issued as NASA Contractor report.
5. Mensing, A. E. and J. S. Kendall: Experimental Investigation of the Effect of Heavy-to-Light-Gas Density Ratio on Two-Component Vortex Tube Containment Characteristics. United Aircraft Research Laboratories Report D-910091-9, prepared under Contract NASw-847, September 1965. To be issued as NASA Contractor report.
6. Kendall, J. S. and A. E. Mensing: Experimental Investigation of the Effect of Heavy-to-Light-Gas Density Ratio on Vortex Containment Characteristics. United Aircraft Research Laboratories Report UAR-E54, prepared under Contract NASw-847, April 1966. Paper presented at AIAA Second Propulsion Joint Specialists Conference, Colorado Springs, Colo., June 13-17, 1966.
7. Travers, A.: Experimental Investigation of Flow Patterns in Radial-Outflow Vortexes Using a Rotating-Peripheral-Wall Water Vortex Tube. United Aircraft Research Laboratories Report F-910091-10, prepared under Contract NASw-847, May 1967. To be issued as NASA Contractor report.
8. Kendall, J. S., A. E. Mensing and B. V. Johnson: Containment Experiments in Vortex Tubes with Radial Outflow and Large Superimposed Axial Flows. United Aircraft Research Laboratories Report F-910091-12, prepared under Contract NASw-847, May 1967. To be issued as NASA Contractor report.

## REFERENCES (Cont'd)

9. Clark, J. W., B. V. Johnson, J. S. Kendall, A. E. Mensing, and A. Travers: Summary of Gaseous Nuclear Rocket Fluid Mechanics Research Conducted under Contract NASw-847. United Aircraft Research Laboratories Report F-910091-13, prepared under Contract NASw-847, May 1967. To be issued as NASA Contractor report.
10. Johnson, B. V., A. Travers, and R. W. Hale: Measurements of Flow Patterns in a Jet-Driven Vortex. Air Force Systems Command Report RTD-TDR-63-1094, prepared by United Aircraft Research Laboratories under Contract AF 04(611)-8189, November 1963.
11. Johnson, B. V. and A. Travers: Analytical and Experimental Investigation of Flow Control in a Vortex Tube by End-Wall Suction and Injection. United Aircraft Research Laboratories Report D-910091-8, prepared under Contract NASw-847, September 1965. To be issued as NASA Contractor report.
12. Mensing, A. E. and J. S. Kendall: Experimental Investigation of Containment of Gaseous Iodine in a Jet-Driven Vortex. Air Force Systems Command Report RTD-TDR-63-1093, prepared by United Aircraft Research Laboratories under Contract AF 04(611)8189, November 1963.
13. Kao, S. K.: Turbulence Criteria for a Circumpolar Vortex in a Rotating Gravity Field. The Physics of Fluids, Vol. 7, No. 3, May 1964.
14. Kurzweg, U. H.: Criteria for the Stability of Heterogeneous Swirling Flows. United Aircraft Research Laboratories Report UAR-F96, May 1967.
15. Johnson, B. V.: Analytical Study of Propellant Flow Requirements for Reducing Heat Transfer to the End Walls of Vortex Stabilized Gaseous Nuclear Rocket Engines. United Aircraft Research Laboratories Report D-910091-6, prepared under Contract NASw-847, September 1965. To be issued as NASA Contractor report.

LIST OF SYMBOLS

$A_f$	Heavy-gas injection area, $\text{ft}^2$ or $\text{in.}^2$
$A_j$	Peripheral-wall simulated-propellant injection area, $\text{ft}^2$ or $\text{in.}^2$
$L$	Length of vortex tube, ft or in.
$p$	Local pressure, $\text{lb}/\text{ft}^2$
$P_F$	Pressure of heavy gas or simulated fuel at injection, psia
$P_P$	Pressure of light gas or simulated propellant at injection, psia
$P_{ref}$	Pressure at $r = 4.75$ in. on nonaxial-flow end wall, $\text{lb}/\text{ft}^2$
$r$	Local radius from centerline of vortex tube, ft or in.
$r_1$	Radius of vortex tube and outer radius of axial-flow exhaust annulus (see Fig. 5), ft or in.
$r_3$	Inner radius of axial-flow exhaust annulus (see Fig. 5), ft or in.
$Re_r$	Radial Reynolds number, indicates thru-flow rate injected (negative) or withdrawn (positive) through ducts at the centers of both end walls for flow visualization tests and velocity measurements; indicates thru-flow rate withdrawn (positive), if any, through ducts at center of axial-flow end wall for heavy-gas containment tests, $W_t / 2 \pi \mu_{P_1} L$ , dimensionless
$Re_{t,j}$	Tangential injection Reynolds number based on peripheral-wall simulated-propellant tangential injection velocity, $V_{\phi,j} r_1 \rho_{P_1} / \mu_{P_1}$ , dimensionless
$Re_{z,w}$	Equivalent axial-flow Reynolds number based on average velocity at an exhaust annulus extending from $r/r_1 = 0.75$ to $r/r_1 = 1.0$ , $W_p / (7/16) \pi r_1 \mu_{P_1}$ , dimensionless
$T_F$	Temperature of heavy gas or simulated fuel at injection, deg F
$T_P$	Temperature of light gas or simulated propellant at injection, deg F
$t_F$	Average dwell time of heavy gas in vortex, $\gamma_F / W_F$ , sec

LIST OF SYMBOLS (Cont'd)

$t_{FMIN}$	Average dwell time of light gas in vortex, $\sqrt{V \rho_p} / W_p$ , sec
$V$	Volume of vortex tube, $V = \pi r_1^2 L$ , ft <sup>3</sup>
$V_j$	Local simulated-propellant peripheral-wall injection velocity, ft/sec
$\bar{V}_j$	Average simulated-propellant peripheral-wall injection velocity, $W_p / (\rho_p A_j)$ , ft/sec
$V_z$	Local axial velocity, ft/sec
$V_{z,j}$	Local axial component of peripheral-wall injection velocity, $V_{z,j} = V_j \sin \beta_j$ , ft/sec
$\bar{V}_z$	Average axial velocity across $r-\phi$ plane of vortex tube at local axial station, ft/sec
$\bar{V}_{z,w}$	Average axial velocity that the simulated propellant would have if exhausted through an annulus extending from $r/r_1 = 0.75$ to $r/r = 1.0$ , $W_p / (7/16) \pi r_1^2 \mu_p$ , ft/sec
$V_\phi$	Local tangential velocity, ft/sec
$V_{\phi,j}$	Local tangential component of peripheral-wall injection velocity, $V_j \cos \beta_j$ , ft/sec
$\bar{V}_{\phi,j}$	Average tangential component of peripheral-wall injection velocity, ft/sec
$V_{\phi,jAF}$	Tangential injection velocity of light gas injected from axial-flow end wall with swirl, ft/sec
$V_{\phi,jNF}$	Tangential injection velocity of light gas injected from nonaxial-flow end wall with swirl, ft/sec
$W_F$	Total weight flow rate of heavy gas or simulated fuel, lb/sec
$W_{FAX}$	Weight flow rate of heavy gas or simulated propellant withdrawn through axial-flow exhaust annulus, lb/sec
$W_p$	Total weight flow rate of light gas or simulated propellant, lb/sec

LIST OF SYMBOLS (Cont'd)

$W_t$	Weight flow rate injected or withdrawn through ducts at both end walls for flow visualization tests and velocity measurements; weight flow rate withdrawn through duct at center of axial-flow end wall for heavy-gas containment tests, lb/sec
$W_F$	Total heavy gas or simulated fuel stored in vortex tube, lb
$W_P$	Total light gas or simulated propellant stored in vortex tube, lb
$z$	Axial location measured from nonaxial-flow end wall, ft or in.
$\beta_j$	Angle between $\beta_j$ plane and centerline of peripheral-wall simulated-propellant injection jet (see sketch in Table I), $\beta_j = \tan^{-1}(V_{z,j}/V_{\phi,j})$ deg
$(\beta_j)_{MAX}$	Maximum value of peripheral-wall simulated-propellant injection angle, deg
$\beta_P$	Angle between $r-\phi$ plane and centerline of velocity probe, (see Fig. 9), deg
$\mu_{P_1}$	Dynamic viscosity of light gas or simulated propellant at injection, lb/(sec-ft)
$\rho_{F_1}$	Heavy-gas or simulated-fuel density at injection, lb/ft <sup>3</sup>
$\bar{\rho}_{F_1}$	Volume-averaged density of heavy gas stored in vortex tube, $\bar{\rho}_{F_1} = W_F / \pi r_1^2 L$ , lb/ft <sup>3</sup>
$\rho_{P_1}$	Light-gas or simulated-propellant density at injection, lb/ft <sup>3</sup>
$\tau_{F_1}$	Dimensionless average time constant for heavy gas or simulated fuel $\tau_{F_1} = t_F / (\rho_{P_1} r_1^2 / \mu_{P_1})$
$\tau_{F_{1MIN}}$	Dimensionless average time constant for light gas or propellant, $\tau_{F_{1MIN}} = t_{F_{1MIN}} / (\rho_{P_1} r_1^2 / \mu_{P_1})$
$\phi$	Azimuthal angle, deg or radians

## APPENDIX

### RELATIONS BETWEEN DIMENSIONLESS AND DIMENSIONAL VORTEX FLOW CONTAINMENT PARAMETERS

All data described in the present report were obtained using a vortex tube having the following geometry:

$$\begin{aligned} \text{radius, } r_1 &= 0.416 \text{ ft} \\ \text{length, } L &= 2.5 \text{ ft} \\ \text{volume, } V &= 1.36 \text{ ft}^3 \end{aligned}$$

The approximate properties of the simulated-propellant and simulated-fuel gases at injection into the vortex tube were as follows:

<u>Property</u>	<u>Simulated Propellant</u>	<u>Simulated Fuel</u>
Gas	Air	Fluorocarbon, FC-77
Temperature	$T_{P_1} = 260 \text{ F}$	$T_{F_1} = 300 \text{ F}$
Pressure	$P_{P_1} = 10 \text{ psia}$	$P_{F_1} = 10 \text{ psia}$
Density	$\rho_{P_1} = 0.038 \text{ lb/ft}^3$	$\rho_{F_1} = 0.49 \text{ lb/ft}^3$
Viscosity	$\mu_{P_1} = 1.536 \times 10^{-5} \text{ lb/ft-sec}$	

To compare with engine performance studies and with previous and concurrent heavy-gas containment results, the results for a given test are presented in terms of three nondimensional parameters. These parameters, with typical values from test data, are presented in the following sample calculations:

$$\begin{aligned} \text{Heavy-gas density ratio, } \bar{\rho}_{F_1}/\rho_{P_1} &= 0.2 \\ \text{Containment parameter, } \tau_{F_1}/\tau_{F_1 \text{ MIN}} &= 8.0 \\ \text{Axial-flow Reynolds number, } Re_{z,w} &= 74,000 \end{aligned}$$

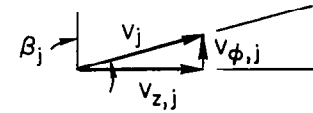
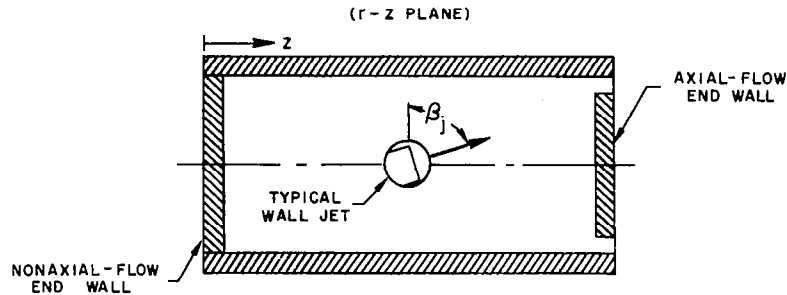
These dimensionless parameters are converted to dimensional parameters in the following table.

Symbol	Parameter	Equation for Conversion	Sample Calculation
$\mathcal{V}_P$	Light gas stored	$\approx V \rho_{P_1}$	$(1.36)(0.038) = 0.052 \text{ lb}$
$\mathcal{V}_F$	Heavy gas stored	$(\bar{\rho}_{F_1} / \rho_{P_1}) V \rho_{P_1}$	$(0.2)(1.36)(0.038) = 0.0104 \text{ lb}$
$W_P$	Light-gas flow rate	$Re_{z,w} \left[ (7/16) \pi r_1 \mu_{P_1} \right]$	$(74,000) \left[ (7/16) \pi (0.416) (1.536 \times 10^{-5}) \right] = 0.65 \text{ lb/sec}$
$W_F$	Heavy-gas flow rate	$\left[ (\bar{\rho}_{F_1} / \rho_{P_1}) / (\tau_{F_1} / \tau_{F_1 \text{ MIN}}) \right] W_P$	$\frac{0.2}{8.0} (0.65) = 0.0164 \text{ lb/sec}$
$W_P / W_F$	Ratio of light-gas flow rate to heavy-gas flow rate	$(\tau_{F_1} / \tau_{F_1 \text{ MIN}}) / (\bar{\rho}_{F_1} / \rho_{P_1})$	$\frac{8.0}{0.2} = 40$
$\mathcal{V}_F / \mathcal{V}_P$	Ratio of heavy gas stored to light gas stored	$\approx \bar{\rho}_{F_1} / \rho_{P_1}$	$\approx 0.2$
$t_{F \text{ MIN}}$	Approximate dwell time of simulated propellant	$V \rho_{P_1} / W_P$	$(1.36)(0.038) / 0.65 = 0.080 \text{ sec}$
$t_F$	Dwell time of simulated fuel	$(\tau_{F_1} / \tau_{F_1 \text{ MIN}}) t_{F \text{ MIN}}$	$(8)(0.080) = 0.64 \text{ sec}$

TABLE I

## SUMMARY OF PERIPHERAL - WALL SIMULATED - PROPELLANT INJECTION CONFIGURATIONS INVESTIGATED

600 DIRECTED WALL JETS; SLOT WIDTH = 0.300 IN.



$V_{\phi,j}$  INDEPENDENT OF AXIAL STATION UNLESS OTHERWISE NOTED

36

DESIGNATION	DISTRIBUTION OF AXIAL COMPONENT OF INJECTION VELOCITY	APPROXIMATE INJECTION AREA, $A_j$ , SQ IN.	$\bar{V}_{z,w} / V_{\phi,j}$	DESCRIPTION OF INJECTION CONFIGURATION
a) $\beta_j = 0$ DEG	$V_{z,j} = 0$	10.8	0.314	SLOT HEIGHT = 0.060 IN.; $\beta_j = 0$ DEG
b) $\beta_j = 0$ TO 45 DEG	$V_{z,j} = V_{\phi,j}(z/L)$	9.7	0.314	SLOT HEIGHT $\approx L/16.7 \sqrt{z^2 + L^2}$ IN.; $\beta_j = \tan^{-1} z/L$
c) $\beta_j = 0$ TO 63.5 DEG	$V_{z,j} = V_{\phi,j}(2z/L)$	7.9	0.314	SLOT HEIGHT $\approx L/16.7 \sqrt{4z^2 + L^2}$ IN.; $\beta_j = \tan^{-1}(2z/L)$
d) $\beta_j = 26.5$ DEG	$V_{z,j} = 0.5V_{\phi,j}$	10.8	0.351	SLOT HEIGHT = 0.060 IN.; $\beta_j = 26.5$ DEG
e) $\beta_j = 45$ DEG	$V_{z,j} = V_{\phi,j}$	10.8	0.444	SLOT HEIGHT = 0.060 IN.; $\beta_j = 45$ DEG
f) $\beta_j = 63.5$ DEG	$V_{z,j} = 2V_{\phi,j}$	10.8	1.422	SLOT HEIGHT = 0.060 IN.; $\beta_j = 63.5$ DEG
g) $\beta_j = 90$ DEG	$V_{z,j} = V_j (V_{\phi,j} = 0)$	10.8	$\infty$	SLOT HEIGHT = 0.060 IN.; $\beta_j = 90$ DEG

TABLE II  
SUMMARY OF SIMULATED - FUEL INJECTION CONFIGURATIONS INVESTIGATED

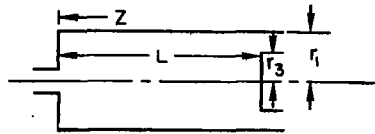
Configuration in Fig. 6	Nomenclature Used for Simulated-Fuel Injection Configuration	Approximate Injection Area $A_f$ , sq in.	Location of Injection	Description of Injection Configuration
a	Nonaxial-Flow End Wall	0.634	Center of Nonaxial-Flow End Wall	0.9-in.-dia duct
a	Axial-Flow End Wall	0.634	Center of Axial-Flow End Wall	0.9-in.-dia duct
a	Both End Walls	1.268	Centers of Both End Walls	0.9-in.-dia ducts
b	1.25-in.-dia Porous Tube	78.5	Centerline	1.0-in.-dia tube, covered with multiple layers of glass cloth to provide a uniform porosity from $z = 5$ in. to $z = 25$ in. Tube was located concentric with the vortex tube centerline
c	Showerhead	0.212	Center of Nonaxial-Flow End Wall	30 1/8-in.-dia hypo tubes (0.095 ID) in 2-1/4-in.-dia cluster projecting inward approximately 1.5 in. from wall
d	6-in.-dia Screen	25.3	Center of Nonaxial-Flow End Wall	6-in.-dia screen, open area of screen approximately 10 percent
e	Swirl through 16 0.030-in. Wall Jets	0.288	Nonaxial-Flow End Wall	16 wall jets on nonaxial-flow end wall, equally spaced at radii of 0.875 and 1.5 in.; slot height = 0.060 in., width = 0.300 in.; $\beta_j = 0$ deg, $\xi_f \approx 30$ deg inward with respect to local tangent
-	Swirl through 16 0.030-in. Wall Jets	0.144	Nonaxial-Flow End Wall	16 wall jets on nonaxial-flow end wall, equally spaced at radii of 0.875 and 1.5 in.; slot height = 0.030 in., width = 0.300 in.; $\beta_j = 0$ deg, $\xi_f \approx 30$ deg inward with respect to local tangent
f	Peripheral-Wall Tubes - 60 deg	0.151	Peripheral Wall, $z = 1.5$ in.	15 1/8-in.-dia hypo tubes equally spaced on peripheral wall at $z = 1.5$ in. and extending 1 in. into vortex tube; $\beta_j = 0$ deg, $\xi_f = 60$ deg
-	Peripheral-Wall Tubes - 90 deg	0.106	Peripheral Wall, $z = 1.5$ in.	15 1/8-in.-dia hypo tubes equally spaced on peripheral wall at $z = 1.5$ in. and extending 1 in. into vortex tube; $\beta_j = 0$ deg, $\xi_f = 90$ deg
g	Swirl through 12 Wall Jets	0.472	Nonaxial-Flow End Wall	4 wall jets, slot height = 0.060 in., slot width = 0.30 in., equally spaced at radius of 0.41 in.; 8 wall jets, slot height = 0.100 in.; slot width = 0.50 in., equally spaced at radius of 1.12 in.; $\xi_f = 30$ deg inward with respect to local tangent
h	12 0.5-in.-dia Ducts	2.35	Nonaxial-Flow End Wall	12 1/2-in.-dia ducts, 4 equally spaced at radius of 0.41 in., 8 equally spaced at radius of 1.12 in.

**TABLE III**  
**SUMMARY OF FLOW CONDITIONS INVESTIGATED**

VORTEX TUBE CONFIGURATION : L = 30 IN.

$r_1 = 5$  IN.

$r_3 = 4.5$  IN.  
(STANDARD)



See Table I for Descriptions of Peripheral-Wall Simulated-Propellant Injection Configurations  
See Table II and Fig. 6 for Descriptions of Simulated-Fuel Injection Configurations

Type of Tests	Fluids	Axial-Flow Reynolds Number, $Re_{z,w}$	Thru-Flow Radial Reynolds Number, $Re_r^*$	Simulated-Propellant Injection Configuration, $\beta_1$ - Deg	Simulated-Fuel (Water, Air or Heavy-Gas) Injection Configuration	Primary Variables	Figures for Photos or Data	Summary Figures	
Flow Visualization Tests	Water with Trace of Dye	53,000	-40 (Outflow)	0	Centers of Both End Walls Fig. 6a	Peripheral-Wall Injection Configuration	10		
				45			11		
				0 to 45			12		
				+40 (Inflow)			0		13
				45			14		
			+80	0 to 45	None; See Note at Right	Flow Withdrawn at Centers of Both End Walls, $Re_r$	15		
Axial and Tangential Velocity Measurements; Peripheral-Wall Pressure Measurements	Air	$\approx 108,000$	$\approx -103$	0	Centers of Both End Walls Fig. 6a	Peripheral-Wall Injection Configuration	16	22 to 27	
				0 to 45			17		
				0 to 63.5			18		
				26.5			19		
				45			20		
				63.5			21		
				-105, 0			0 to 45		28
				+24, +28			0 to 63.5		29
-103	0 to 63.5	30							
Heavy-gas Containment Tests	Air and FC-77 with Trace of Iodine	74,000	0*	0, 45, 90 0 to 45, 0 to 63.5	Centers of Nonaxial-Flow and Both End Walls Fig. 6a	Peripheral-Wall and Heavy-Gas Injection Configurations	31	32, 33	
				0, +51 +68, +23	0 to 63.5	Center of Nonaxial-Flow End Wall - Fig. 6a	Flow Withdrawn at Center of Axial-Flow End Wall		34
					0 to 63.5		Light-Gas Injection Rate with Axial Distance		35
		74,000 40,000	0	0, 45, 90		$Re_{z,w}$	36		
		74,000	0, +50, +110	0 to 45	1 1/4-in.-dia Porous Tube Fig. 6b	Heavy-Gas Injection Configuration	37		
				0 to 63.5	"Showerhead" Fig. 6c		38		
				0 to 63.5	6-in.-dia Screen Fig. 6d		39		
				0	Swirl through 16 Wall Jets Fig. 6e		40, 41		
				0	15 1/8-in.-dia Tubes from Peripheral Wall Fig. 6f		42		
		40,000	0	0 to 45	Swirl through 12 Wall Jets Fig. 6g	Light-Gas Injection from End Walls with Swirl	43		
					12 1/2-in.-dia Ducts Fig. 6h		44		

\*For heavy-gas containment tests,  $Re_r$  indicates rate of thru-flow withdrawal at center of axial-flow end wall, if any.

# SKETCH OF VORTEX TUBE ASSEMBLY

ASSEMBLY SHOWN WITH SIMULATED-FUEL INJECTION FROM DUCTS AT CENTERS OF BOTH END WALLS

SEE FIG. 6 FOR ADDITIONAL SIMULATED-FUEL INJECTION CONFIGURATIONS

SEE TABLE I AND FIGS. 3 AND 4 FOR DETAILS OF PERIPHERAL-WALL SIMULATED-PROPELLANT INJECTION CONFIGURATIONS

69

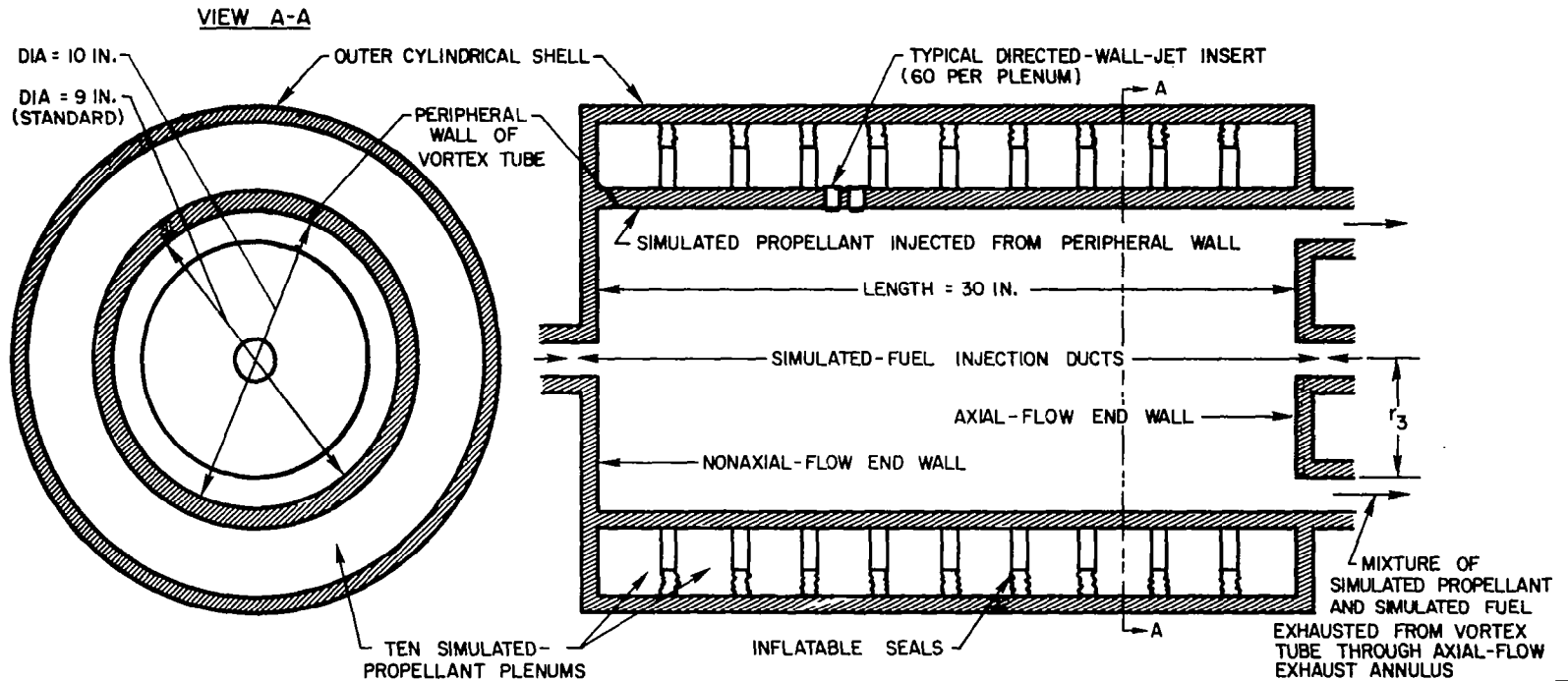
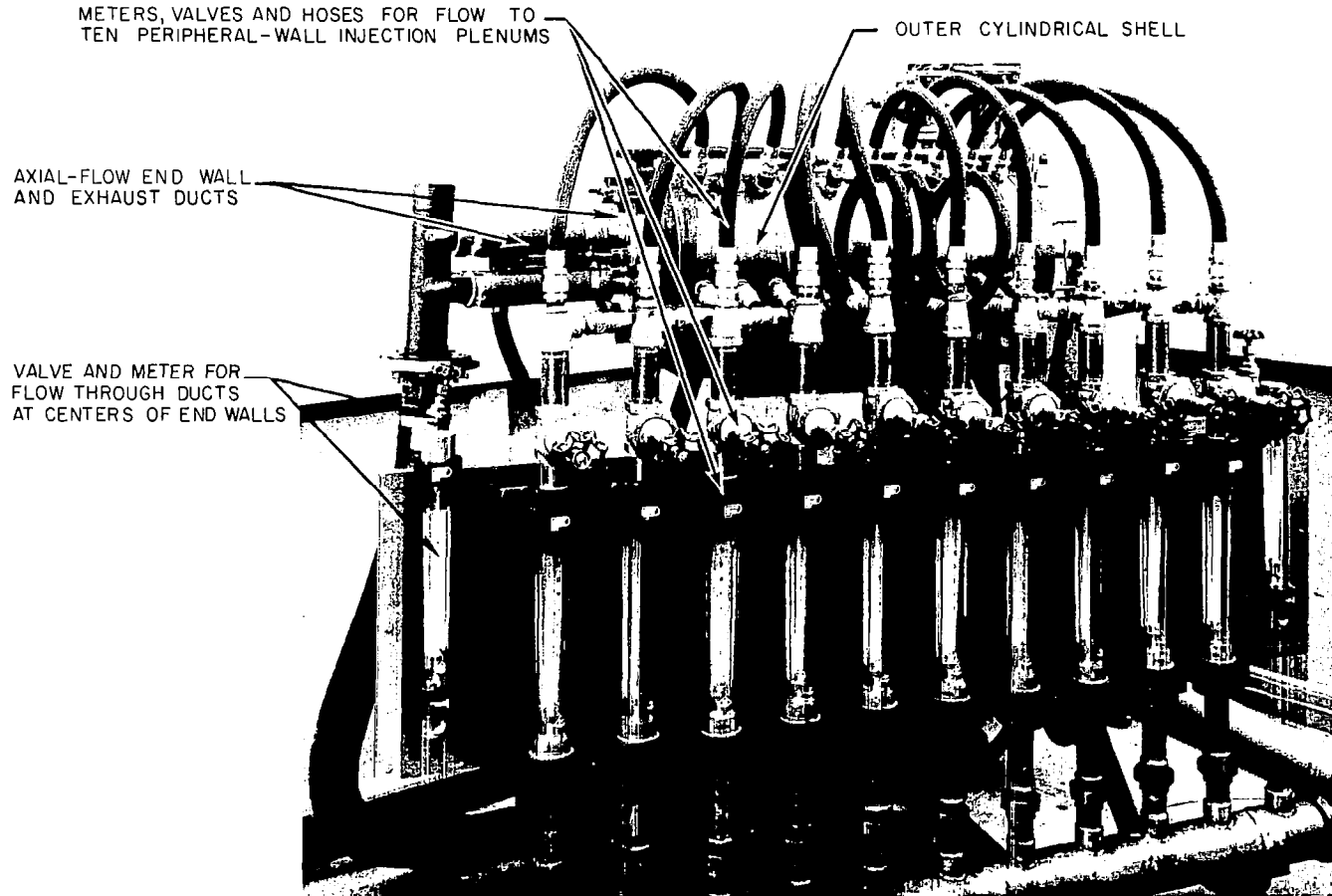


FIG. 1

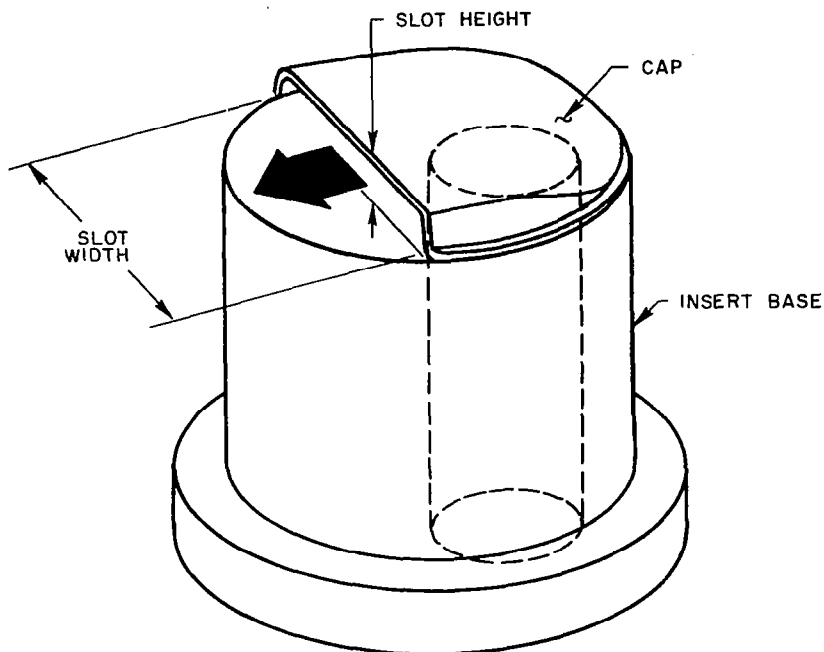
# PHOTOGRAPH OF VORTEX TEST APPARATUS USED FOR VELOCITY MEASUREMENTS AND HEAVY-GAS CONTAINMENT TESTS

APPARATUS SHOWN ASSEMBLED FOR VELOCITY MEASUREMENT TESTS

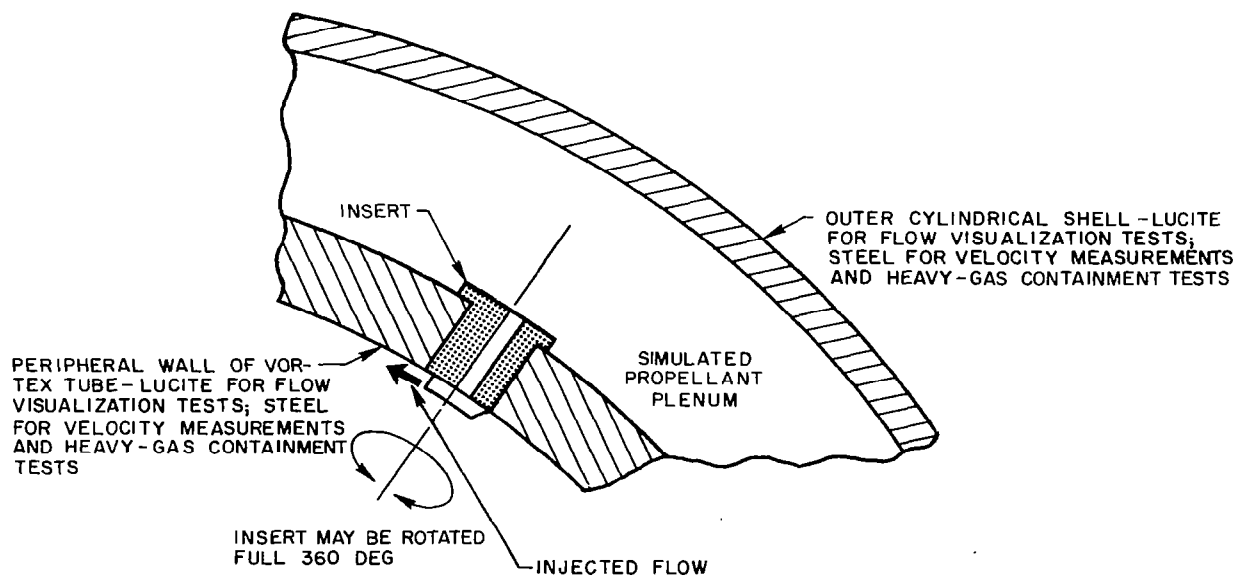


SKETCHES OF DIRECTED-WALL-JET INSERT AND PERIPHERAL-WALL SIMULATED-PROPELLANT INJECTION SYSTEM

a) DETAILS OF INSERT



b) INSERT INSTALLATION

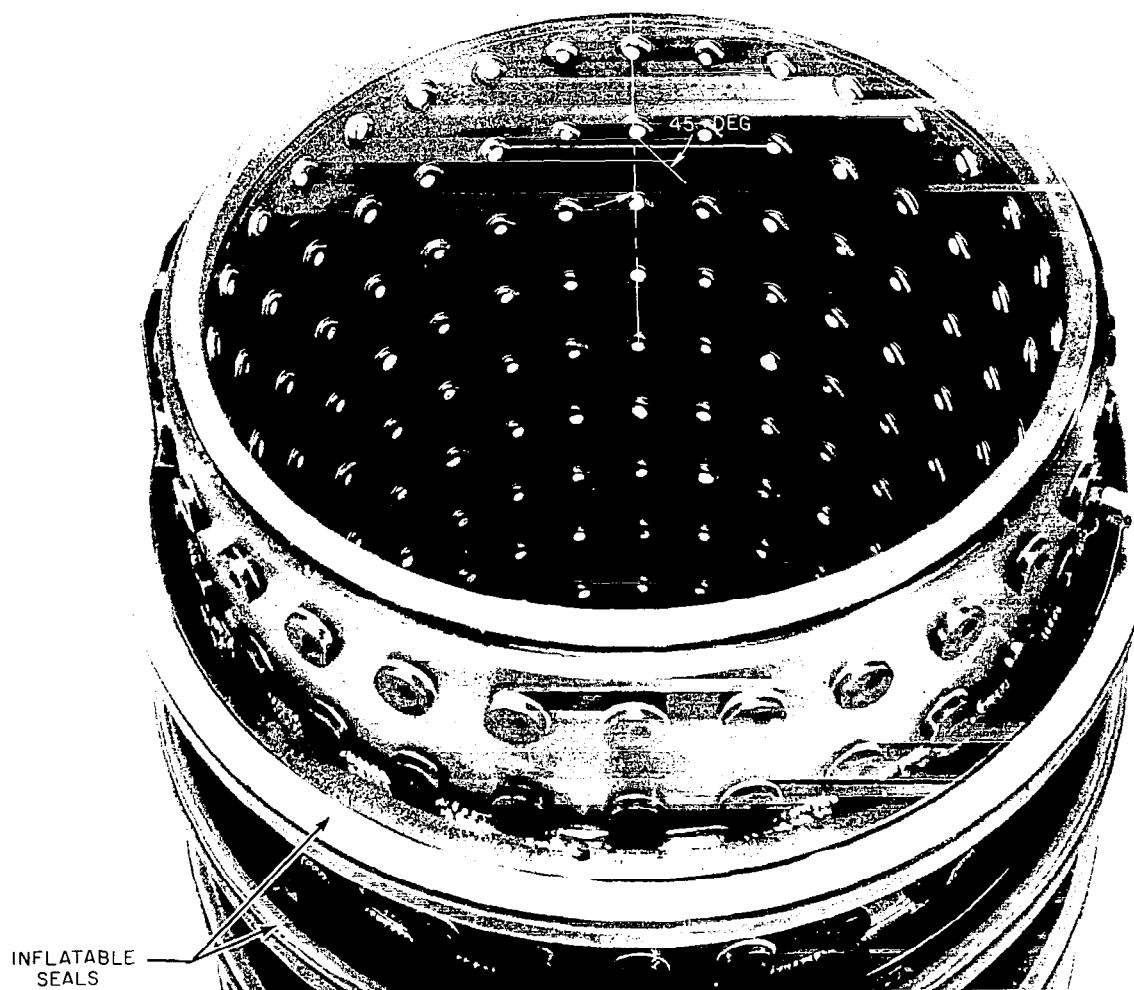


# PHOTOGRAPH OF VORTEX TUBE USED FOR VELOCITY MEASUREMENTS AND HEAVY-GAS CONTAINMENT TESTS

VIEW FROM NONAXIAL-FLOW END

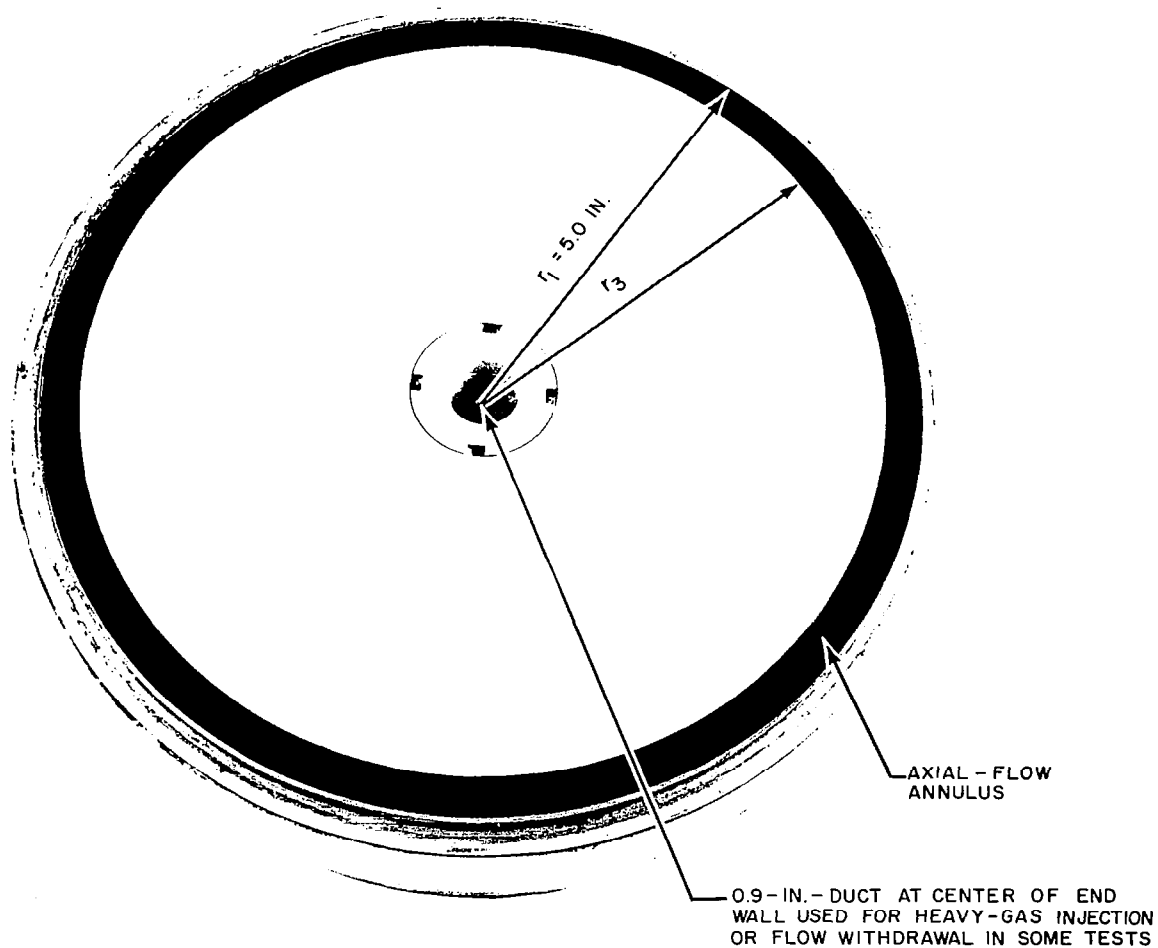
INJECTION CONFIGURATION SHOWN,  $\beta_j = 45 \text{ DEG}$ ,  $V_{z,j} = V_{\phi,j}$

GEOMETRICALLY SIMILAR LUCITE VORTEX TUBE USED FOR FLOW VISUALIZATION TESTS



## PHOTOGRAPH OF AXIAL-FLOW END WALL USED FOR VELOCITY MEASUREMENTS AND HEAVY-GAS CONTAINMENT TESTS

- NOTES: (1)  $r_3 = 4.5$  IN. FOR MOST VELOCITY MEASUREMENTS; HOWEVER, ONE SERIES OF MEASUREMENTS WAS MADE FOR  $r_3 = 4.75, 4.50, 4.00, 3.50$  AND  $3.00$  IN.
- (2)  $r_3 = 4.5$  IN. FOR ALL HEAVY-GAS CONTAINMENT TESTS
- (3)  $r_3 = 4.5$  IN. FOR ALL FLOW VISUALIZATION TESTS (GEOMETRICALLY SIMILAR LUCITE END WALL WAS USED WITH A LUCITE VORTEX TUBE)

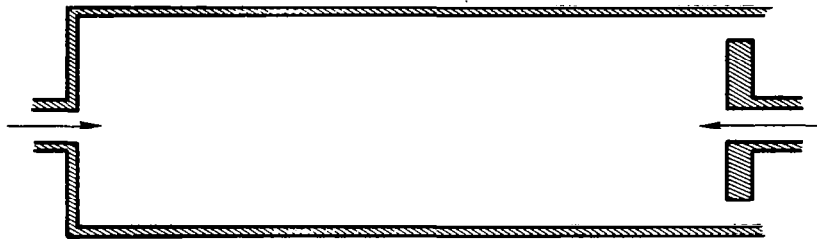


# SKETCHES OF HEAVY-GAS INJECTION CONFIGURATIONS INVESTIGATED FIG. 6a-d

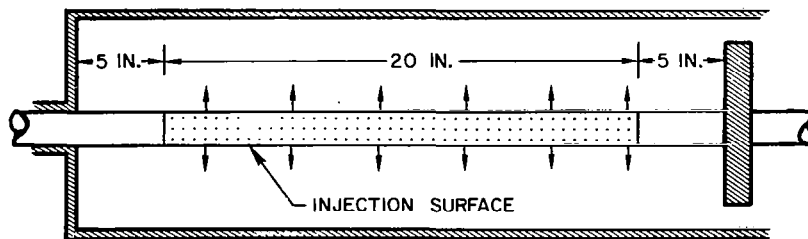
NOTES: (1) FOR SOME HEAVY-GAS CONTAINMENT TESTS, FLOW WAS WITHDRAWN THROUGH A 0.9-IN.-DIA DUCT AT CENTER OF AXIAL-FLOW END WALL.

(2) FOR RADIAL-INFLOW FLOW VISUALIZATION TESTS AND VELOCITY MEASUREMENTS, FLOW WAS WITHDRAWN THROUGH BOTH DUCTS OF CONFIGURATION a).

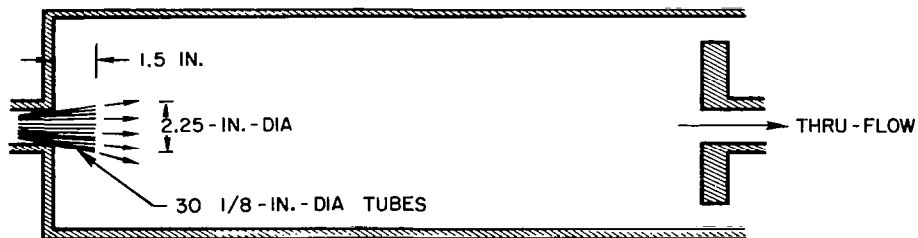
a) INJECTION FROM 0.9-IN.-DIA DUCTS AT CENTERS OF NONAXIAL-FLOW AND/OR AXIAL-FLOW END WALLS



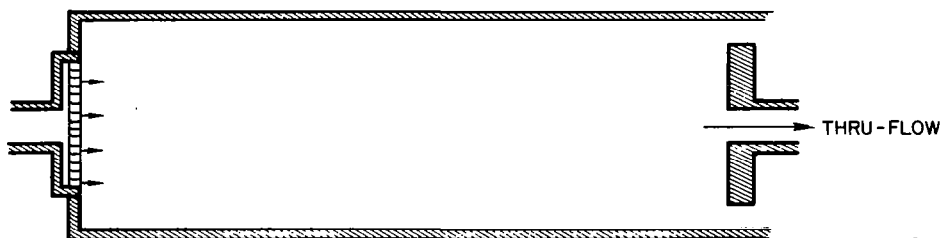
b) INJECTION FROM 1 1/4 - IN.-DIA POROUS TUBE



c) INJECTION FROM "SHOWERHEAD"



d) INJECTION THROUGH 6-IN.-DIA SCREEN

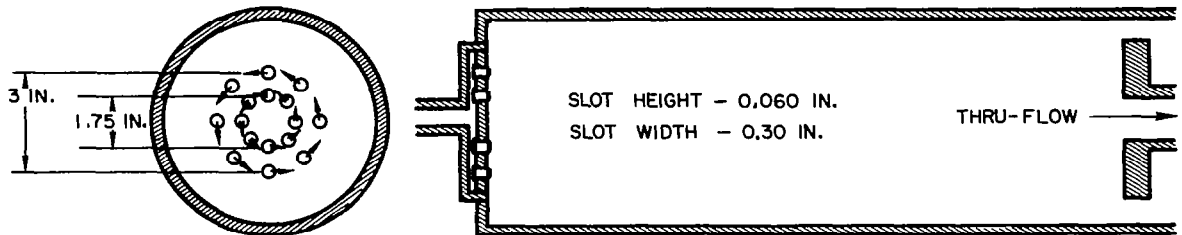


CONTINUED

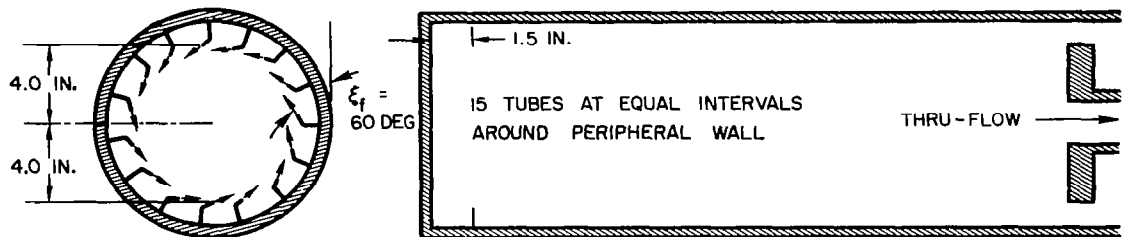
SKETCHES OF HEAVY-GAS INJECTION CONFIGURATIONS INVESTIGATED

SEE NOTES ON PRECEDING PAGE

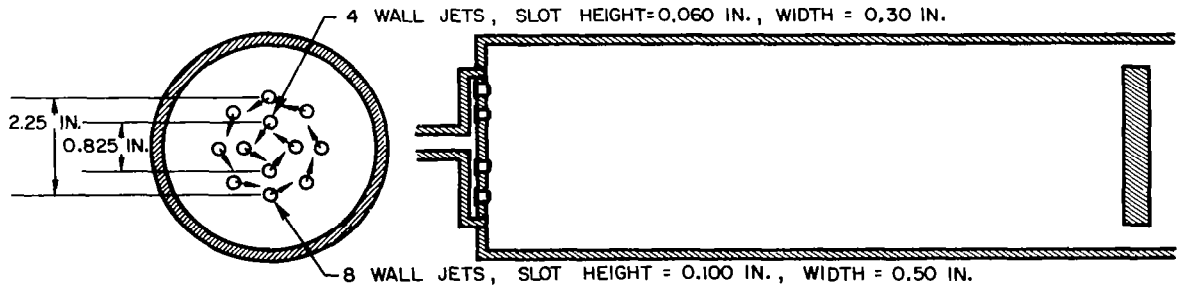
e) INJECTION WITH SWIRL THROUGH 16 WALL JETS



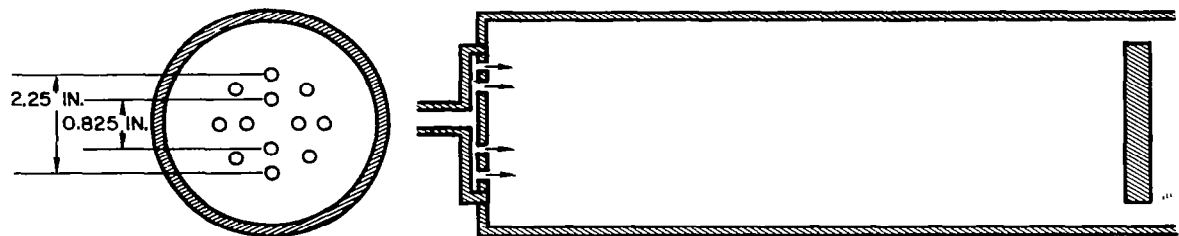
f) INJECTION THROUGH 15 1/8-IN.-DIA TUBES FROM PERIPHERAL WALL



g) INJECTION WITH SWIRL THROUGH 12 WALL JETS



h) INJECTION THROUGH 12 1/2-IN.-DIA DUCTS

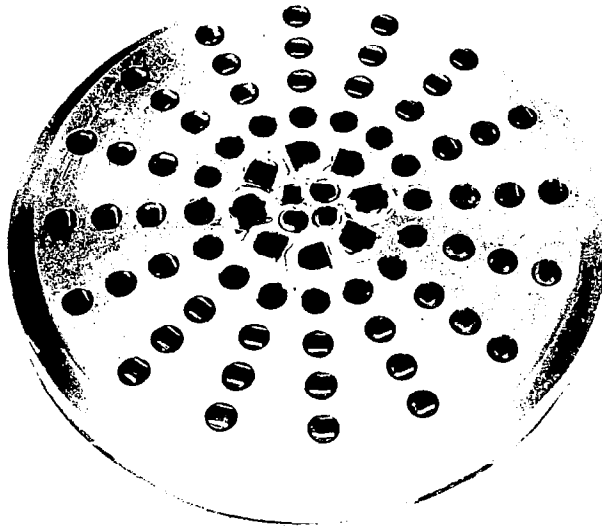


# PHOTOGRAPHS OF END WALLS USED FOR TESTS WITH LIGHT-GAS INJECTION WITH SWIRL

## a) NONAXIAL-FLOW END WALL

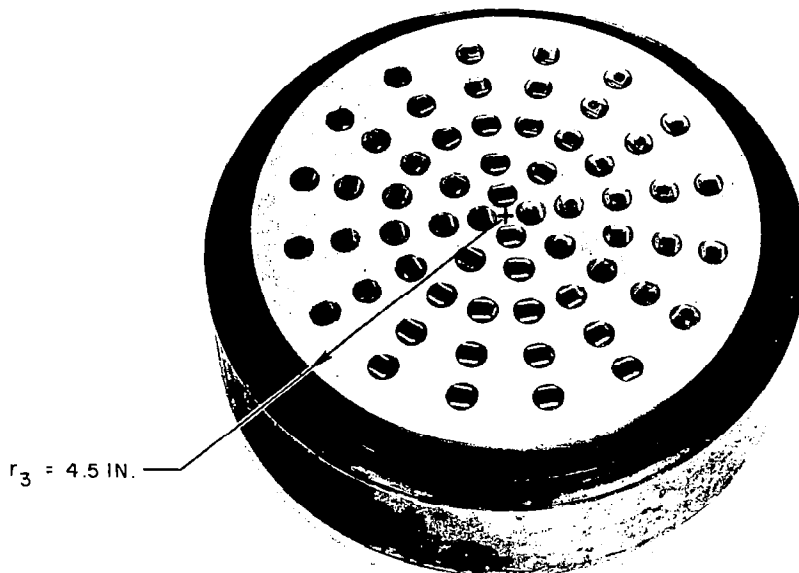
HEAVY-GAS INJECTION CONFIGURATION - CONFIGURATION g) IN FIG. 6 SHOWN;  
CONFIGURATION h) ALSO USED WITH THIS END WALL

LIGHT-GAS INJECTION CONFIGURATION - 48 WALL JETS, SLOT HEIGHT = 0.03 IN.,  
SLOT WIDTH = 0.30 IN.; 16 WALL JETS AT RADII OF 2.87, 3.68, AND 4.50 IN.

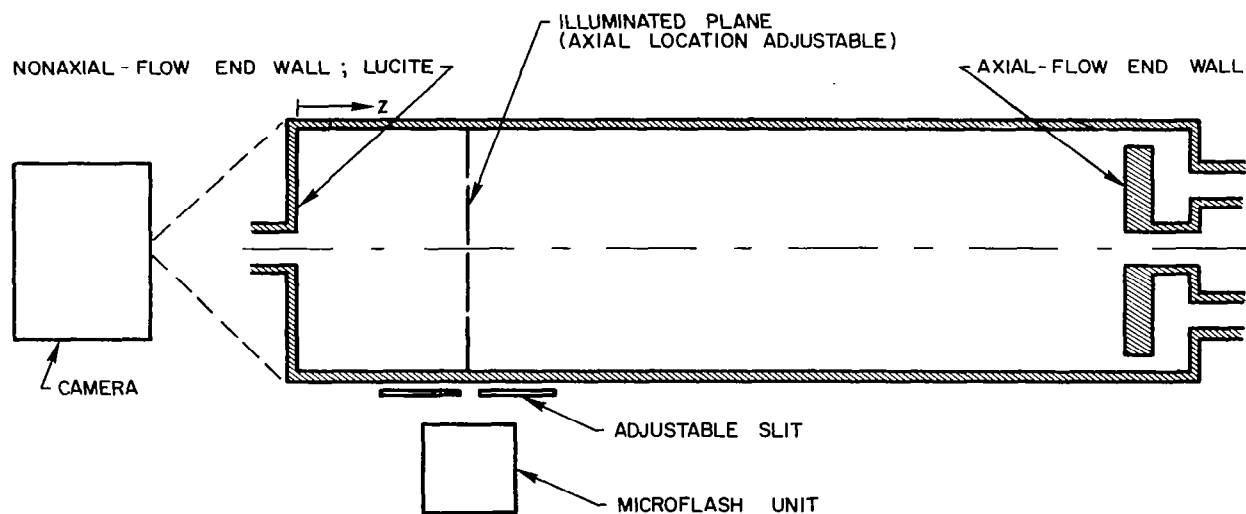


## b) AXIAL-FLOW END WALL

LIGHT-GAS INJECTION CONFIGURATION - 60 WALL JETS, SLOT HEIGHT = 0.03 IN.,  
SLOT WIDTH = 0.30 IN.; 4 WALL JETS AT RADIUS OF 0.41 IN., 8 WALL JETS AT  
RADIUS OF 1.12 IN., 16 WALL JETS AT RADII OF 2.00, 2.87, AND 3.68 IN.

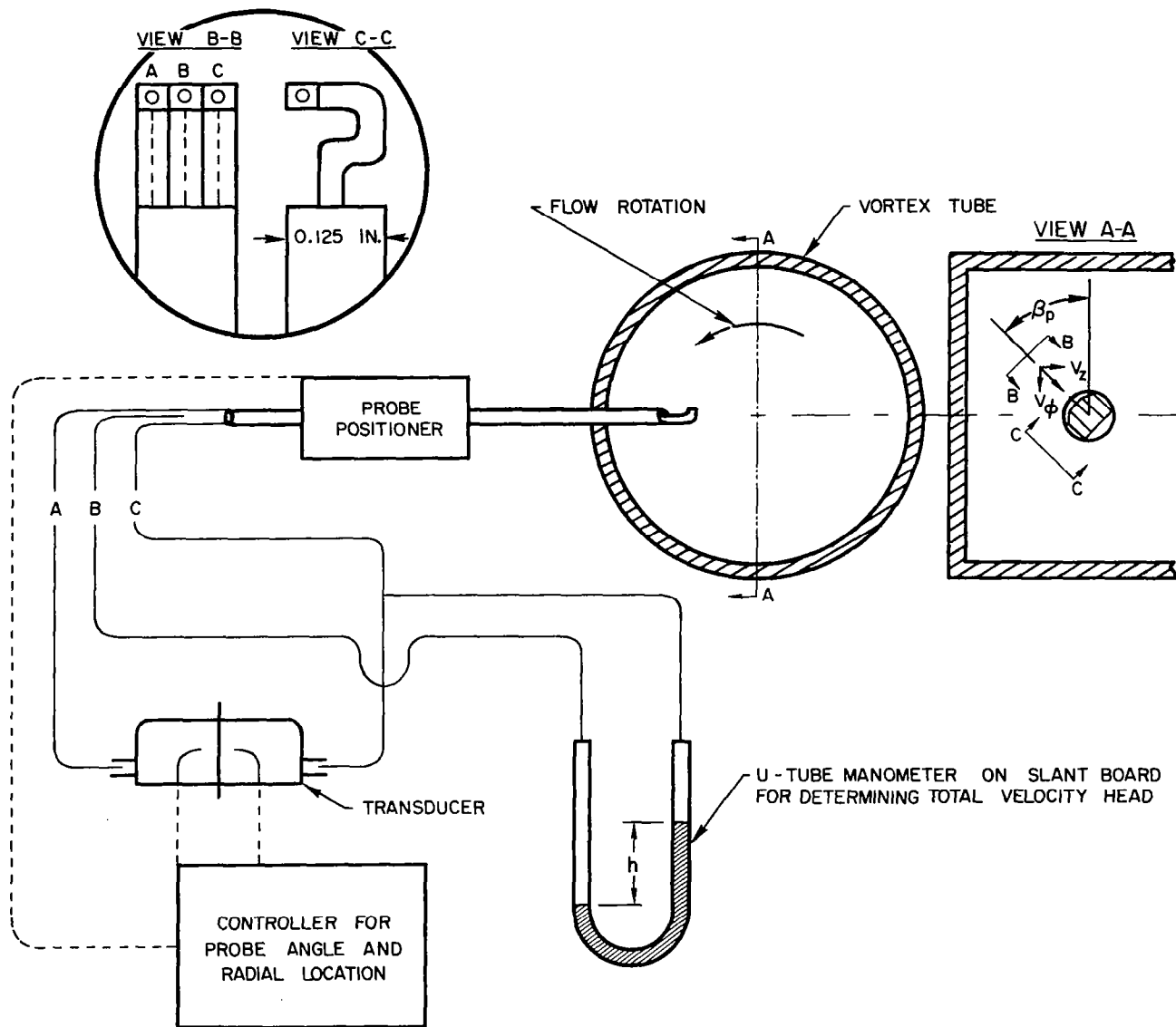


OPTICAL SYSTEM USED TO OBTAIN MICROFLASH PHOTOGRAPHS



SCHMATIC OF EQUIPMENT USED FOR VELOCITY MEASUREMENTS

DETAILS OF COBRA PROBE HEAD



NOTES: (1) RADIAL LOCATION OF PROBE WAS CONTROLLED MANUALLY

(2) PROBE ANGLE,  $\beta_p$ , WAS CONTROLLED MANUALLY OR AUTOMATICALLY BY TRANSDUCER AND PROBE CONTROLLER TO OBTAIN NULL POSITION

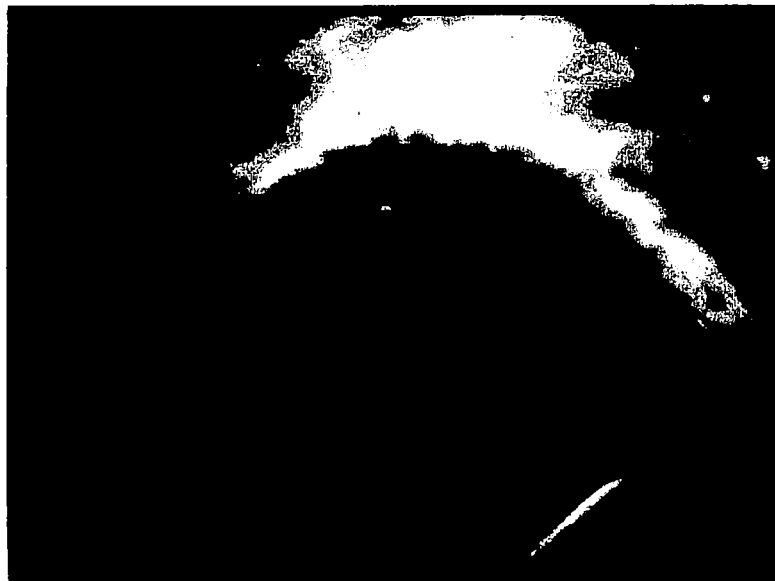
PHOTOGRAPHS OF DYE PATTERNS FOR  $\beta_j = 0$  DEG  
AND RADIAL OUTFLOW

AXIAL-FLOW REYNOLDS NUMBER,  $Re_{z,w} = 53,000$   
TANGENTIAL INJECTION REYNOLDS NUMBER,  $Re_{t,j} = 164,000$   
RADIAL REYNOLDS NUMBER,  $Re_r = -40$

FLUID INJECTED AT CENTERS OF BOTH END WALLS  
SEE TABLE I AND FIGS. 3 AND 4 FOR DETAILS OF PERIPHERAL-WALL INJECTION CONFIGURATION  
PHOTOGRAPH TAKEN AT  $Z = 7.5$  IN.  
FLOW ROTATION



FLOW PATTERN NEAR PERIPHERAL WALL

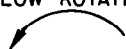


FLOW PATTERN IN CENTRAL REGION



# PHOTOGRAPHS OF DYE PATTERNS FOR $\beta_j = 45$ DEG AND RADIAL OUTFLOW

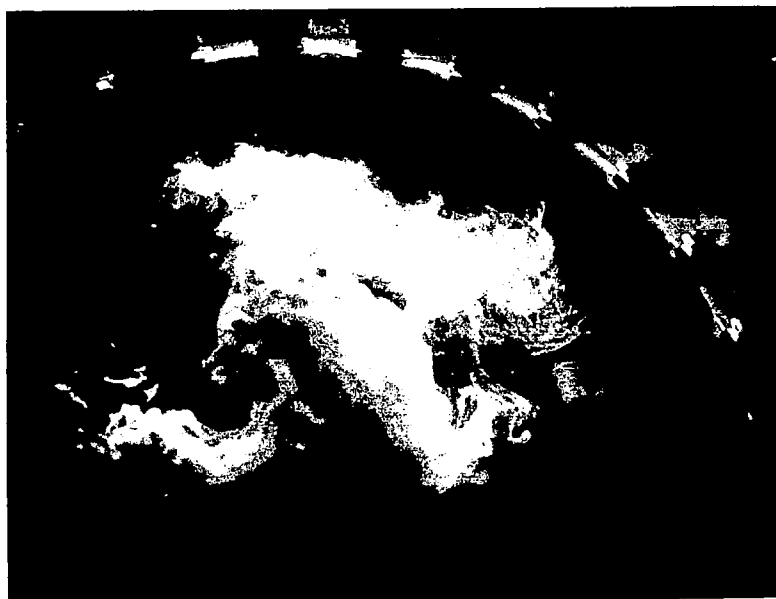
$Re_{z,w} = 53,000$   
 $Re_{t,j} = 116,000$   
 $Re_r = -40$   
 $Z = 7.5$  IN.  
FLOW ROTATION



FLOW PATTERN NEAR PERIPHERAL WALL



FLOW PATTERN IN CENTRAL REGION



PHOTOGRAPHS OF DYE PATTERNS FOR  $\beta_j = 0$  TO 45 DEG AND RADIAL OUTFLOW

FIG. 12

$Re_{z,w} = 53,000$   
 $Re_{t,j} = 164,000$   
 $Re_r = -40$   
 $Z = 7.5$  IN.

FLOW ROTATION  


FLOW PATTERN NEAR PERIPHERAL WALL



FLOW PATTERN IN CENTRAL REGION



PHOTOGRAPHS OF DYE PATTERNS FOR  $\beta_j = 0$  DEG  
AND MODERATE RADIAL INFLOW

AXIAL-FLOW REYNOLDS NUMBER,  $Re_{z,w} = 53,000$   
TANGENTIAL INJECTION REYNOLDS NUMBER,  $Re_{t,j} = 164,000$   
RADIAL REYNOLDS NUMBER,  $Re_r = +40$

FLUID WITHDRAWN AT CENTERS OF BOTH END WALLS  
SEE TABLE I AND FIGS. 3 AND 4 FOR DETAILS OF PERIPHERAL-WALL INJECTION CONFIGURATION  
PHOTOGRAPH TAKEN AT  $z = 7.5$  IN.  
FLOW ROTATION



FLOW PATTERN NEAR PERIPHERAL WALL



FLOW PATTERN IN CENTRAL REGION

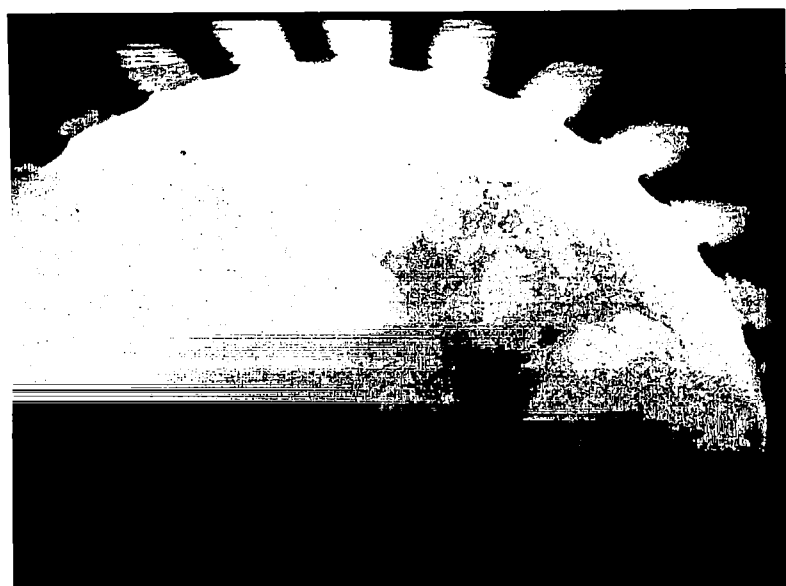


# PHOTOGRAPHS OF DYE PATTERNS FOR $\beta_j = 45$ DEG AND MODERATE RADIAL INFLOW

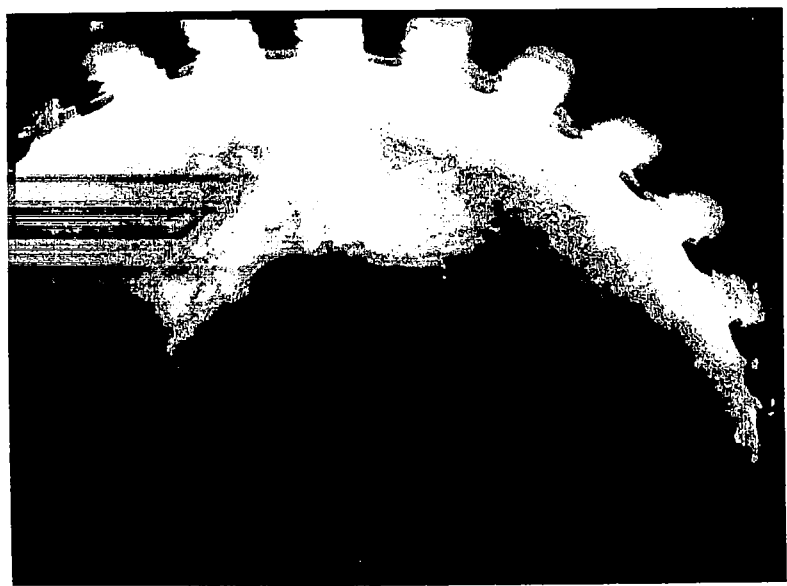
$Re_{z,w} = 53,000$   
 $Re_{t,j} = 116,000$   
 $Re_r = +40$   
 $Z = 7.5$  IN.  
FLOW ROTATION



FLOW PATTERN NEAR PERIPHERAL WALL



FLOW PATTERN IN CENTRAL REGION

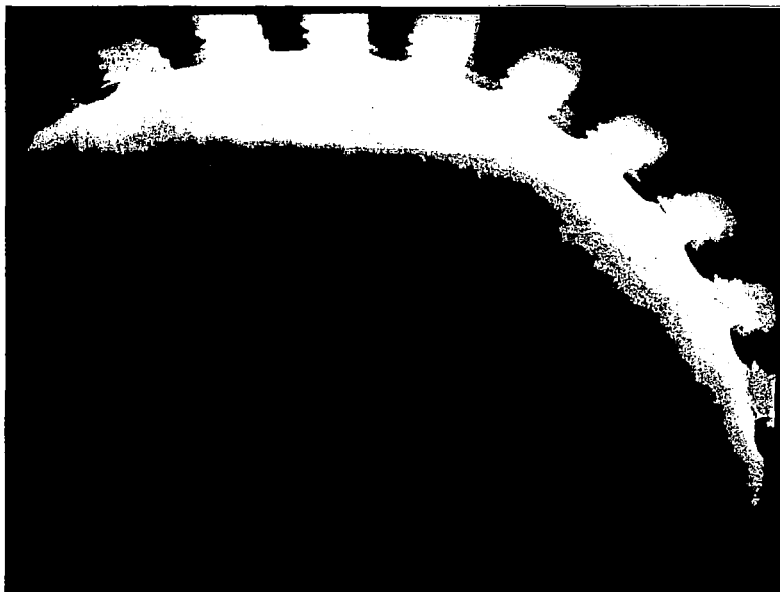


# PHOTOGRAPHS OF DYE PATTERNS FOR $\beta_j = 45$ DEG AND LARGE RADIAL INFLOW

$Re_{z,w} = 53,000$   
 $Re_{t,j} = 116,000$   
 $Re_r = +80$   
 $Z = 7.5$  IN.  
FLOW ROTATION



FLOW PATTERN NEAR PERIPHERAL WALL



FLOW PATTERN IN CENTRAL REGION



# AXIAL AND TANGENTIAL VELOCITY PROFILES FOR $\beta_j = 0$ DEG

$Re_{z,w} = 108,500$        $Re_{r,j} = 291,000$        $Re_r = -103$

SYMBOL	◇	▷	□	△	○
z - IN.	4.5	10.5	16.5	22.5	28.5
$V_{z,j}$ - FT/SEC	0	0	0	0	0

z = DISTANCE FROM NONAXIAL - FLOW END WALL

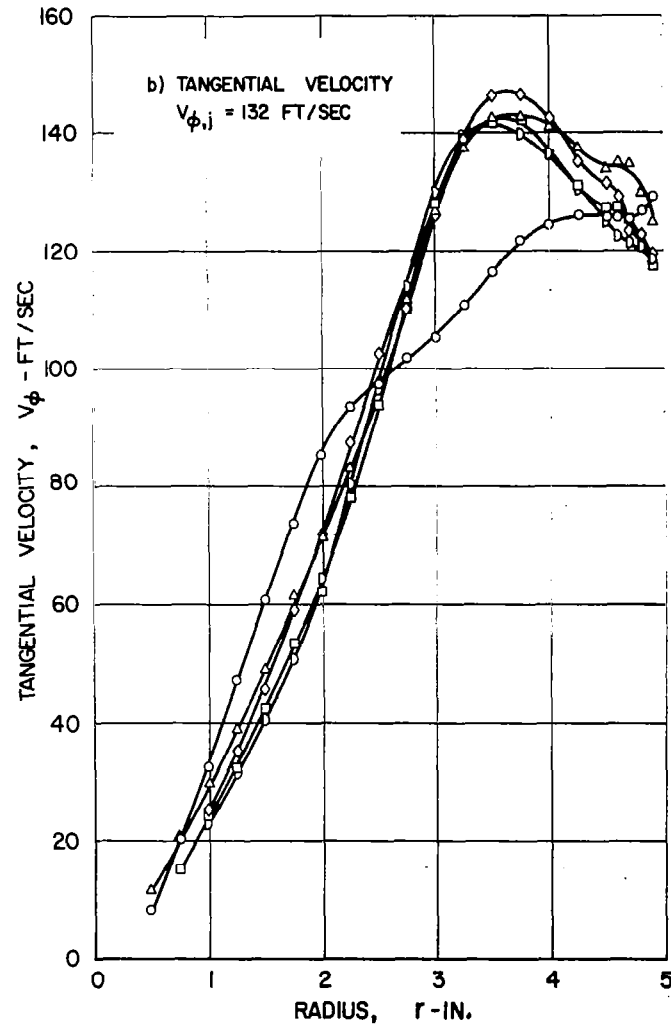
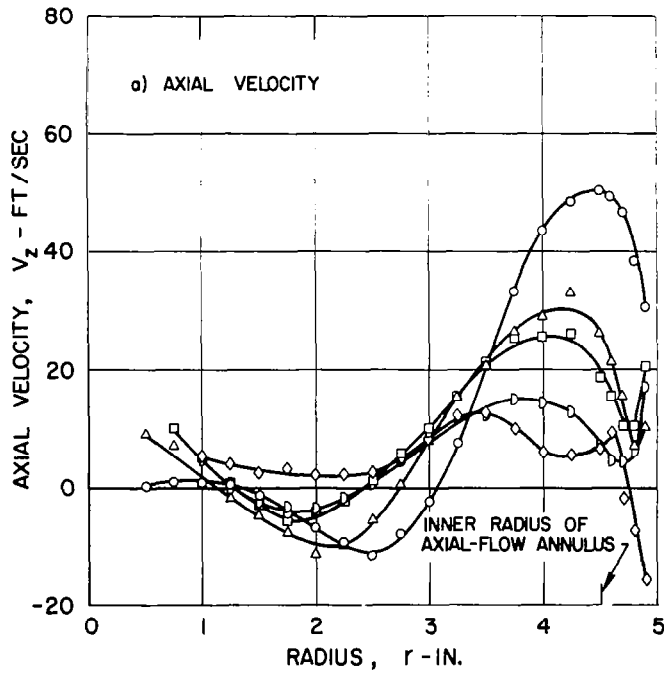


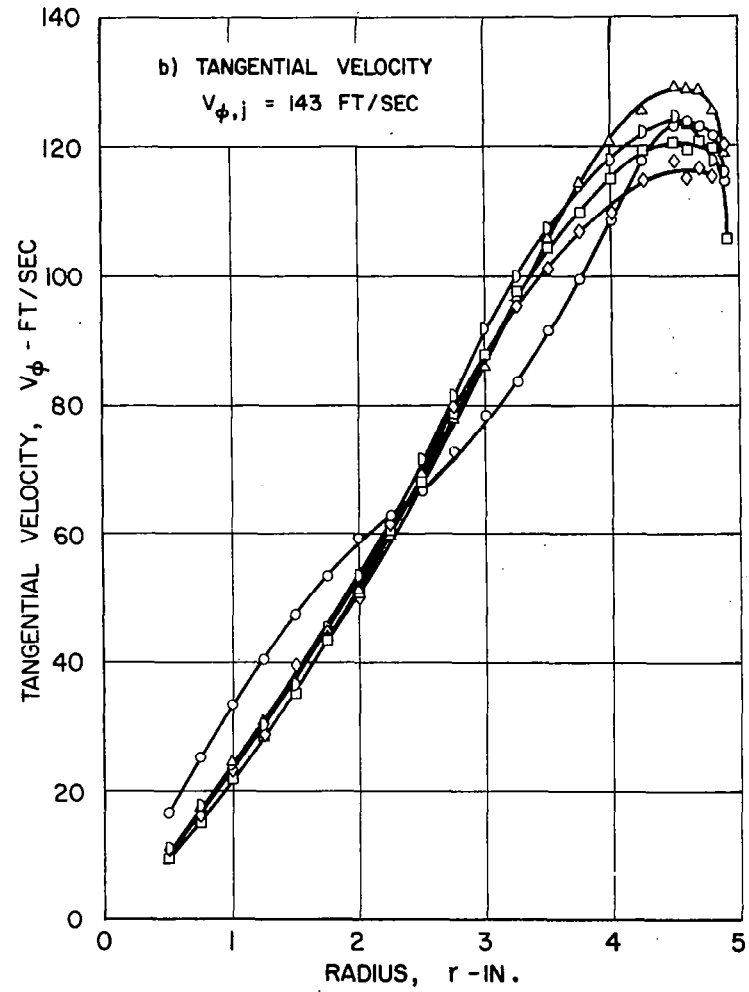
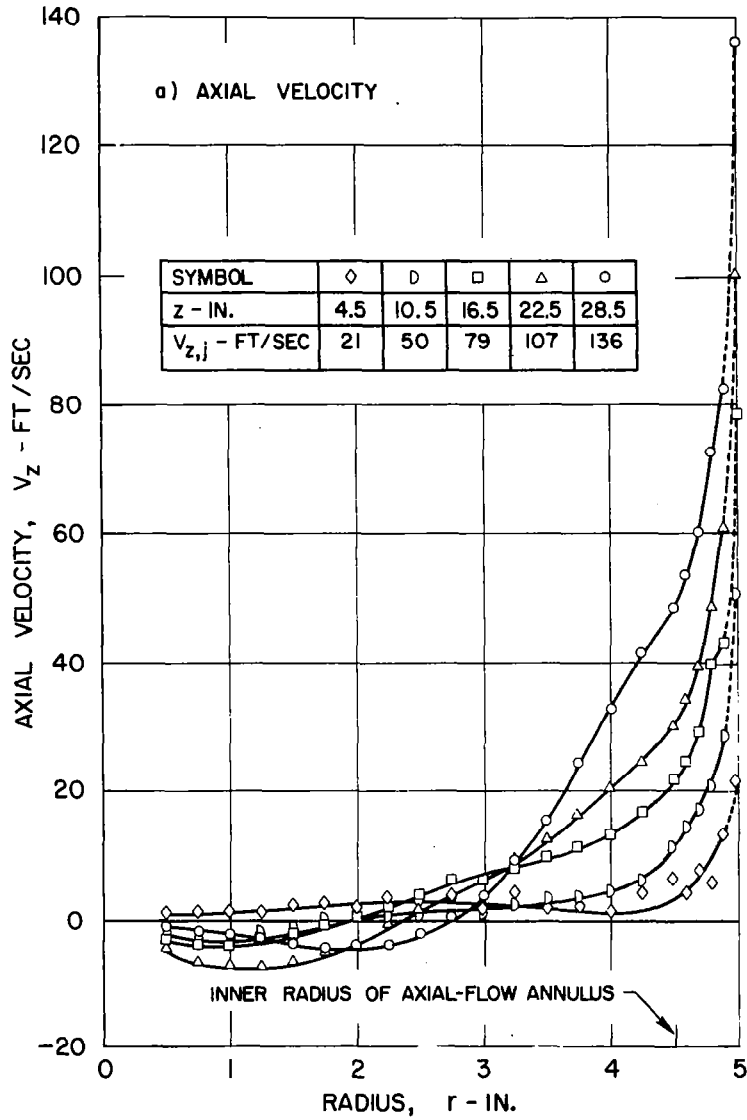
FIG. 16

# AXIAL AND TANGENTIAL VELOCITY PROFILES FOR $\beta_j = 0$ TO 45 DEG

$Re_{z,w} = 109,000$

$Re_{t,j} = 328,000$

$Re_r = -103$

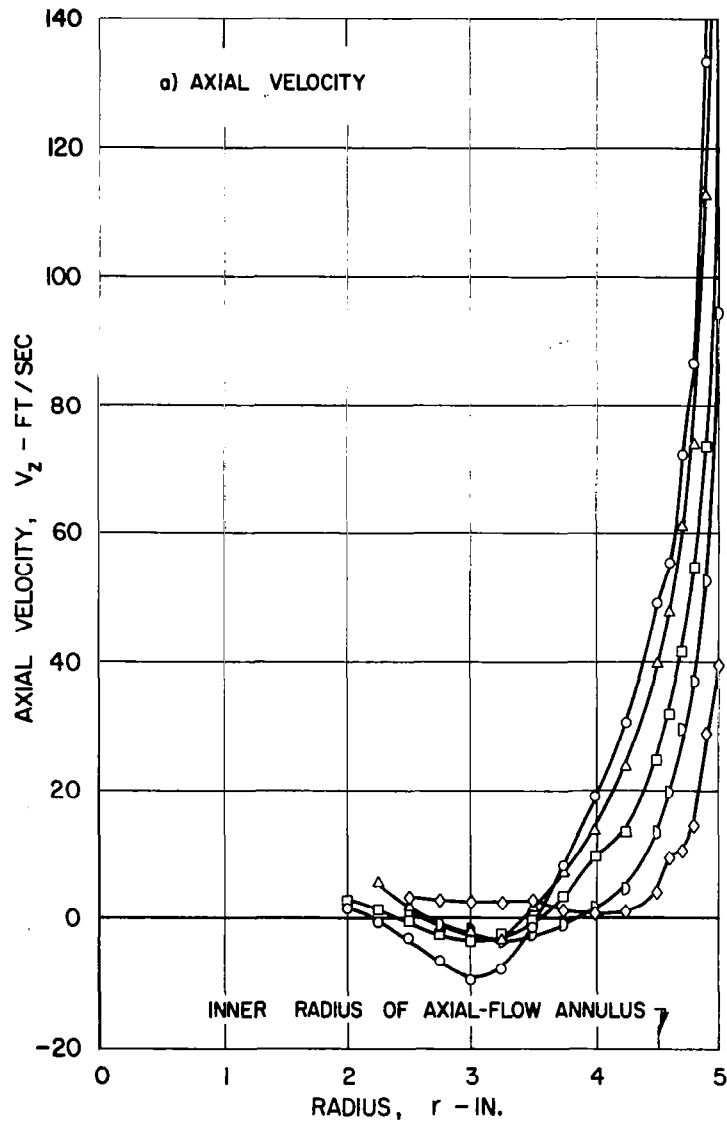


# AXIAL AND TANGENTIAL VELOCITY PROFILES FOR $\beta_j = 0$ TO 63.5 DEG

$Re_{z,w} = 102,000$

$Re_{t,j} = 304,000$

$Re_r = -103$



SYMBOL	◇	D	□	△	○
$z$ - IN.	4.5	10.5	16.5	22.5	28.5
$V_{z,j}$ - FT/SEC	41	123	150	205	259

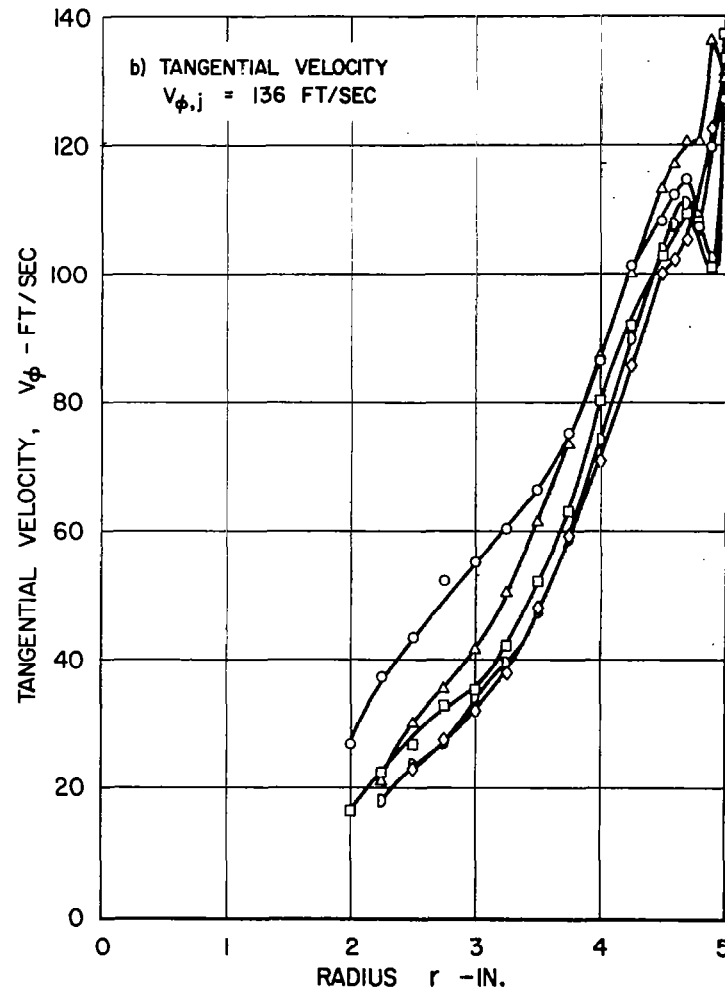


FIG. 18

# AXIAL AND TANGENTIAL VELOCITY PROFILES FOR $\beta_j = 26.5$ DEG

$Re_{z,w} = 109,000$

$Re_{t,j} = 265,000$

$Re_r = -103$

SYMBOL	◇	□	○
z - IN.	4.5	16.5	28.5

88

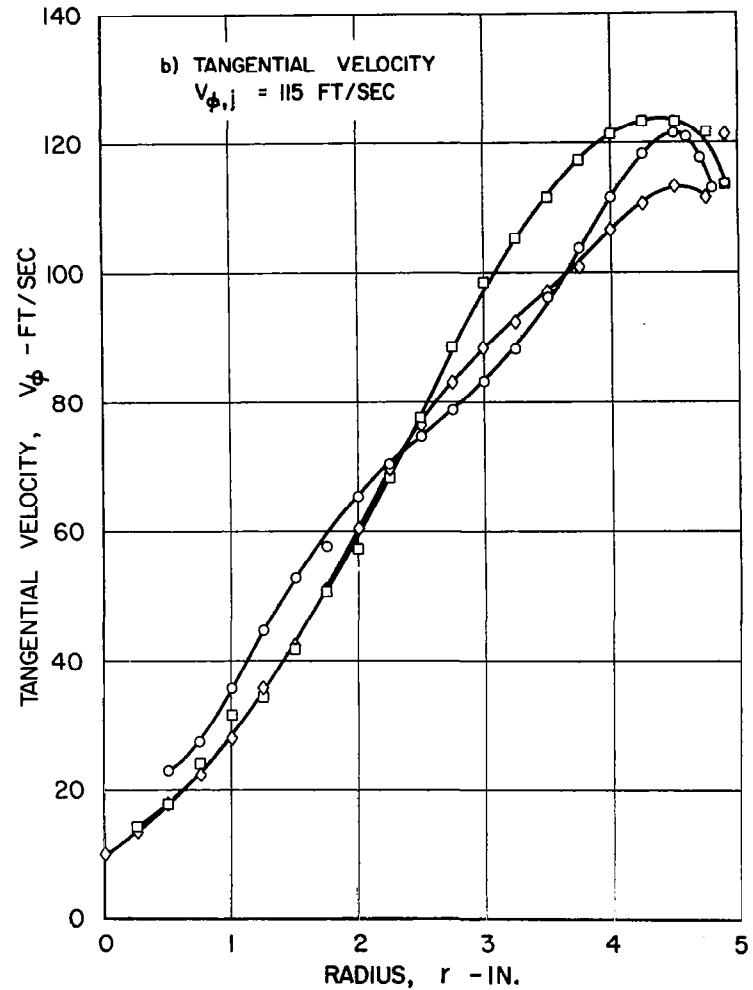
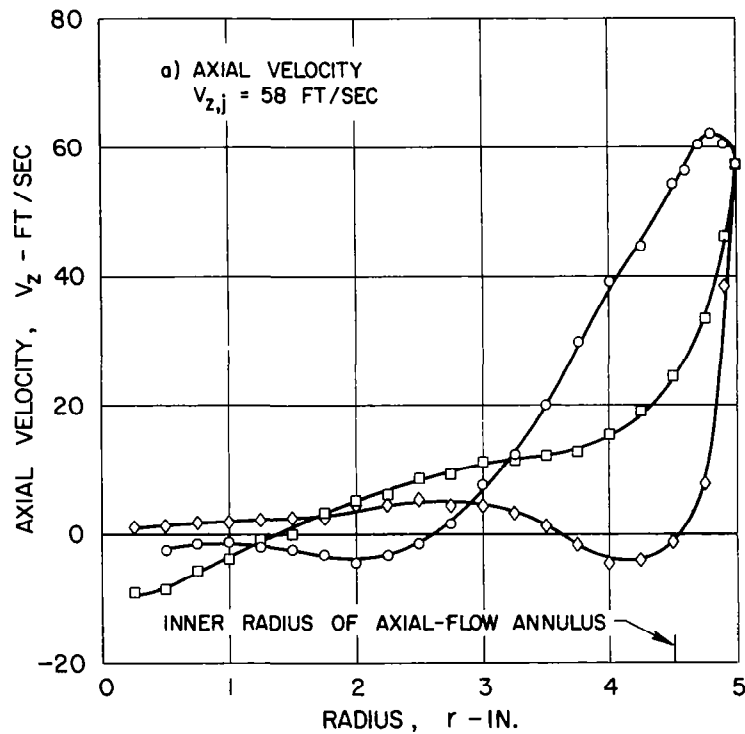


FIG. 19

# AXIAL AND TANGENTIAL VELOCITY PROFILES FOR $\beta_j = 45$ DEG

$Re_{z,w} = 108,000$

$Re_{t,j} = 209,000$

$Re_r = -103$

SYMBOL	◇	□	○
z - IN.	4.5	16.5	28.5

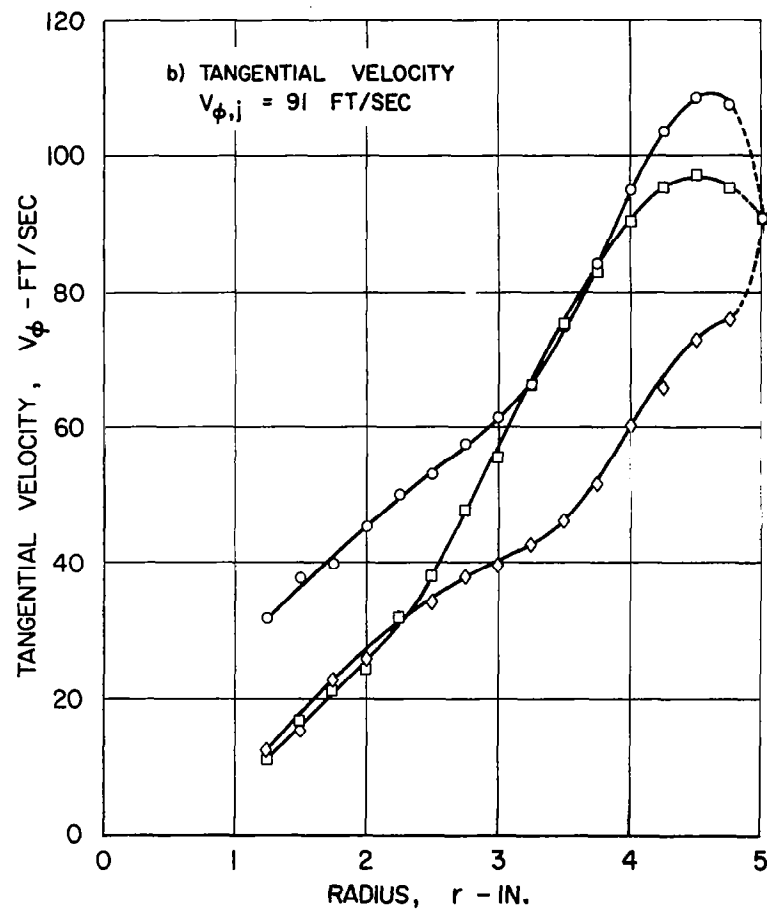
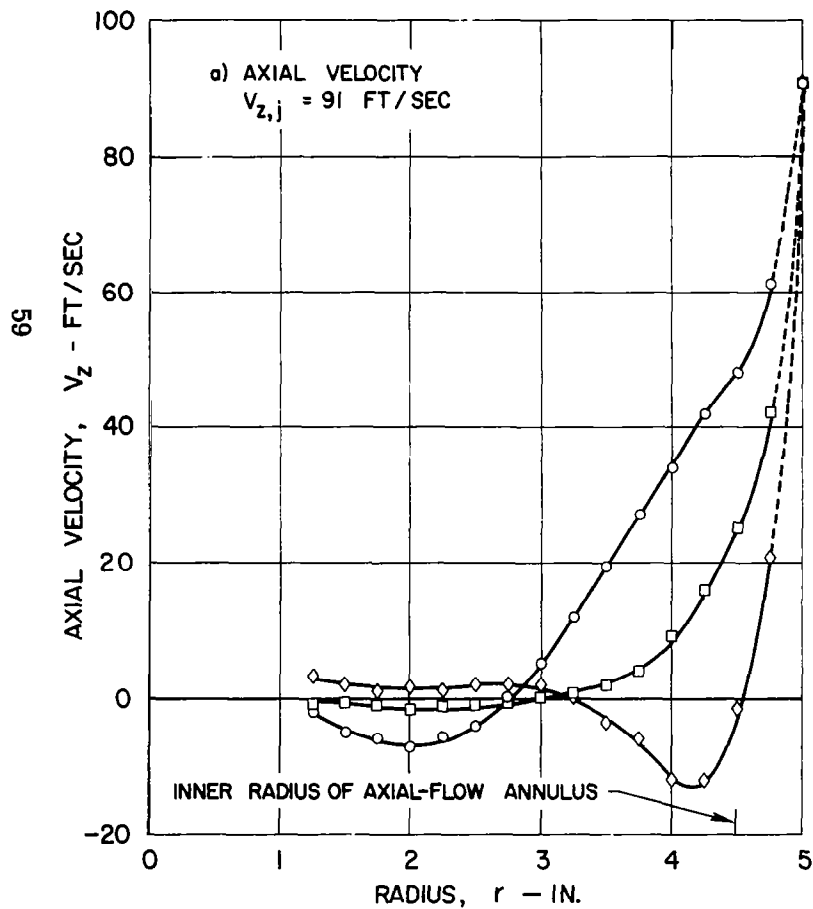


FIG. 20

# AXIAL AND TANGENTIAL VELOCITY PROFILES FOR $\beta_j = 63.5$ DEG

$Re_{z,w} = 109,000$

$Re_{t,j} = 133,000$

$Re_r = -104$

SYMBOL	◇	□	○
z - IN.	4.5	16.5	28.5

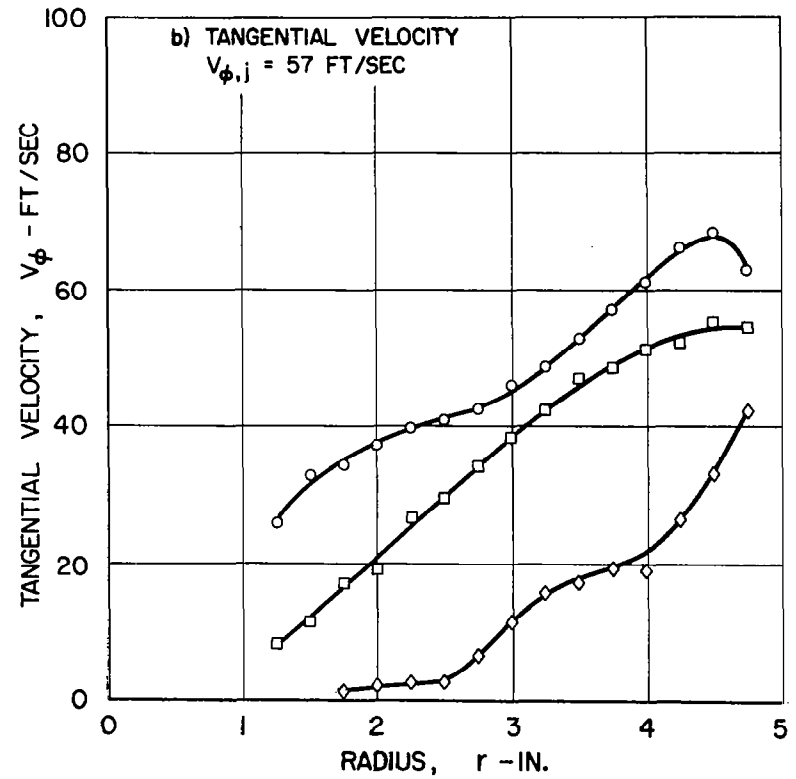
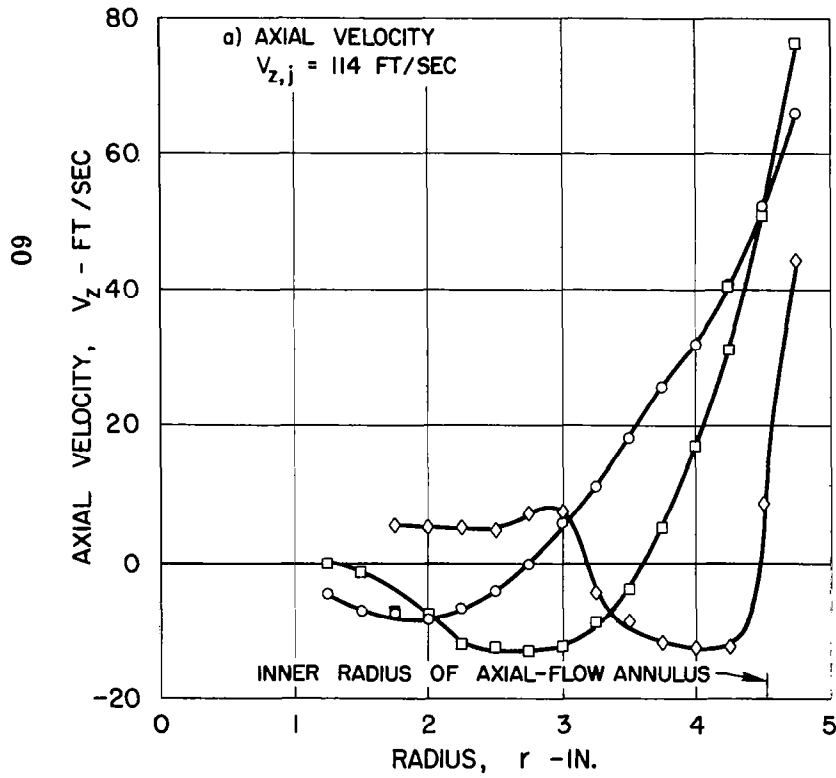
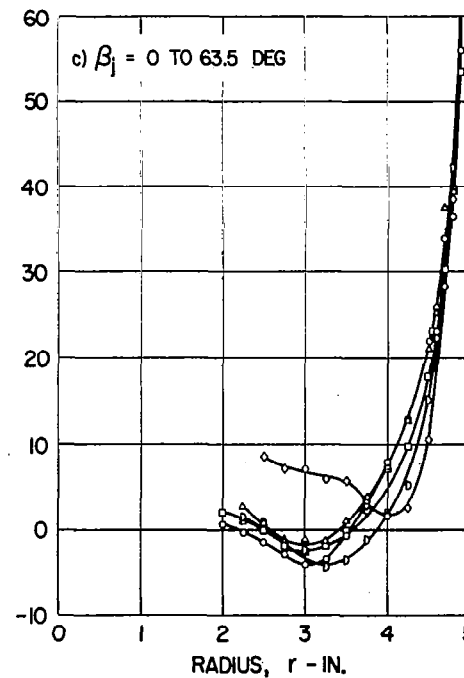
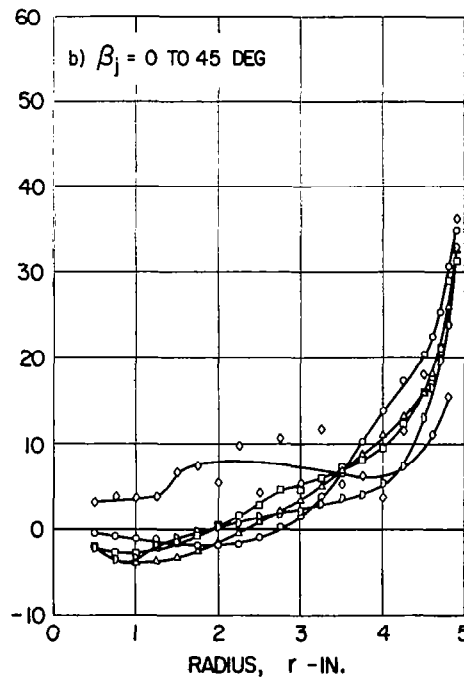
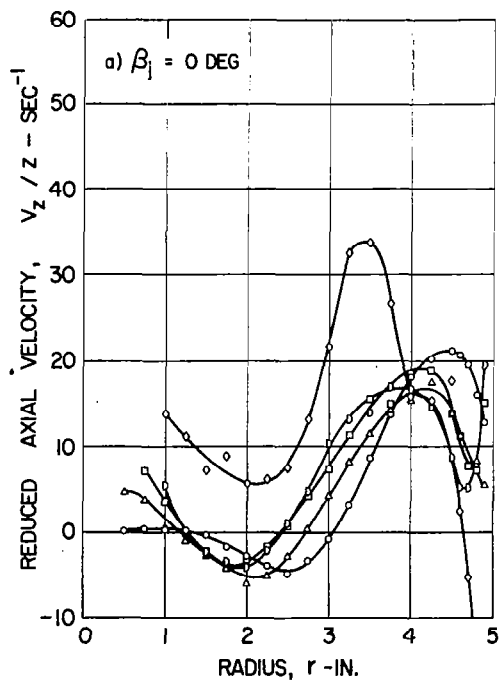


FIG. 21

# REDUCED AXIAL VELOCITY PROFILES FOR $\beta_j = 0, 0 \text{ TO } 45 \text{ AND } 0 \text{ TO } 63.5 \text{ DEG}$

DATA FROM FIGS. 16, 17 AND 18

SYMBOL	◇	◊	□	△	○
z - IN.	4.5	10.5	16.5	22.5	28.5



# COMPARISON OF AXIAL AND TANGENTIAL VELOCITY PROFILES FOR $\beta_j = 0, 0 \text{ TO } 45 \text{ AND } 0 \text{ TO } 63.5 \text{ DEG}$

PROFILES MEASURED AT  $z = 16.5 \text{ IN.}$

$Re_{z,w} \approx 109,000$        $Re_{t,j} \approx 300,000$        $Re_r = -103$

DATA FROM FIGS. 16, 17 AND 18

SYMBOL	PERIPHERAL-WALL INJECTION CONFIGURATION, $\beta_j$ - DEG	V <sub>z,j</sub> AT z = 16.5 IN. - FT/SEC
○	0	0
□	0 TO 45	79
◇	0 TO 63.5	150

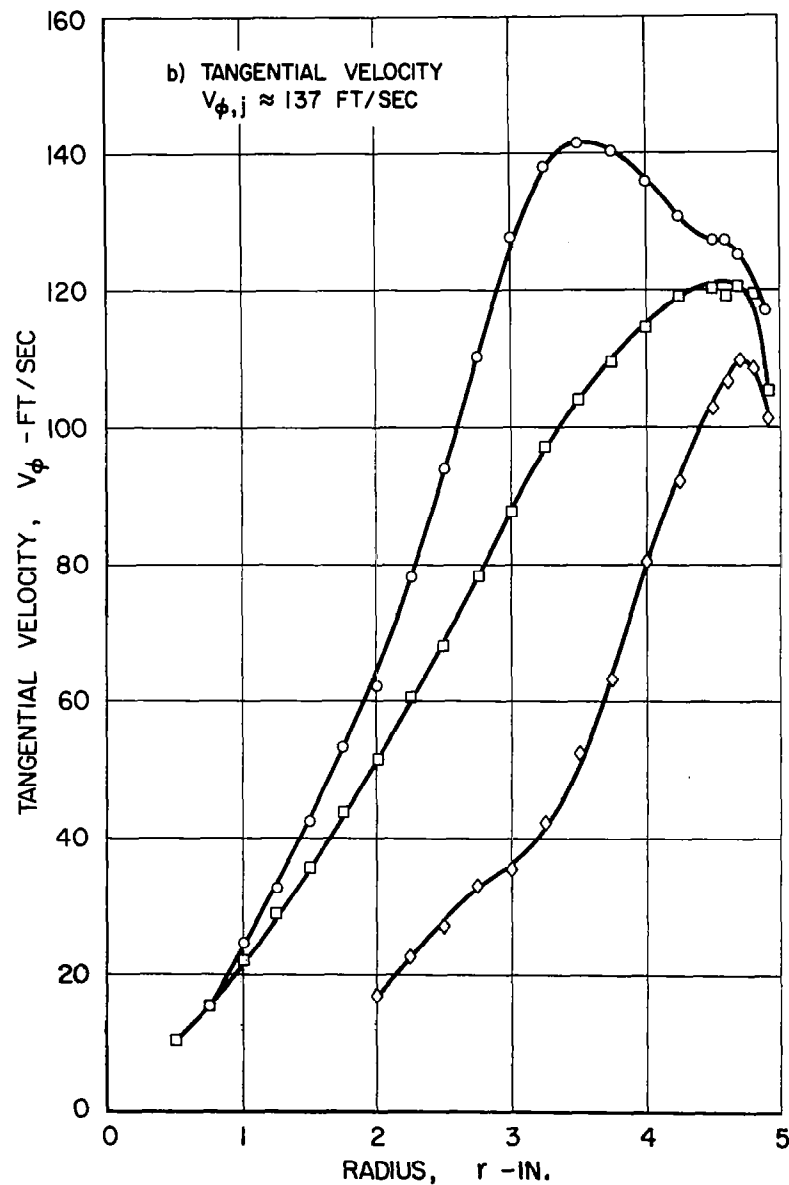
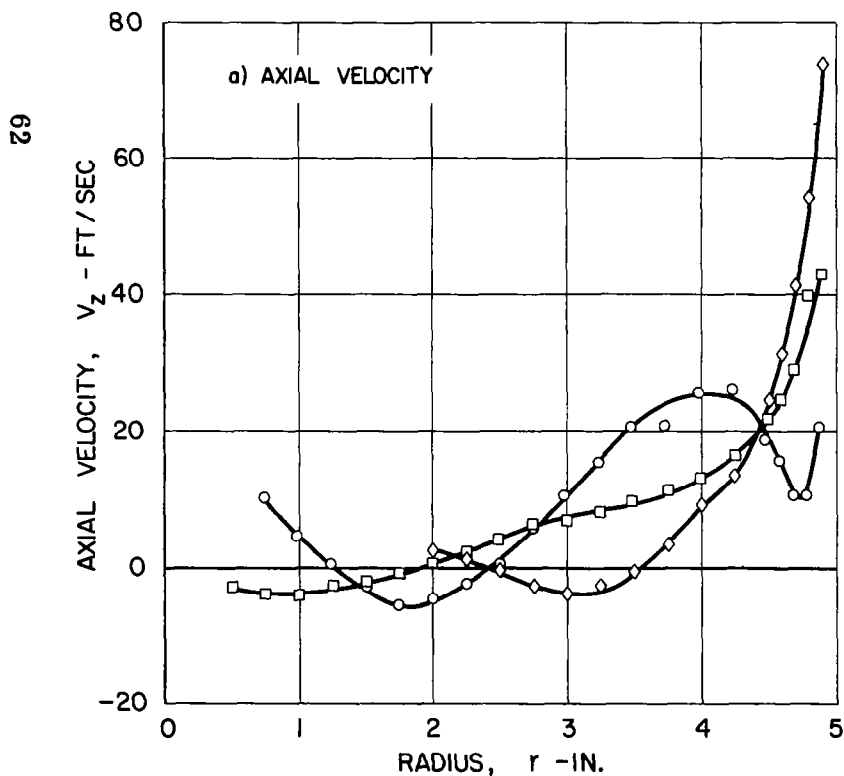


FIG. 23

# COMPARISON OF AXIAL AND TANGENTIAL VELOCITY PROFILES FOR $\beta_j = 0, 26.5, 45$ AND $63.5$ DEG

PROFILES MEASURED AT  $z = 16.5$  IN.

$Re_{z,w} \approx 108,000$

$Re_r = -103$

DATA FROM FIGS. 19, 20 AND 21

SYMBOL	PERIPHERAL-WALL INJECTION CONFIGURATION, $\beta_j$ - DEG	$V_{z,j}$ - FT/SEC	$V_{\phi,j}$ - FT/SEC	$Re_{t,j}$
$\Delta$	0	0	132	291,000
$\square$	26.5	58	115	265,000
$\circ$	45	91	91	209,000
$\square$	63.5	114	57	133,000

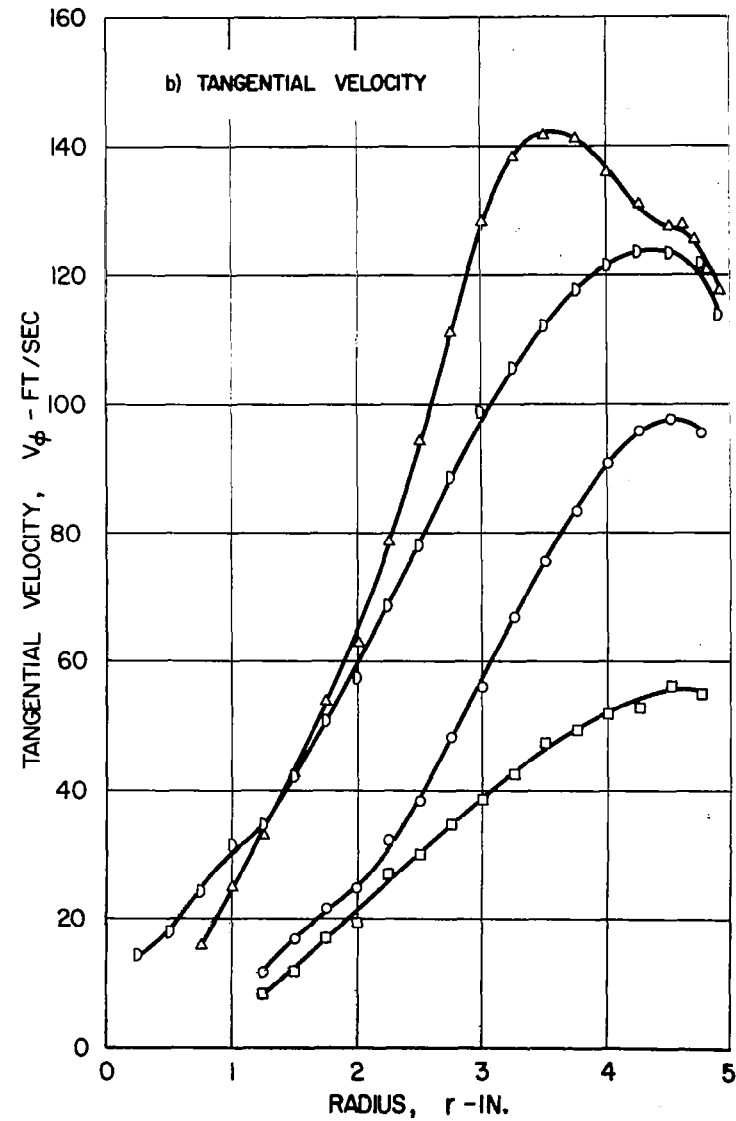
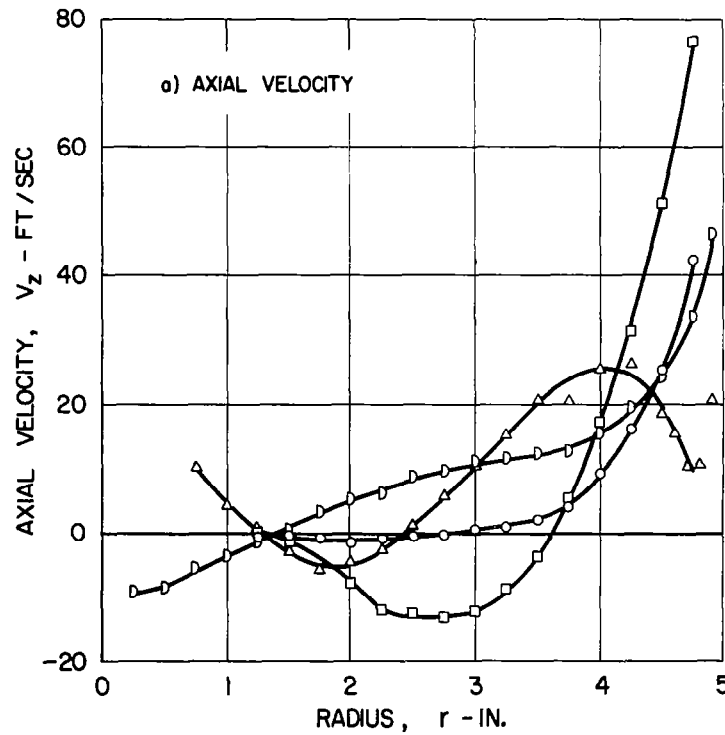


FIG. 24

# COMPARISON OF PERIPHERAL-WALL STATIC PRESSURE DISTRIBUTIONS FOR $\beta_j = 0, 0 \text{ TO } 45 \text{ AND } 0 \text{ TO } 63.5 \text{ DEG}$

$Re_{z,w} \approx 109,000$

$Re_{t,j} \approx 300,000$

$Re_r = -103$

64

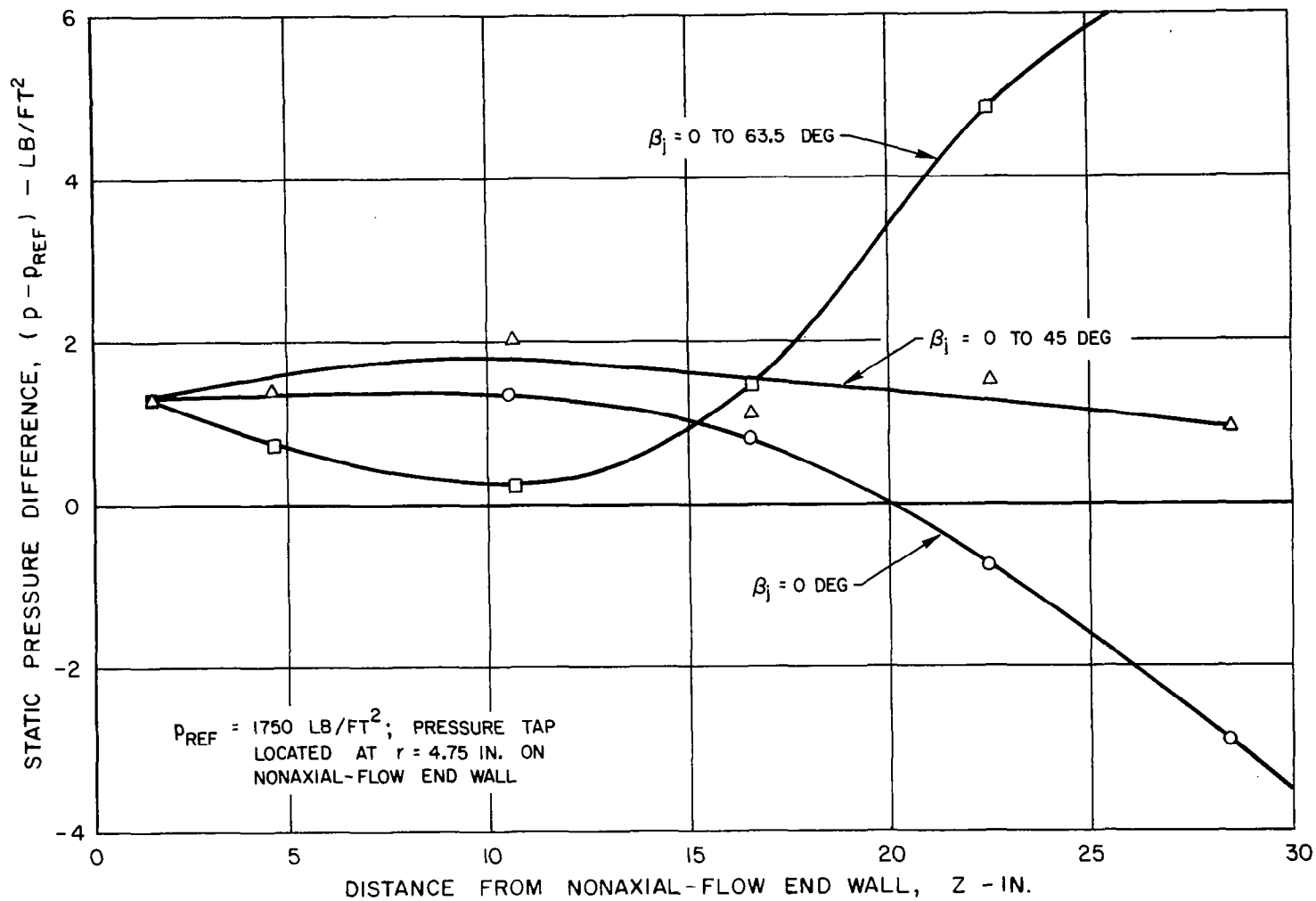


FIG. 25

COMPARISON OF PERIPHERAL-WALL STATIC PRESSURE DISTRIBUTIONS FOR  
 $\beta_j = 0, 26.5, 45$  AND  $63.5$  DEG

$Re_{z,w} \approx 108,000$

$Re_r = -103$

SYMBOL	○	□	◇	D
$\beta_j$ - DEG	0	26.5	45	63.5
$Re_{t,j}$	291,000	265,000	209,000	133,000

69

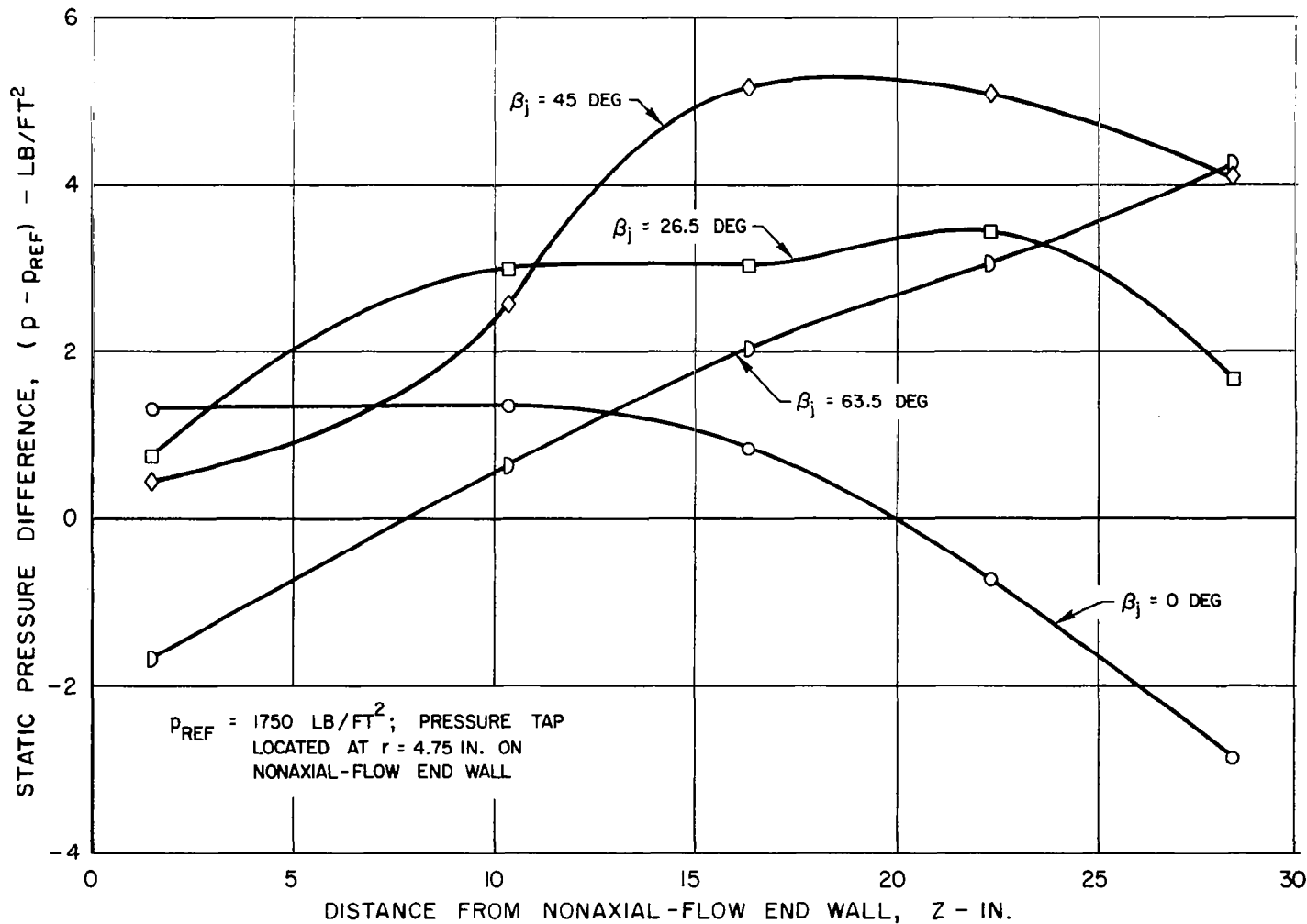


FIG. 26

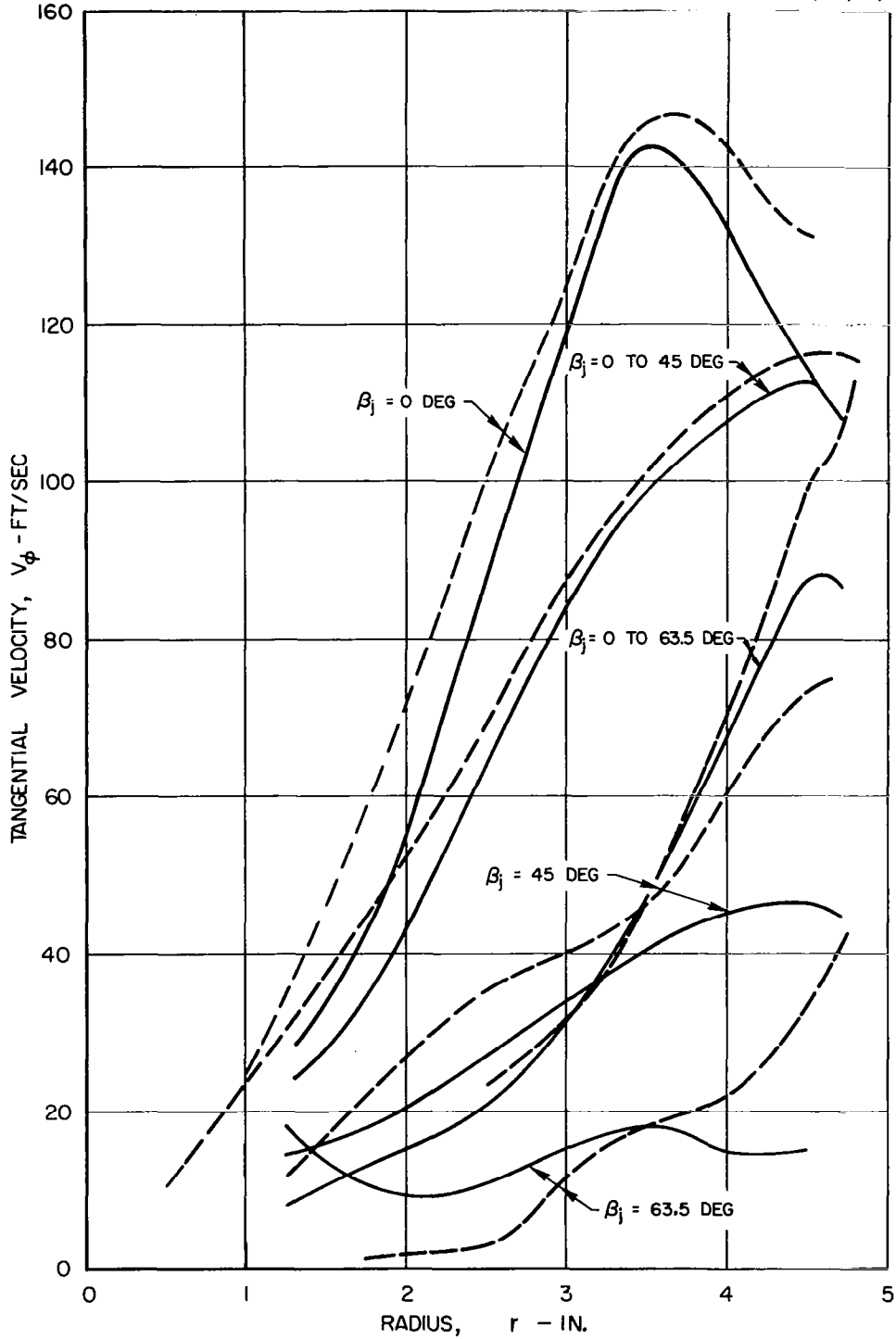
FIG. 27

# COMPARISON OF TANGENTIAL VELOCITY PROFILES OBTAINED WITH PROBE AND END-WALL STATIC PRESSURE MEASUREMENTS

$Re_{z,w} \approx 109,000$

$Re_r = -103$

VELOCITY PROFILES FROM END-WALL PRESSURE MEASUREMENTS  
 VELOCITY PROFILES FROM PROBE MEASUREMENTS AT  $z = 4.5$  IN. (FIGS. 16, 17, 18, 20 AND 21)



# EFFECT OF RADIAL REYNOLDS NUMBER ON VELOCITY PROFILES FOR $\beta_j = 0$ TO 45 DEG

PROFILES MEASURED AT  $z = 16.5$  IN.

$Re_{z,w} \approx 109,000$

$Re_{t,j} \approx 327,000$

SYMBOL	○	□	◇	△
$Re_r$	-103	0	+24	+96

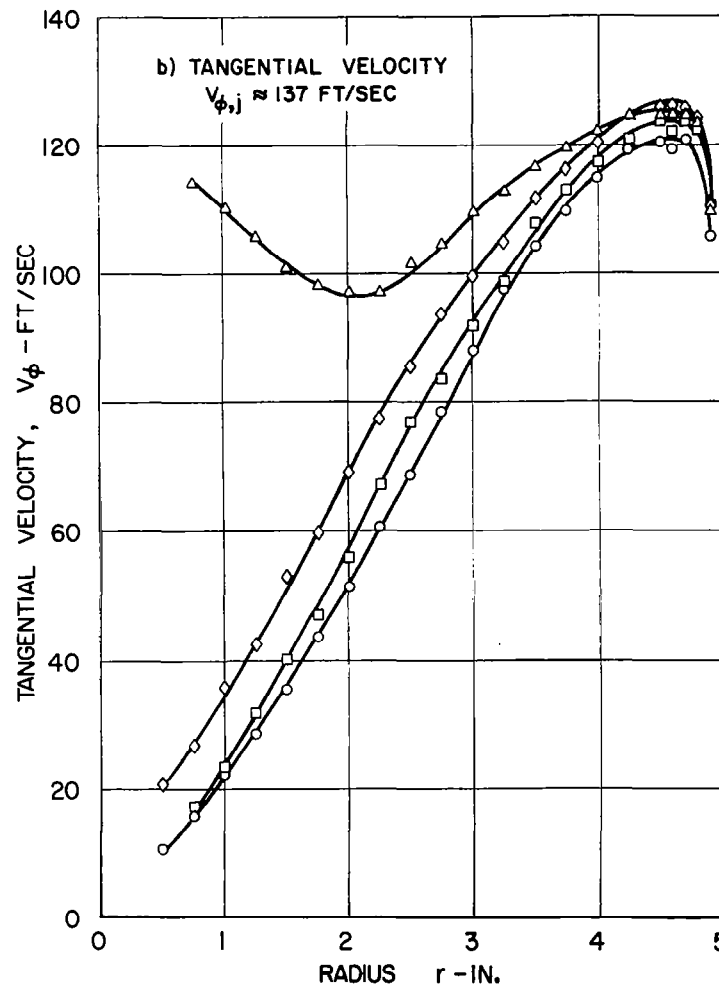
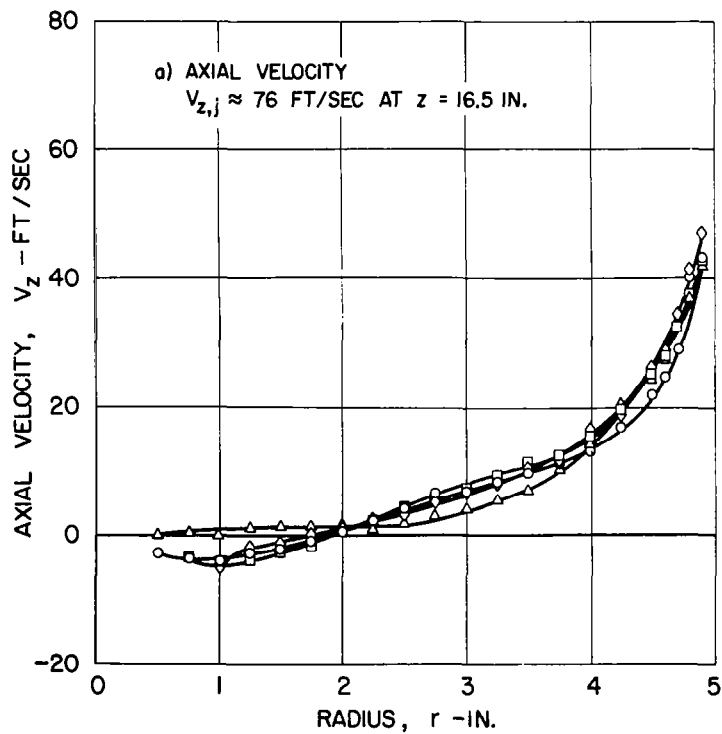


FIG. 28

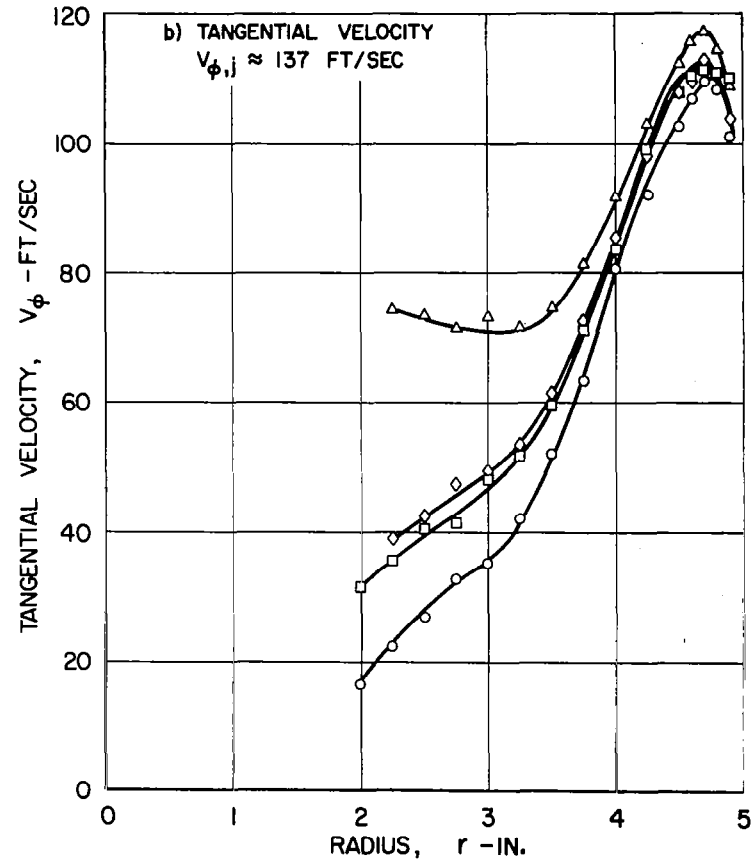
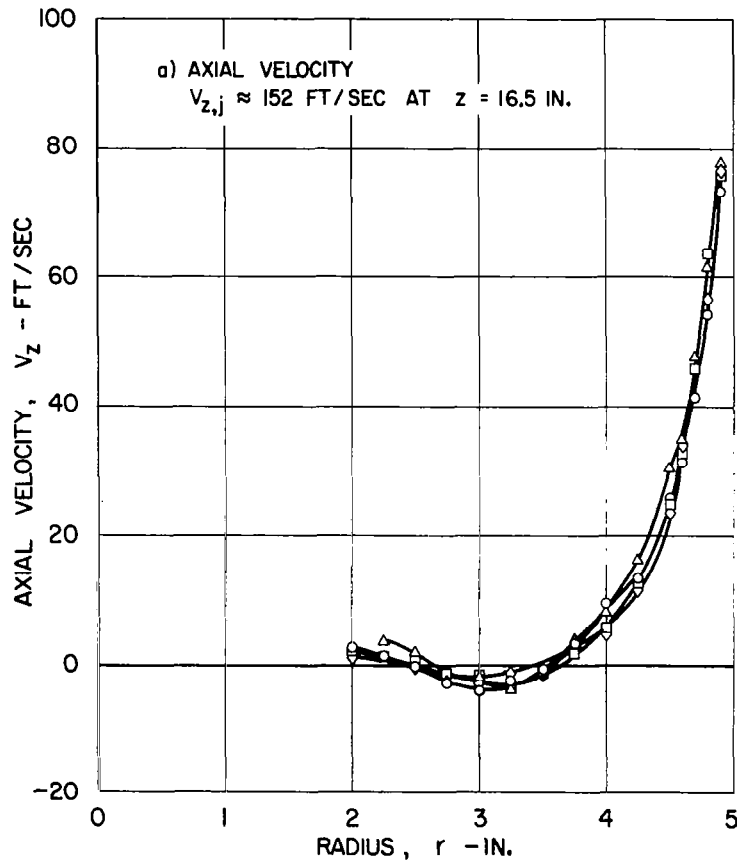
# EFFECT OF RADIAL REYNOLDS NUMBER ON VELOCITY PROFILES FOR $\beta_j = 0$ TO 63.5 DEG

PROFILES MEASURED AT  $z = 16.5$  IN.

$Re_{z,w} \approx 102,000$

$Re_{t,j} = 303,000$

SYMBOL	○	□	◇	△
$Re_r$	-103	0	+24	+96



# EFFECT OF INNER RADIUS OF AXIAL-FLOW EXHAUST ANNULUS ON VELOCITY PROFILES

PERIPHERAL-WALL INJECTION CONFIGURATION,  $\beta_j = 0$  TO 63.5 DEG

PROFILES MEASURED AT  $z = 16.5$  IN.

$Re_{z,w} \approx 102,000$

$Re_{t,j} = 302,000$

$Re_r = -105$

SEE FIG. 5 FOR PHOTOGRAPH OF AXIAL-FLOW END WALL

SYMBOL	○	□	◇	△	D
INNER RADIUS OF ANNULUS, $r_3$ - IN.	4.75	4.50	4.00	3.50	3.00

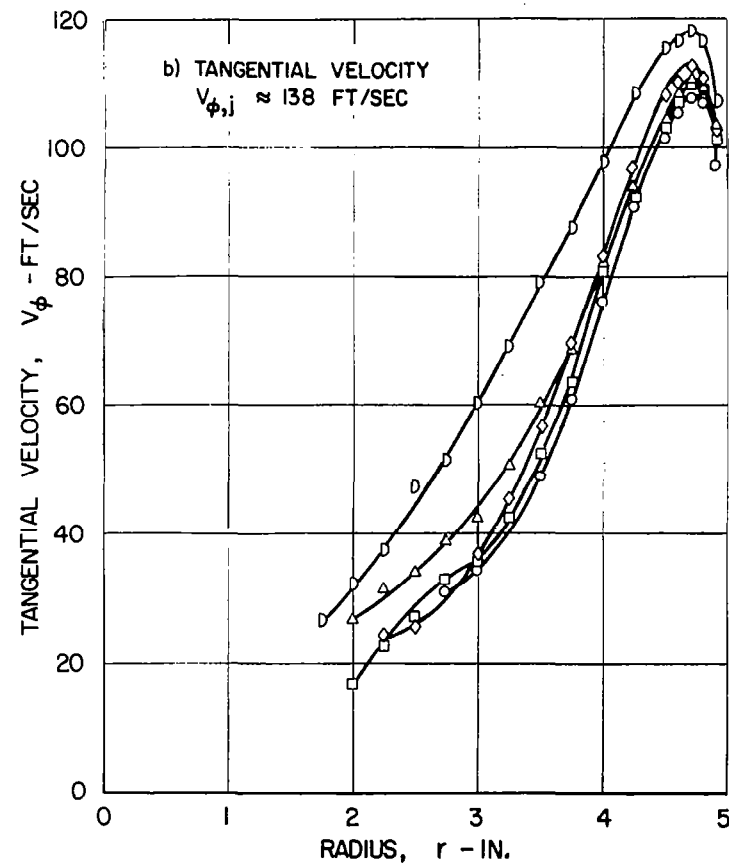
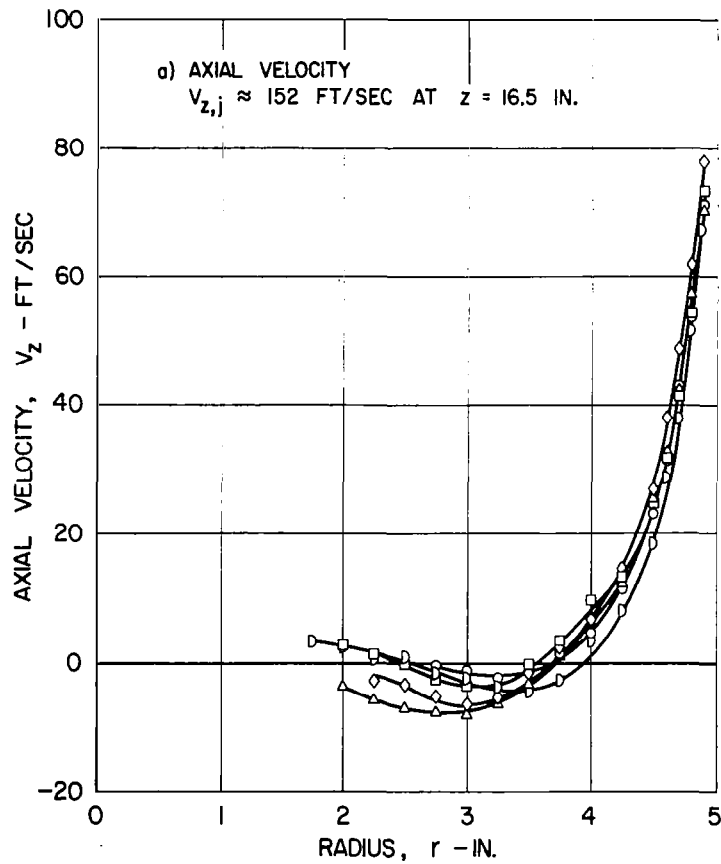


FIG. 30

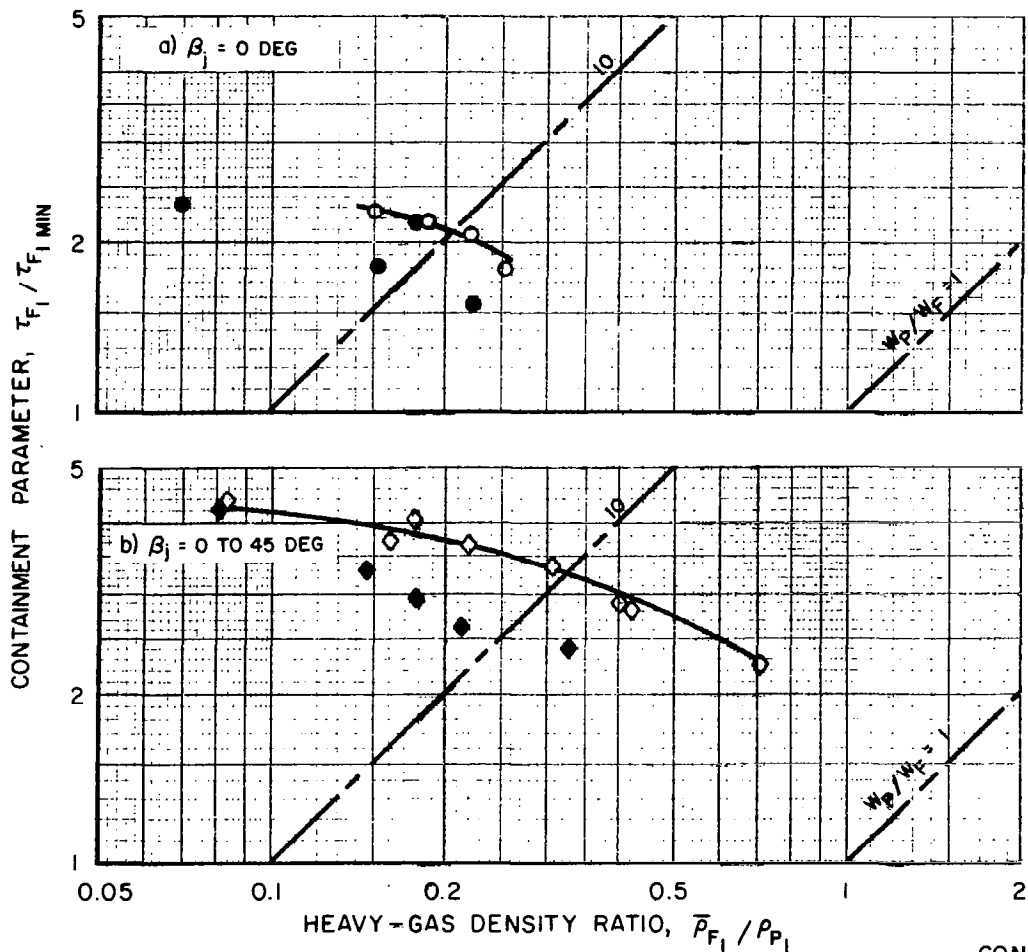
# CONTAINMENT PARAMETERS FOR ALL PERIPHERAL-WALL INJECTION CONFIGURATIONS TESTED WITH HEAVY-GAS INJECTION AT CENTERS OF END WALLS

AXIAL-FLOW REYNOLDS NUMBER,  $Re_{z,w} \approx 74,000$

DIMENSIONLESS TIME CONSTANT FOR FULLY MIXED FLOW,  $\tau_{F1, MIN} \approx 0.00019$

SEE TABLE II AND FIG. 60 FOR DETAILS OF HEAVY-GAS INJECTION CONFIGURATIONS

SYMBOL	PERIPHERAL-WALL INJECTION CONFIGURATION	AXIS ORIENTATION	HEAVY-GAS INJECTION CONFIGURATION	$Re_{t,j}$	$\bar{v}_{z,w} / v_{\phi,j}$
○	$\beta_j = 0$ DEG	HORIZONTAL	CENTER, NONAXIAL-FLOW END WALL	230,000	0.314
●	$\beta_j = 0$ DEG		CENTERS, BOTH END WALLS		
◇	$\beta_j = 0$ TO 45 DEG		CENTER, NONAXIAL-FLOW END WALL		
◆	$\beta_j = 0$ TO 45 DEG		CENTERS, BOTH END WALLS		



CONTINUED

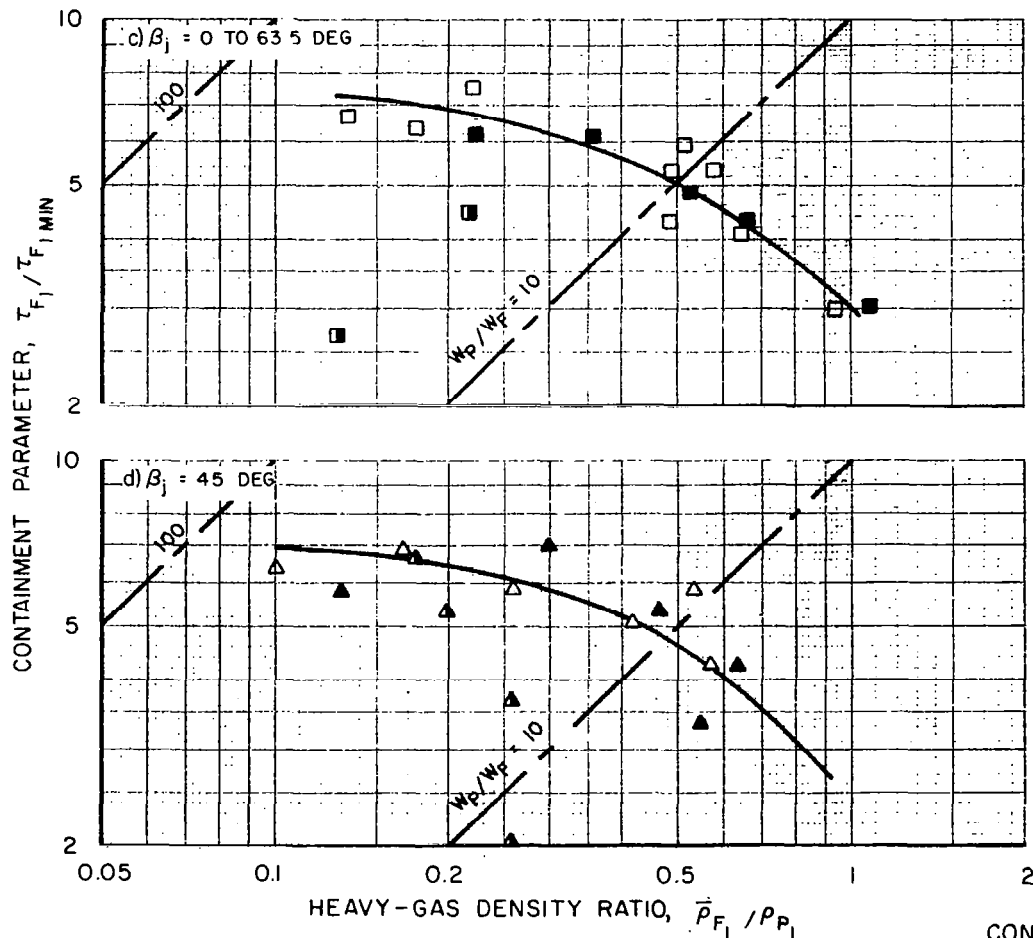
# CONTAINMENT PARAMETERS FOR ALL PERIPHERAL - WALL INJECTION CONFIGURATIONS TESTED WITH HEAVY - GAS INJECTION AT CENTERS OF END WALLS

$$Re_{z,w} \approx 74,000$$

$$\tau_{F1 \text{ MIN}} \approx 0.00019$$

SEE TABLE II AND FIG. 6d FOR DETAILS OF HEAVY-GAS INJECTION CONFIGURATIONS

SYMBOL	PERIPHERAL - WALL INJECTION CONFIGURATION	AXIS ORIENTATION	HEAVY-GAS INJECTION CONFIGURATION	$Re_{t,j}$	$\bar{v}_{z,w} / v_{\phi,j}$
□	$\beta_j = 0$ TO 63.5 DEG	HORIZONTAL	CENTER, NONAXIAL-FLOW END WALL	230,000	0.314
▣	↓		CENTER, AXIAL-FLOW END WALL		
■	↓		CENTERS, BOTH END WALLS		
△	$\beta_j = 45$ DEG		CENTER, NONAXIAL-FLOW END WALL	160,000	0.444
▴	↓		CENTER, AXIAL-FLOW END WALL		
▲	↓		CENTERS, BOTH END WALLS		



CONTINUED

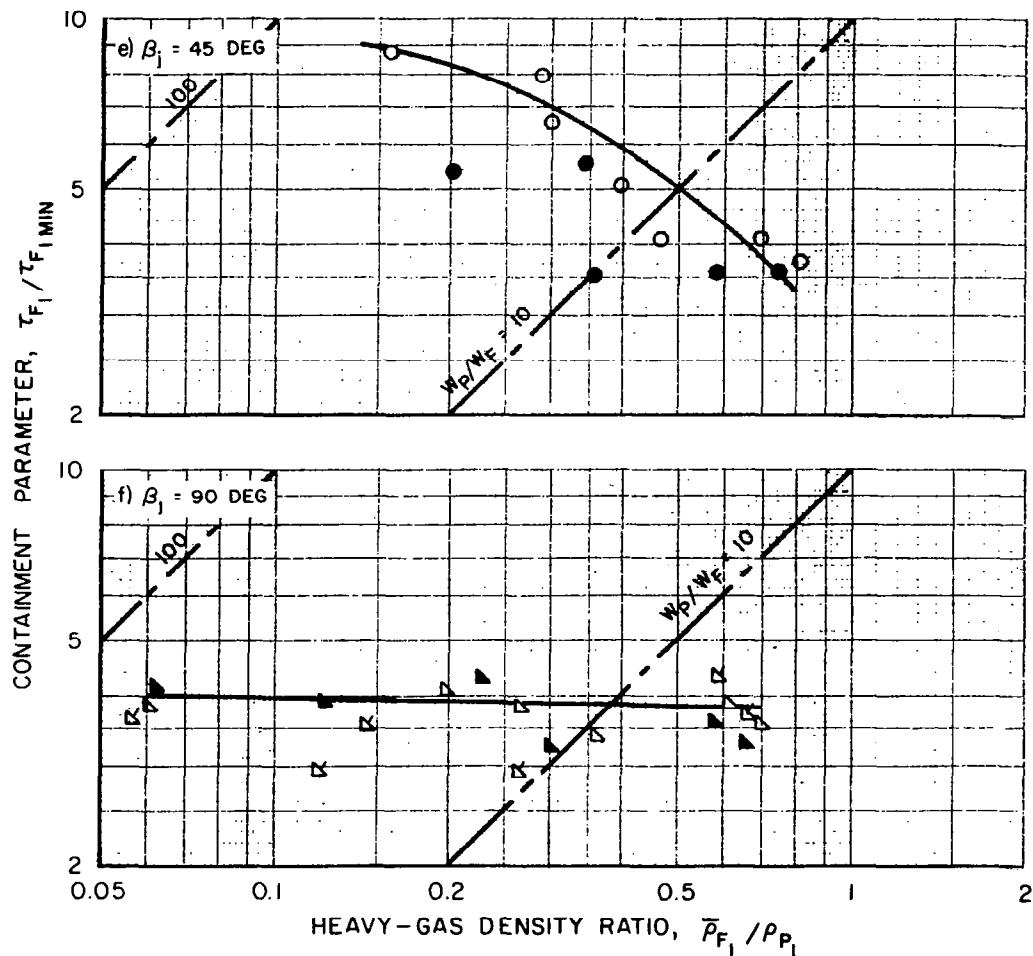
## CONTAINMENT PARAMETERS FOR ALL PERIPHERAL - WALL INJECTION CONFIGURATIONS TESTED WITH HEAVY - GAS INJECTION AT CENTERS OF END WALLS

$$Re_{z,w} \approx 74,000$$

$$\tau_{F_{MIN}} \approx 0.00019$$

SEE TABLE II AND FIG. 6d FOR DETAILS OF HEAVY - GAS INJECTION CONFIGURATIONS

SYMBOL	PERIPHERAL-WALL INJECTION CONFIGURATION	AXIS ORIENTATION	HEAVY-GAS INJECTION CONFIGURATION	$Re_{t,j}$	$\bar{v}_{z,w}/v_{\phi,j}$
○	$\beta_j = 45$ DEG	VERTICAL	CENTER, NONAXIAL-FLOW END WALL	160,000	0.444
●	$\beta_j = 45$ DEG		CENTERS, BOTH END WALLS	160,000	0.444
△	$\beta_j = 90$ DEG		CENTER, NONAXIAL-FLOW END WALL	0	∞
▽			CENTER, AXIAL-FLOW END WALL		
▶			CENTERS, BOTH END WALLS		



# COMPARISON OF CONTAINMENT PARAMETERS FOR ALL PERIPHERAL-WALL INJECTION CONFIGURATIONS TESTED

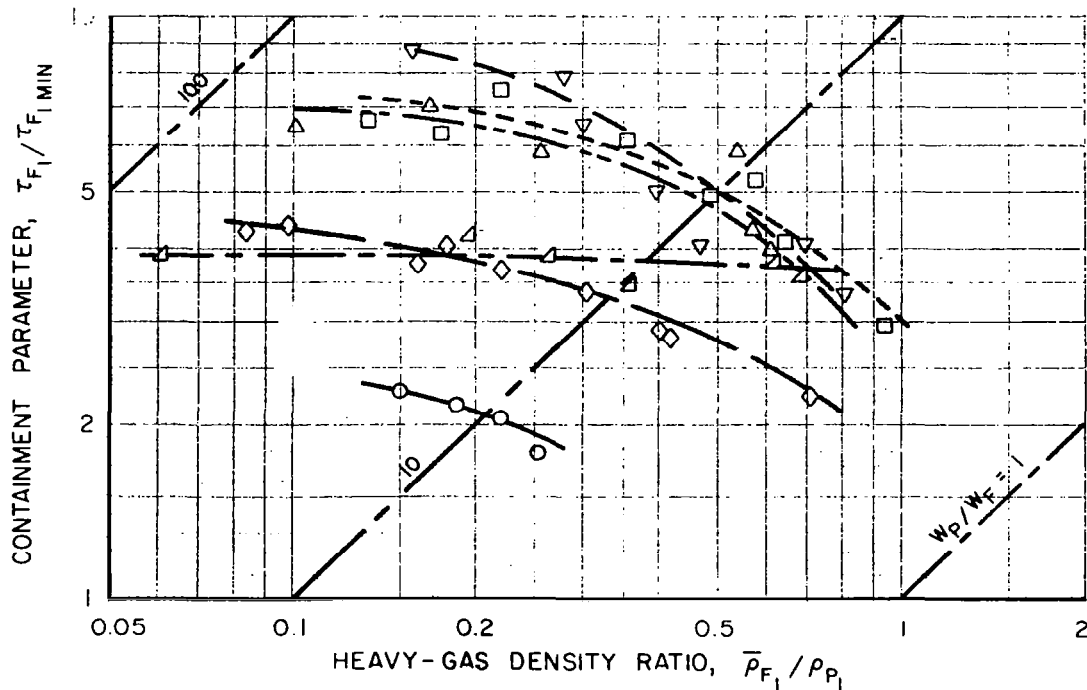
HEAVY-GAS INJECTION AT CENTER OF NONAXIAL-FLOW END WALL

AXIAL-FLOW REYNOLDS NUMBER,  $Re_{z,w} \approx 74,000$

DIMENSIONLESS TIME CONSTANT FOR FULLY MIXED FLOW,  $\tau_{F1, MIN} \approx 0.00019$

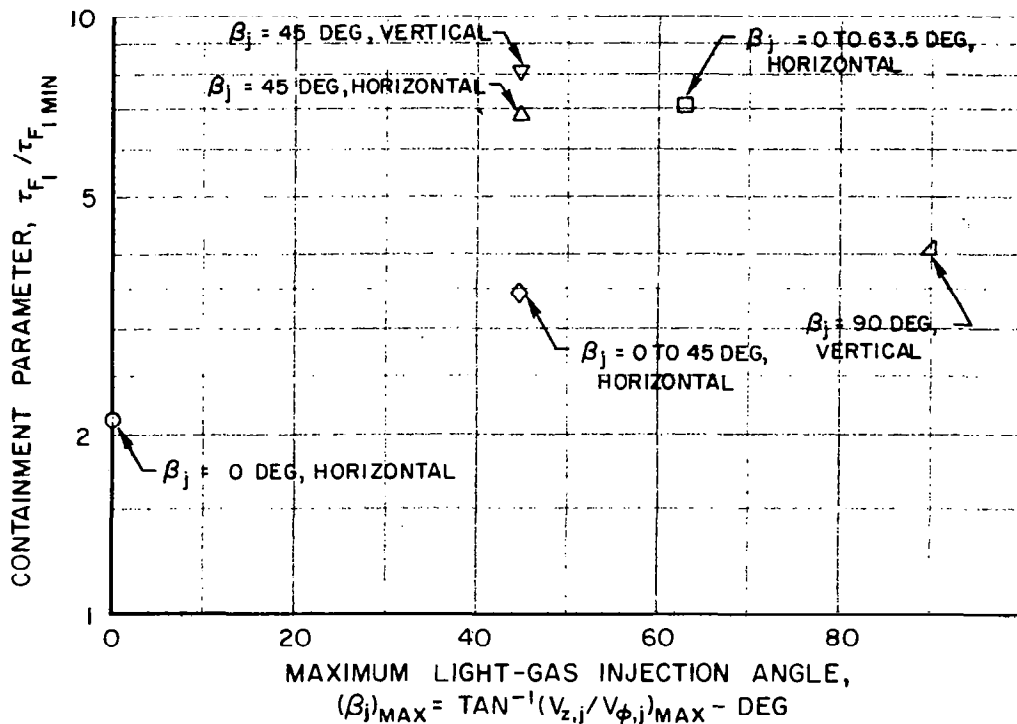
DATA FROM FIG. 31

SYMBOL	PERIPHERAL-WALL INJECTION CONFIGURATION	AXIS ORIENTATION	$Re_{t,j}$	$\bar{v}_{z,w}/v_{\phi,j}$
○ ———	$\beta_j = 0$ DEG	HORIZONTAL	230,000	0.314
◇ ———	$\beta_j = 0$ TO 45 DEG	↓	↓	↓
□ - - - -	$\beta_j = 0$ TO 63.5 DEG			
△ - - - -	$\beta_j = 45$ DEG	VERTICAL	160,000	0.444
▽ - - - -	$\beta_j = 45$ DEG		160,000	0.444
△ - - - -	$\beta_j = 90$ DEG	VERTICAL	0	$\infty$



SUMMARY OF EFFECT OF PERIPHERAL-WALL INJECTION CONFIGURATION ON CONTAINMENT PARAMETER FOR  $\bar{\rho}_{F_1} / \rho_{P_1} = 0.2$

HEAVY-GAS INJECTION AT CENTER OF NONAXIAL-FLOW END WALL  
 AXIAL-FLOW REYNOLDS NUMBER,  $Re_{z,w} \approx 74,000$   
 DIMENSIONLESS TIME CONSTANT FOR FULLY MIXED FLOW,  $\tau_{F_1 \text{ MIN}} \approx 0.00019$   
 CROSS-PLOT OF DATA FROM FIG. 32



# EFFECT OF FLOW WITHDRAWAL AT CENTER OF AXIAL-FLOW END WALL ON CONTAINMENT PARAMETER

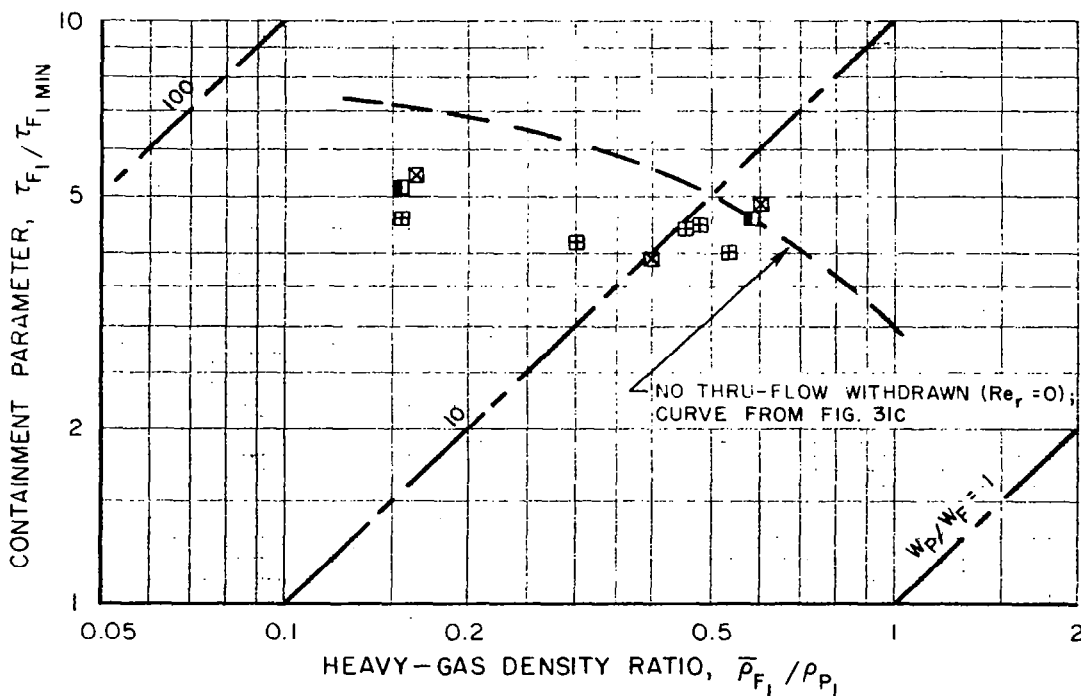
PERIPHERAL-WALL INJECTION CONFIGURATION,  $\beta_j = 0$  TO 63.5 DEG  
 HEAVY-GAS INJECTION AT CENTER OF NONAXIAL-FLOW END WALL

$Re_{z,w} \approx 74,000$

$\tau_{F1,MIN} \approx 0.00019$

THRU-FLOW WITHDRAWN AT CENTER OF AXIAL-FLOW END WALL INDICATED BY  $Re_r$

SYMBOL	$Re_r$	$Re_{t,j}$	$\bar{v}_{z,w}/v_{\phi,j}$
■	+ 51	230,000	0.314
⊗	+ 68	↓	↓
⊕	+ 93	↓	↓



EFFECT OF CHANGES IN LIGHT-GAS INJECTION RATE WITH AXIAL DISTANCE ON CONTAINMENT PARAMETER

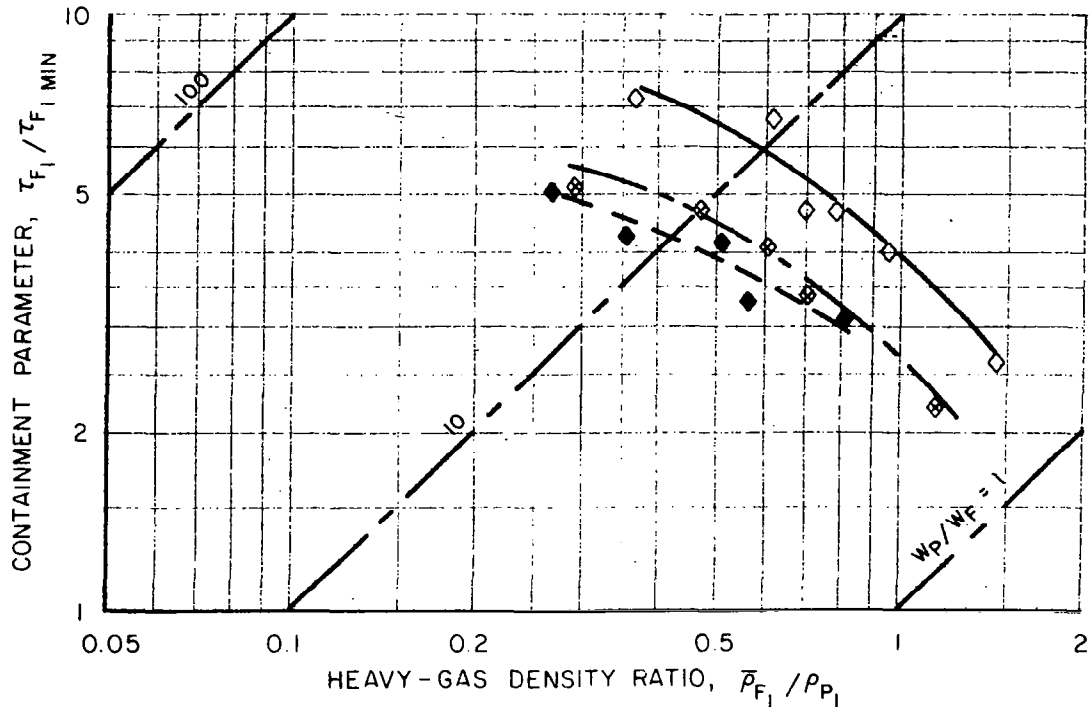
PERIPHERAL-WALL INJECTION CONFIGURATION,  $\beta_j = 0$  TO 63.5 DEG

HEAVY-GAS INJECTION AT CENTER OF NONAXIAL-FLOW END WALL

$Re_{z,w} \approx 43,000$

$\tau_{F1 MIN} \approx 0.00034$

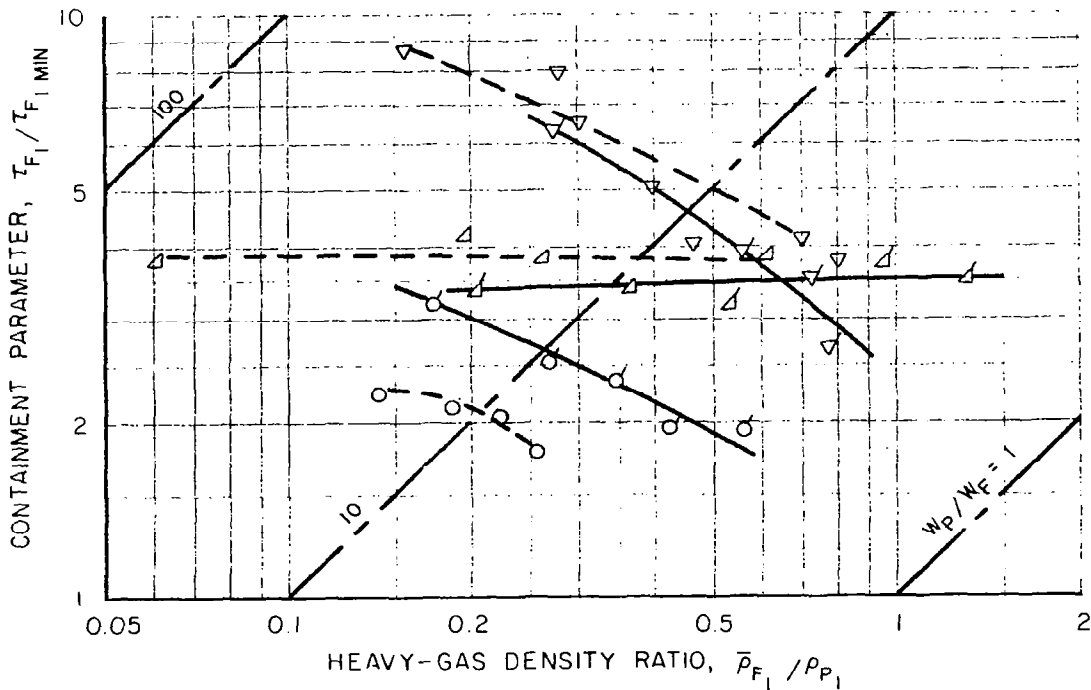
SYMBOL	PERIPHERAL-WALL LIGHT-GAS INJECTION FLOW CONDITION	$v_j$	$v_{\phi,j}$	$Re_{t,j}$
◇ ---	INJECTION FLOW RATE CONSTANT ALONG WALL	$\bar{v}_{\phi,j} \sqrt{1+4(Z/L)^2}$	$\bar{v}_{\phi,j}$ (CONSTANT)	125,000
◆ ---	EQUAL PRESSURES IN ALL PLENUMS	$\approx \bar{v}_j$ ( $\approx$ CONSTANT)	$\frac{\approx \bar{v}_j}{\sqrt{1+4(Z/L)^2}}$	171,000 (Z=0) TO 76,000 (Z=30 IN.)
◇ —	INJECTION FLOW RATE INCREASES LINEARLY WITH DISTANCE FROM NONAXIAL-FLOW END WALL	$\bar{v}_j \left[ 0.8 + 0.4 \left( \frac{Z}{L} \right) \right]$	$\bar{v}_{\phi,j} \left[ 0.8 + 0.4 \left( \frac{Z}{L} \right) \right]$	100,000 (Z=0) TO 150,000 (Z=30 IN.)



## COMPARISON OF CONTAINMENT PARAMETERS FOR $Re_{z,w} = 40,000$ AND $74,000$

HEAVY-GAS INJECTION AT CENTER OF NONAXIAL-FLOW END WALL

SYMBOL	PERIPHERAL - WALL INJECTION CONFIGURATION	AXIS ORIENTATION	$Re_{t,j}$	$\bar{V}_{z,w}/V_{\phi,j}$	$Re_{z,w}$	$\tau_{F,MIN}$
---○---	$\beta_j = 0$ DEG	HORIZONTAL	230,000	0.314	74,000	0.00019
---○---			128,000		40,000	0.00034
---▽---	$\beta_j = 45$ DEG	VERTICAL	160,000	0.444	74,000	0.00019
---▽---			91,000		40,000	0.00034
---△---	$\beta_j = 90$ DEG	VERTICAL	0	$\infty$	74,000	0.00019
---△---			0		40,000	0.00034



## EFFECT OF HEAVY-GAS INJECTION FROM POROUS TUBE ON CONTAINMENT PARAMETER

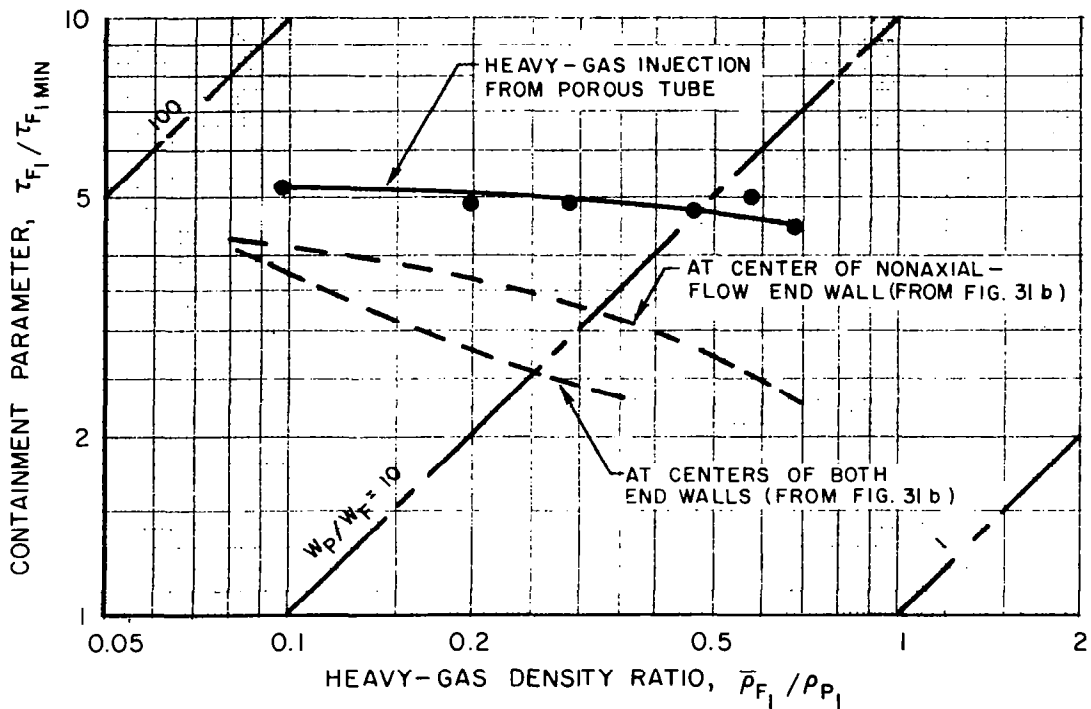
PERIPHERAL-WALL INJECTION CONFIGURATION,  $\beta_j = 0$  TO 45 DEG

$Re_{z,w} \approx 74,000$

$\tau_{F1 MIN} \approx 0.00019$

$Re_{t,j} = 230,000$

SEE TABLE II AND FIG. 6B FOR DETAILS OF HEAVY-GAS INJECTION CONFIGURATIONS



# EFFECT OF HEAVY-GAS INJECTION FROM "SHOWERHEAD" ON CONTAINMENT PARAMETER

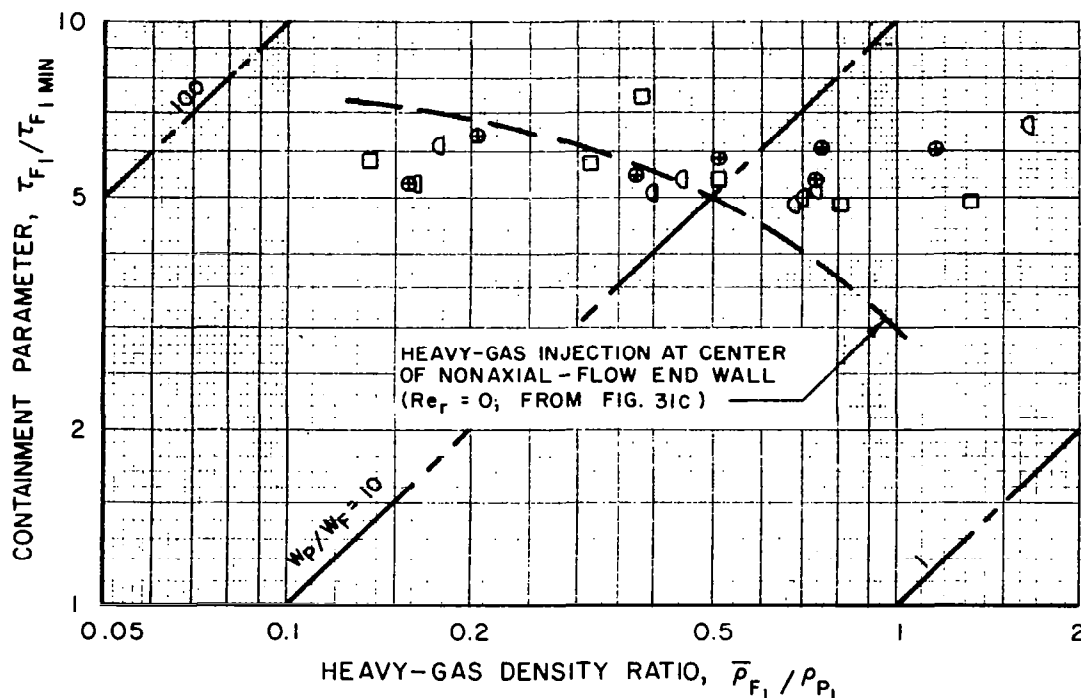
PERIPHERAL-WALL INJECTION CONFIGURATION,  $\beta_j = 0$  TO 63.5 DEG

$Re_{z,w} \approx 74,000$

$\tau_{F1 MIN} \approx 0.00019$

SEE TABLE II AND FIG. 6c FOR DETAILS OF HEAVY-GAS INJECTION CONFIGURATIONS  
THRU-FLOW WITHDRAWN AT CENTER OF AXIAL-FLOW END WALL INDICATED BY  $Re_r$

SYMBOL	$Re_r$	$Re_{t,j}$
□	0	230,000
⊕	+50	↓
⊖	+110	↓



## EFFECT OF HEAVY-GAS INJECTION FROM 6-IN.-DIA SCREEN ON CONTAINMENT PARAMETER

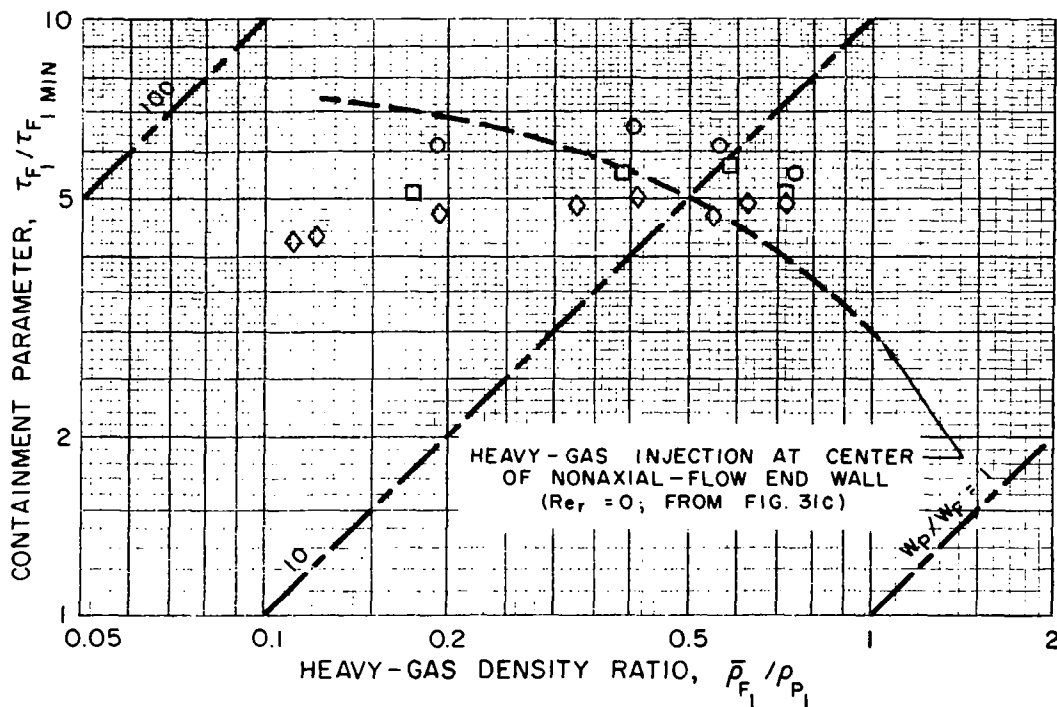
PERIPHERAL-WALL INJECTION CONFIGURATION,  $\beta_j = 0$  TO 63.5 DEG

$Re_{z,w} \approx 74,000$

$\tau_{F1 MIN} \approx 0.00019$

SEE TABLE II AND FIG. 6d FOR DETAILS OF HEAVY-GAS INJECTION CONFIGURATION  
THRU-FLOW WITHDRAWN AT CENTER OF AXIAL-FLOW END WALL INDICATED BY  $Re_r$

SYMBOL	$Re_r$	$Re_{t,j}$
○	0	230,000
□	+74	↓
◇	+110	↓



# EFFECT OF HEAVY-GAS INJECTION FROM END WALL WITH SWIRL ON CONTAINMENT PARAMETER

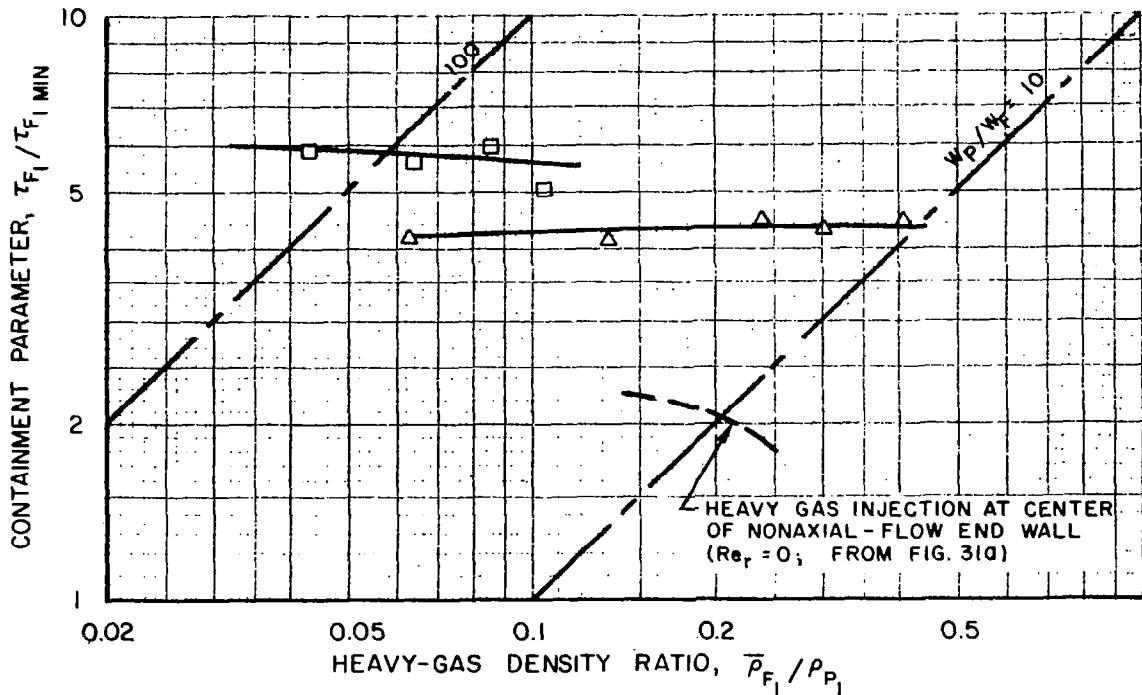
PERIPHERAL-WALL INJECTION CONFIGURATION,  $\beta_j = 0$  DEG

$Re_{z,w} \approx 74,000$

$\tau_{F1 MIN} \approx 0.00019$

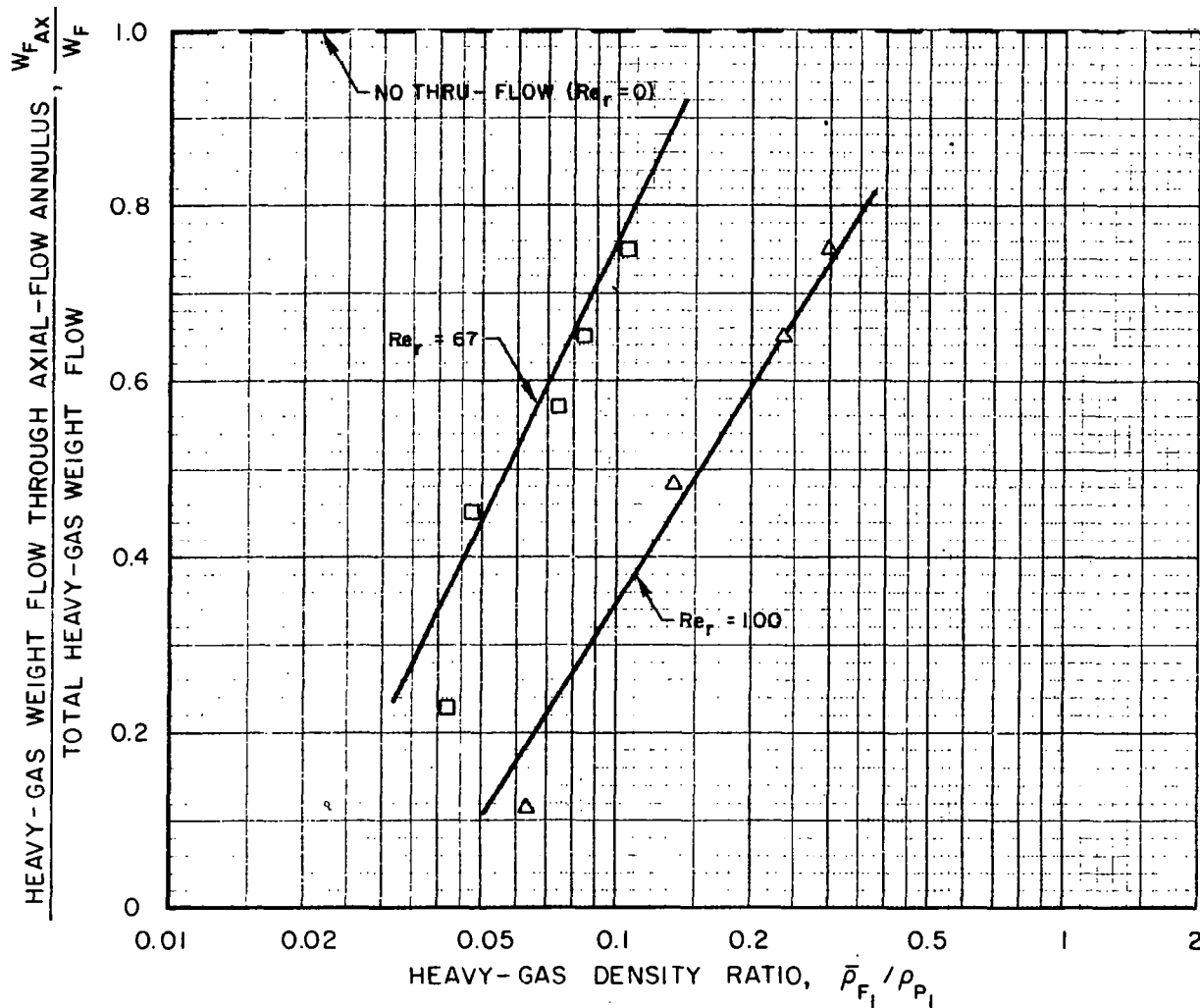
SEE TABLE II AND FIG. 6e FOR DETAILS OF HEAVY-GAS INJECTION CONFIGURATION THRU-FLOW WITHDRAWN AT CENTER OF AXIAL-FLOW END WALL INDICATED BY  $Re_r$

SYMBOL	$Re_r$	$Re_{t,j}$
□	+67	230,000
△	+100	230,000



### EFFECT OF RADIAL REYNOLDS NUMBER ON FRACTION OF TOTAL HEAVY-GAS WEIGHT FLOW THAT EXHAUSTS THROUGH AXIAL-FLOW ANNULUS

SEE FIG. 40 FOR DETAILS OF CONFIGURATION AND FLOW CONDITIONS  
 THRU-FLOW WITHDRAWN AT CENTER OF AXIAL-FLOW END WALL INDICATED BY  $Re_r$



# EFFECT OF HEAVY-GAS INJECTION THROUGH TUBES FROM PERIPHERAL WALL WITH SWIRL ON CONTAINMENT PARAMETER

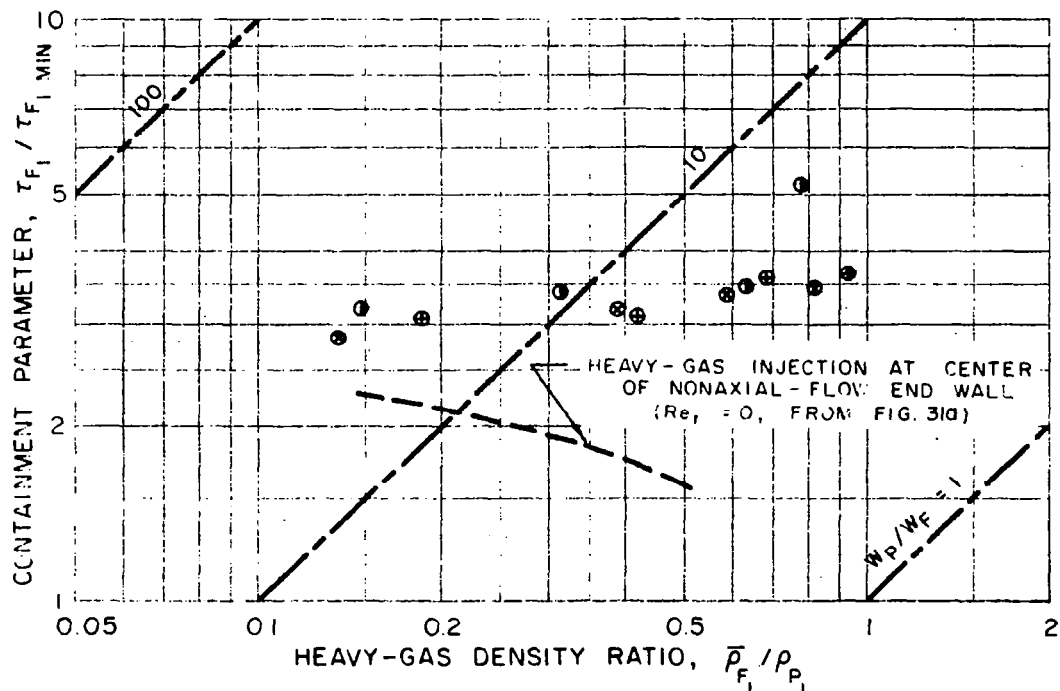
PERIPHERAL-WALL INJECTION CONFIGURATION,  $\beta_j = 0$  DEG

$Re_{2,w} \approx 40,000$

$\tau_{F1, MIN} \approx 0.00034$

SEE TABLE II AND FIG. 6f FOR DETAILS OF HEAVY-GAS INJECTION CONFIGURATION THRU-FLOW WITHDRAWN AT CENTER OF AXIAL-FLOW END WALL INDICATED BY  $Re_r$

SYMBOL	$Re_r$	$Re_{t,j}$
●	0	125,000
⊗	+59	
⊕	+104	



## COMPARISON OF CONTAINMENT PARAMETERS FOR LIGHT-GAS INJECTION WITH SWIRL FROM AXIAL-FLOW END WALL AND BOTH END WALLS

HEAVY GAS INJECTED WITH SWIRL FROM NONAXIAL-FLOW END WALL

PERIPHERAL-WALL INJECTION CONFIGURATION,  $\beta_j = 0$  TO 45 DEG

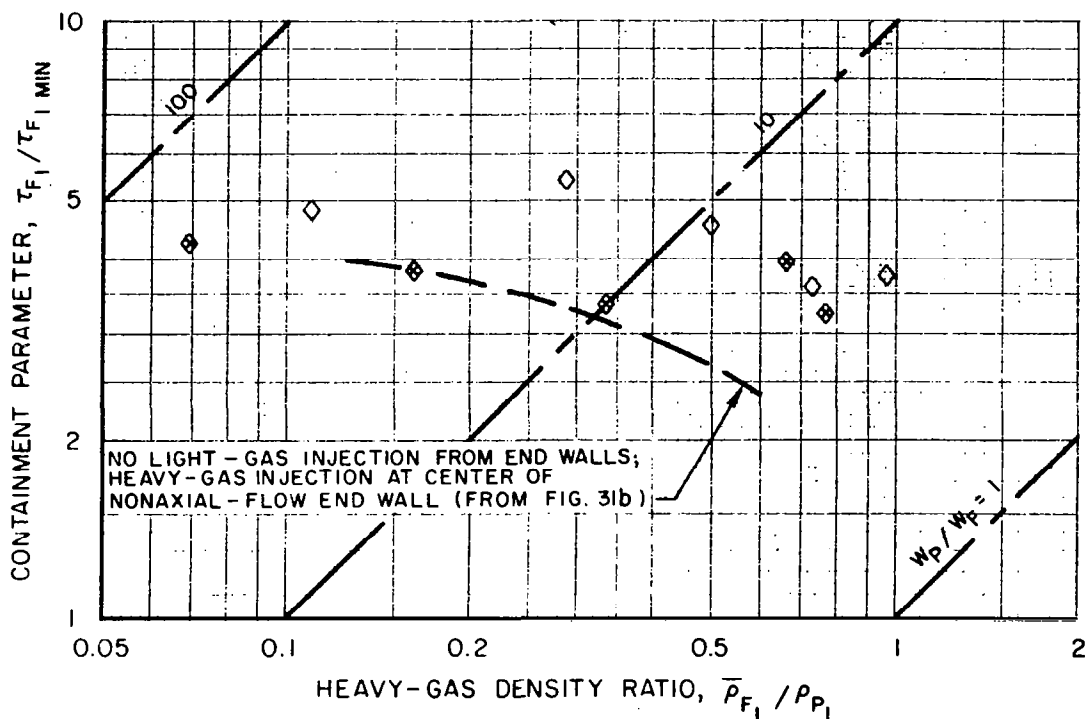
$Re_{z,w} \approx 42,000$

$\tau_{F1 MIN} \approx 0.00032$

SEE TABLE II AND FIG. 6g FOR DETAILS OF HEAVY-GAS INJECTION CONFIGURATION

SEE FIG. 7 FOR PHOTOGRAPHS AND DETAILS OF LIGHT-GAS END-WALL INJECTION CONFIGURATIONS

SYMBOL	$Re_{t,j}$	LIGHT-GAS INJECTION VELOCITIES		
		PERIPHERAL WALL $V_{\phi,j}$ - FT/SEC	AXIAL-FLOW END WALL $V_{\phi,j AF}$ - FT/SEC	NONAXIAL-FLOW END WALL $V_{\phi,j NF}$ - FT/SEC
◇	135,000	150	228	0
◈	135,000	150	226	173



## COMPARISON OF CONTAINMENT PARAMETERS FOR HEAVY-GAS INJECTION FROM NONAXIAL-FLOW END WALL WITH AND WITHOUT SWIRL

LIGHT GAS INJECTED WITH SWIRL FROM AXIAL-FLOW END WALL  
 PERIPHERAL-WALL INJECTION CONFIGURATION,  $\beta_j = 0$  TO 45 DEG  
 $Re_{z,w} \approx 40,000$        $Re_{t,j} = 135,000$        $\tau_{F1 MIN} \approx 0.00032$

SEE FIG. 7 FOR PHOTOGRAPHS AND DETAILS OF LIGHT-GAS END-WALL INJECTION CONFIGURATIONS

SYMBOL	HEAVY-GAS INJECTION CONFIGURATION	LIGHT-GAS INJECTION VELOCITIES		
		PERIPHERAL WALL $V_{\phi,j}$ - FT/SEC	AXIAL-FLOW END WALL $V_{\phi,j}$ AF - FT/SEC	NONAXIAL-FLOW END WALL $V_{\phi,j}$ NF - FT/SEC
◇	WITH SWIRL FROM NONAXIAL-FLOW END WALL THROUGH 12 WALL JETS (SEE TABLE II AND FIG. 6g FOR DETAILS)	150	228	0
◆	WITHOUT SWIRL FROM NONAXIAL-FLOW END WALL THROUGH 12 1/2-IN.-DIA DUCTS (SEE TABLE II AND FIG. 6h FOR DETAILS)	150	215	0

